Detection and Quantitation of Reactive Atmospheric Nitrogen Species in Remote Ecosystems

by

© Bryan K. Place

A Thesis submitted to the

School of Graduate Studies

in partial fulfillment of the requirements for the degree of

Masters of Science

Department of Chemistry

Memorial University of Newfoundland

July 2017

St. John's, Newfoundland and Labrador

Abstract

Anthropogenic inputs of nitrogen to the environment have increased by over 150 % in the last 150 years causing concern for vital biophysical processes on Earth. Thus being able to measure these increased inputs in terrestrial, aquatic and atmospheric environments is essential to understanding how the global nitrogen cycle has been impacted since the industrial revolution. With respect to the atmosphere, emissions of reduced and oxidized forms of nitrogen have increased largely due to the anthropogenic activities of agriculture and combustion, respectively. Emissions of these nitrogenous species not only impact regions adjacent to their point sources, but also have the ability to influence ecosystems hundreds of kilometers away due to the long-range transport of some of these compounds. This can impact sensitive remote ecosystems positively or negatively by either stimulating growth or causing acidification, eutrophication and biodiversity shifts. Therefore developing analytical techniques that are capable of measuring oxidized and reduced atmospheric inputs to remote ecosystems is of great importance.

In part I of this work a method employing custom-built physisorption-based passive samplers coupled with ion chromatography analysis was developed to sample atmospheric nitric acid ($HNO_{3(g)}$) in remote ecosystems. The developed $HNO_{3(g)}$ sampling method was able to detect $HNO_{3(g)}$ mixing ratios as low as 2 parts per trillion by volume (pptv) over a monthly sampling period, following a rigorous quality assurance and quality control procedure. The passive samplers were installed across the Newfoundland and Labrador – Boreal Ecosystem Latitudinal Transect (NL-BELT) in the summer of 2015,

and average mixing ratios of $HNO_{3(g)}$ at the NL-BELT field sites from 2015-16 were determined to be in the tens of parts per trillion by volume (pptv) range. The dry deposition flux of $HNO_{3(g)}$ as nitrogen (N) to the field sites ranged from 3 – 16 mg N yr^{-1}. Through an air mass back trajectory analysis, coupled with a steady-state chemical box model approximation, it was determined that the $HNO_{3(g)}$ quantities observed at a single NL-BELT site likely originated from local production and regional transport from central and eastern Newfoundland, with an additional contribution from the down welling of peroxyacetyl nitrates from the upper troposphere, possibly occurring during the spring and early summer.

In part II of this work, an ion chromatography method was developed to speciate and quantify alkylamines ($NR_{3(g)}$) . $NR_{3(g)}$ have been shown to influence Earth's climate and may be an important source of new nitrogen to remote ecosystems. The developed method was shown to be sensitive, accurate, and robust in separating and quantifying 11 atmospheric alkylamines, including 3 sets of alkylamine isomers, from 5 common atmospheric inorganic cations. The method was able to detect $NR_{3(g)}$ at a picogram per injection level, and the method performed robustly in the presence of a complex biomass-burning matrix containing amounts of inorganic cations up to 3 orders of magnitude larger than the $NR_{3(g)}$ quantified in the samples. Thus the ion chromatography method can be applied to the remote atmosphere where alkylamine concentrations are often detected in quantities 1000 times less than other atmospheric cations. In the biomass-burning particle samples tested using the ion chromatography method unprecedented quantities of dimethylamine and diethylamine were observed, with the summed molar quantity exceeding that of ammonium in the 100 – 560 nm particle diameter fraction.

The applicability of these atmospheric measurement techniques to measure and quantify $HNO_{3(g)}$ and $NR_{3(g)}$ has been demonstrated for remote ecosystems and will hopefully allow for a greater understanding of these two species roles' in remote environments.

Acknowledgements

First and foremost I would like to thank Trevor VandenBoer for all of his guidance and supervision throughout my time at Memorial University. Trevor, without your hands on help, brilliant ideas, and expertise in troubleshooting the damn IC, none of this would have been possible. You also introduced me to the wonderful world of fieldwork, and although I do agree that it is type II fun, it helped me realize that I have a passion for it and that I would like to continue on doing fieldwork during my PhD. You also pushed me to accomplish so much more than I thought I was ever capable of, and for that I am very thankful.

Secondly, I would like to thank Cora Young and Sue Ziegler for all of their wonderful support throughout the completion of my program. Cora, you were a fantastic teacher and mentor, and your helpful feedback, whether it was for the improving of a scientific idea or the preparation of a manuscript, was invaluable. Sue, I learned so much about the world of biogeochemistry from you, and your consistent reminders to take a step back and look at the bigger picture have taught me to remain focused on the true goals when conducting research.

Thirdly, the research conducted in this thesis would not have been possible without the help of the individuals working with the Canadian Forestry Service in Corner Brook. Andrea, Darrell, Kate and Pam, I am so grateful to all the organization, assistance, and

help that all of you provided to make my sample collection and this thesis possible. All of you were wonderful and so adaptable that it made fieldwork seem effortless.

I would also like to thank Rob, Aleya and Joseph for all your help with developing the alkylamine method and John for all your help going back and forth to the field collecting samplers. Jamie, thank you for all of your support with running samples on the IC, I couldn't have done that alone. Thank you to all my friends in the CJY group for their support in the last two years. John, Kathryn, Joseph, Heidi, Devon (that's right, I remembered to mention you), Peter, and Teles, thank you so much for tolerating my stupid jokes in the office and coming on all the Tim's runs with me, I don't think I would have survived my Master's without you guys, honestly.

Finally, I would like to acknowledge all the other people in my life who supported me through the completion of my Masters degree. Sruti, thank you so much for always believing in me and pushing me to do better, without your support through all of this I don't know what I would have done. Mom, Dad and Kara, I can't thank you enough for supporting me through the last two years and thank you again for never questioning my spur of the moment decision to move out to the most easterly point in North America.

TABLE OF CONTENTS

Abstract ii
Acknowledgements v
List of Tables x
List of Figures xi
List of Symbols, Nomenclature, and Abbreviations xv
List of Appendices xvii
Co-authorship Statement xviii
1. Introduction 1
1.1 Introduction to the Atmospheric System 2
1.2 Motivation and Challenges for Characterizing Reactive Nitrogen Species in Remote Ecosystems 3
1.2.1 Anthropogenic Influence on the Global Nitrogen Cycle 3
1.2.2 Analytical Challenges when Sampling and Analyzing Atmospheric Reactive Nitrogen species in remote ecosystems 6
1.3 Passive Sampling of Gaseous Nitric Acid in Canadian Boreal Ecosystems 8
1.3.1 Motivation for Quantifying Nitric Acid Deposition in Remote Ecosystems 8
1.3.2 Properties of Atmospheric Nitric Acid 10
1.3.3 Reactive Sources and Sinks of Atmospheric Nitric Acid 11
1.3.4 Deposition of Nitric Acid to Earth's Surfaces 14
1.3.5 The Atmospheric Passive Sampling Approach 16
1.3.6 Employing a Passive Sampling Technique to Quantify Nitric Acid in Remote Ecosystems 18
1.4 Quantitation of Atmospheric Alkylamines in Remote Ecosystems 18
1.4.1 Motivations for Measuring Atmospheric Alkylamines 18
1.4.2 Properties of Atmospheric Alkylamines 21
1.4.3 Sources and Sinks of Atmospheric Alkylamines 24
1.4.4 Analytical Characterization of Atmospheric Alkylamines 25
1.4.5 Development and Characterization of an Ion Chromatography Method for Measuring Atmospheric Alkylamines in Remote Ecosystems 27
1.5 References 29

2. Passive sampling of gaseous nitric acid along the Newfoundland and Labrador Boreal Ecosystem Latitudinal Transect (NL-BELT) 44
2.1 Abstract 45
2.2 Introduction 46
2.3 Methods 51
2.3.1 Custom Built Nitric Acid Passive Samplers 51
2.3.2 Passive Sampler Deployment Along the Newfoundland and Labrador – Boreal Ecosystem Latitudinal Transect (NL-BELT) 53
2.3.3 Supporting Measurements at the NL-BELT Sites 55

2.3.4 Sample Handling, Analysis and Quality Control 55
2.3.4.1 Handling and Extraction of Nylon and PTFE Filters 55
2.3.4.2 Analysis of Nylon and PTFE Filters by Ion Chromatography 56
2.3.4.3 Washing Procedures and Negative Controls 57
2.3.4.4 Ion Chromatography Instrumental Performance Evaluation 58
2.3.5 Reusability of Nylon Membrane Filters 59
2.3.6 Calculation of $HNO_{3(g)}$ Mixing Ratios from Filter Extracts 59
2.3.7 Calculation of $HNO_{3(g)}$ Annual Fluxes Across the NL-BELT 60
2.3.8 HYSPLIT Model Calculations for Estimating Air Mass Back Trajectories 61
2.4 Results and Discussion 62
2.4.1 Ion Chromatography Method Performance, Quality Assurance, and Quality Control 62
2.4.2 Atmosphere-Biosphere Interactions Through $HNO_{3(g)}$ at the NL-BELT 64
2.4.2.1 Mixing Ratios and Trends in $HNO_{3(g)}$ Collected by Passive Sampling 64
2.4.2.2 Considerations Regarding the Accuracy of Calculated $HNO_{3(g)}$ 67
2.4.2.3 Reusability Nylon Membrane Filters for Passive Sampling of $HNO_{3(g)}$ 72
2.4.3 Annual Fluxes of $HNO_{3(g)}$ to the NL-BELT 73
2.4.4 Assigning a Source of Measured $HNO_{3(g)}$ 78
2.4.4.1 Air Mass Back-Trajectory Analysis and Geographical Sector Assignment 78
2.4.4.2 Steady-State Approximation of Locally-Derived $HNO_{3(g)}$ 83
2.5 Conclusions 90
2.6 References 92

3. Quantitation of 11 Alkylamines in Atmospheric Samples: Separating Structural Isomers by Ion Chromatography 97
3.1 Abstract 98
3.2 Introduction 100
3.3 Methods 104
3.3.1 Chemicals and Materials 104
3.3.2 Ion Chromatography 105
3.3.3 CS19 Separation Optimization 106
3.3.4 Quality Assurance and Quality Control 107
3.3.5 Size-Resolved BB Sample Analysis 109
3.3.6 BC Fire Sample Analysis 110
3.4 Results and Discussion 111
3.4.1 Analytical Method Performance of CS19 Cation-Exchange Column 111
3.4.1.1 Separation Approach and Optimization of Parameters 111

3.4.1.2 Instrumental Performance and Comparison for the Methylamines, Ethylamines, and Inorganic Cations 117
3.4.1.3 Expanded Amine Catalogue for Other Common Atmospheric Species 123
3.4.1.4 Method Development with the Addition of an Inline CG15 Guard Column 126
3.4.1.5 Analytical Column Stability 127
3.4.2 Biomass-Burning Particle Analysis and Discussion 128
3.4.2.1 Size-Resolved Alkylamines in Particles from an Aged Biomass-Burning Plume 128
3.4.2.2 Time Series of Amines in Fresh Biomass-Burning Plume Particles from British Columbia 134
3.5 Conclusions 136
3.6 References 138

4. Conclusions 150
4.1 Summary and General Findings 151
4.2 Summary of the Passive Sampling of $HNO_{3(g)}$ Across the NL-BELT 152
4.3 Summary of the IC Method for Quantifying Atmospheric Alkylamines 153
4.4 References 155

Appendix A Supporting Information for Chapter 2 157
Appendix B Supporting Information for Chapter 3 160

List of Tables

Table 1-1: Most abundant oxidized and reduced N_r compounds in the atmosphere. 6

Table 2-1: Descriptive statistics for correlations between air mass source regions and measured concentrations of $HNO_{3)g)}$ at each site. The coefficient of determination (r^2) describes the strength of fit using a linear regression between two sets of data. The Spearman's rho (ρ) describes the directionality of the correlation and describes the strength of fit when using any appropriate monotonic function to fit the data. 81

Table 3-1: Separation characteristics and statistics for the CS19 gradient method. The retention time (t_r) ranges for the methyl amines, ethyl amines and inorganic cations were determined using retention time windows from a full calibration. The peak width and resolution were determined using the highest calibration standards amines (500 ng) and inorganic (160 – 520 ng) cations. The t_r range and peak width were back-calculated for $iMPAH^+$, $MPAH^+$, $MBAH^+$, $DABH^+$ and $DAPH^+$ based on the other alkyl amines responses to column degradation. Sensitivity, precision, average LOD, and LOD range were analyzed using multiple calibration standards and blanks (see Section 3.3.4). Upper and lower range accuracies were assessed using high and low check standards for the alkyl amines (n=6) and inorganic cations (n=4). The low check standards were 15 times more concentrated than the lowest calibration standard and the high check standards were 150 times more concentrated. 119

Table A-1: Geographical grid sector assignment of air-mass source regions for each month of the study period across all four study sites. 159

Table B-1: Comparison of methyl and ethyl amine external and standard addition calibration slopes and retention times (t_r). 165

Table B-2: Analytical performance of other IC methods used for the determination of atmospheric methyl and ethyl amines. 165

Table B-3. Mass loadings of amines and ammonium in size-resolved particle samples from an aged biomass burning plume sampled in St. John's, Newfoundland on July 6, 2013. 167

Table B-4. Mass loadings of amines and ammonium in a fresh biomass burning plume at Burnaby Kensington Park and North Vancouver/Second Narrows sites in British Columbia in July 2015. 167

List of Figures

Figure 1-1: Fluxes (Tg N yr^{-1}; arrows) and reservoirs (Tg N; boxes) of the modern day global nitrogen cycle (Adapted from Schlesinger and Bernhardt, 2013). 4

Figure 1-2: Chemical formation and loss processes of $HNO_{3(g)}$ in the atmosphere. 12

Figure 1-3: Atmospheric chemistry and climate effects of alkylamines. The K_1 pathway represents equilibrium thermodynamic partitioning between the gas and condensed of alkylamines and the K_2 pathway represents the phase partitioning of amides/imines. 20

Figure 2-1: Schematic of the custom-built $HNO_{3(g)}$ passive samplers. The filter pack assembly (a) consists of a petri dish (60 x 15 mm), a nylon membrane filter (47 mm, 1.0 μm), a supported PTFE filter (47 mm, 1.0 μm), two PTFE rings (50 x 2 mm) and a polycarbonate ring (50 x 5 mm). The weatherproof enclosure (b) consists of an ABS enclosure base and an ABS screw cap with a drilled hole to loop string through for mounting in situ. 52

Figure 2-2: Map of North America (left) highlighting the geographical location of Newfoundland and Labrador and map of the NL-BELT (right) showing the four watershed regions (Grand Codroy (GC), Humber River (HR), Salmon River (SR), and Eagle River (ER)) that comprise the NL-BELT. 53

Figure 2-3: Time-weighted average $HNO_{3\,(g)}$ mixing ratios (red trace) and average air temperatures (dotted black trace) per sampling period in a) GC b) HR c) SR and d) ER from August 2015 to October 2016. The width of each bar represents the period over which the sample was collected. Error bars denote the standard error of triplicate samples collected within each site. 65

Figure 2-4: Schematic of potential effects of temperature, relative humidity and particulate concentrations on $HNO_{3(g)}$ uptake to the nylon filters. 69

Figure 2-5: Annual flux of $HNO_{3(g)}$ as N to the NL-BELT field sites from August 2015 to August 2016 calculated using a deposition velocity of 3 cm s^{-1}. The black error bars represent sum of squares of the triplicate standard error in mixing ratios and the blue error bars represent the variability in the flux calculated by considering depositional velocity (V_d) may range from 2 – 4 cm s^{-1} in these forests. 76

Figure 2-6: Example HYSPLIT model output frequency plots for distribution of air masses arriving at GC during the months of a) July 2016 and b) September 2016. The percentage distribution of air mass back trajectories is calculated by dividing the number of trajectory end point outputs in each 1° x 1° grid square by the total number

of trajectories run in the simulation. 80

Figure 2-7: Conceptual schematic of the chemical box model employed for calculating abundance of $HNO_{3\,(g)}$ across the NL-BELT derived from known atmospheric chemical mechanisms of formation and loss. 84

Figure 2-8: Measured $NO_{2(g)}$ (blue trace) and $HNO_{3(g)}$ (black trace) mixing ratios, and calculated $HNO_{3(g)}$ (red trace) mixing ratios using a steady-state approximation, for GC in the summer of 2016. The error bars for the measured $NO_{2(g)}$ and $HNO_{3(g)}$ mixing ratios represent the standard error in triplicate measurements. The error bars for the calculated $HNO_{3(g)}$ mixing ratios represent the propagation of uncertainty when calculating the mixing ratios. 88

Figure 3-1: Separation of amine and inorganic cation standards with the highest resolution gradient program at (a) 30 and (b) 55°C. The order of elution and mass of cation injected in (a) is as follows: Li^+ (1, 16 ng), Na^+ (2, 158 ng), NH_4^+ (3, 169 ng), $MMAH^+$ (4, 500 ng), $MEAH^+$ (5, 500 ng), K^+ (6, 524 ng), $DMAH^+$ (7, 500 ng), $TMAH^+$ (8, 500 ng), $DEAH^+$ (9, 500 ng), $TEAH^+$ (10, 500 ng), Mg^{2+} (11, 128 ng), and Ca^{2+} (12, 361 ng). Cation peaks represent the same mass injected and are labeled according to the same numeric identities in (b). 113

Figure 3-2: Separation of 1 μg ml^{-1} mixed amines standard with the final method gradient elution program at 30, 40, 50 and 60 °C. The peak elution order was $MMAH^+$ (1), $MEAH^+$ (2), $DMAH^+$ (3), $TMAH^+$ (4), $DEAH^+$ (5), and $TEAH^+$ (6). The separation of diethylamine (DEA) from trimethylamine (TEA) was achieved at column temperatures greater than 50 °C. 116

Figure 3-3: (a) Separation of amine and inorganic cation standards with the addition of $MPAH^+$, $iMPAH^+$ and $MBAH^+$ using the final gradient program. The order of elution and mass of cation injected in (a) is as follows: Li^+ (1, 1.6 ng), Na^+ (2, 16 ng), NH_4^+ (3, 17 ng), $MMAH^+$ (4, 50 ng), K^+ (5, 52 ng), $MEAH^+$ (6, 50 ng), $DMAH^+$ (7, 50 ng), $iMPAH^+$ (8, 50 ng), $MPAH^+$ (9, 50 ng), $TMAH^+$ (10, 50 ng), $DEAH^+$ (11, 50 ng), $MBAH^+$ (12, 50 ng), and $TEAH^+$ (13, 50 ng). (b) Separation of amine and inorganic cation standards with the addition of $MPAH^+$, $iMPAH^+$ and $MBAH^+$ and the addition of the CG15 column using a modified gradient program. Cation peaks are labeled accordingly to the same identities in (b) and the mass of analyte injected is as follows: Li^+ (1.6 ng), Na^+ (16 ng), NH_4^+ (17 ng), $MMAH^+$ (500 ng), K^+ (52 ng), $MEAH^+$ (500 ng), $DMAH^+$ (500 ng), $iMPAH^+$ (500 ng), $MPAH^+$ (500 ng), $TMAH^+$ (500 ng), $DEAH^+$ (500 ng), $MBAH^+$ (500 ng), and $TEAH^+$ (500 ng). 124

Figure 3-4: Overlaid chromatograms of MOUDI size-fractionated particle samples collected in St John's on July 6, 2013 during the intrusion of a biomass-burning plume that originated from Northern Labrador and Quebec. The robustness of the separation method for $MMAH^+$, $DMAH^+$ and $DEAH^+$ from the common inorganic cations is demonstrated for the 320-560 nm (Black) and 100-180 nm (Red) size bins. 129

Figure 3-5: (a) Amines to ammonium ratio in the size-resolved aged biomass-burning sample originating from Quebec and Labrador in the summer of 2013. (b) Amines to ammonium ratio for the Burnaby/Kensington Park (BKP) site and North Vancouver/Second Narrows (NVSN) site in British Columbia during the summer 2015 wildfires. The error bars in the graph represent propagated error in the amine and ammonium quantities resulting from variability in the field blanks and check standards during the analysis of the samples. 132

Figure A-1: Procedure developed for geographical sector assignment of air mass back trajectory endpoints for use with Igor Pro. Trajectory endpoints are assigned to one of four quadrants (NE, NW, SW, SE) surrounding the coordinates centered on the desired NL-BELT field site. Any trajectory endpoints directly on top of the field site were not counted in the analysis. The procedure takes in 3 waves (columns) named latitude_points, longitude_points, and site_coordinates and creates the wave sector_points. The wave latitude_points contains all the latitude coordinates of the air mass trajectory endpoints for a given sampling period, while longitude_points contains all of the matching longitude coordinates. The wave site_coordinates contains the latitude and longitude points in that order within the wave for the field site of interest (ie. GC, HR, SR or ER). The procedure then takes each longitude and latitude trajectory endpoint and decides whether it is greater than or less than the corresponding site coordinate. It outputs the final result in the wave sector_points, which is a counting-based wave that contains the following rows: northwest points, northeast points, southwest points, southeast points, and total points. The procedure adds a value of one to the quadrant in which the trajectory endpoint lies and then adds a value of one to the total points. The probability density for air transit duration in each sector is calculated later by dividing the quadrant points by the total points counted. 157

Figure A-2: Ion chromatograph of separations achieved between the inorganic anions (red line: fluoride, nitrite, chloride, nitrate, bromide, sulfate, and phosphate) and organic anions (black line: succinate, formate, acetate, lactate, propionate, and butyrate) running the gradient program described in Sect 2.3.4.2. Ions are listed in order of appearance from left to right. The two system peaks present in the chromatogram where both traces overlap result from carbonate and bicarbonate present in the ultrapure water eluent source. 158

Figure A-3: Overlaid chromatograms of a nylon filter sample extract, a nylon filter field blank extract, and a 1 mM KOH reagent blank collected from GC in November 2015. 158

Figure B-1: Chromeleon method data file for final gradient method at 55 °C. 160

Figure B-2: Sample chromatograms of a calibration blank and a size-resolved BB MOUDI foil substrate field blank. The peaks labelled above are as follows: Na^+ (1), K^+ (2), System peak (3), and Ca^{2+} (4). 161

Figure B-3: (a) Resolution of the six inorganic cation peak pairs using isocratic eluent methods at a flow rate of 0.75 ml min^{-1}. (b) Resolution of the six inorganic cation peak pairs using isocratic eluent methods at a flow rate of 1.25 ml min^{-1}. The resolution axis is split to indicate eluent concentrations where dramatic increases in separation occurred. 162

Figure B-4: (a) Resolution of the six alkyl amine cation peak pairs using isocratic eluent methods at a flow rate of 0.75 ml min^{-1}. (b) Resolution of the six alkyl amine cation peak pairs using isocratic eluent methods at a flow rate of 1.25 ml min^{-1}. 163

Figure B-5: Calculated Van Deemter plots for the isocratic elutions of (a) $MMAH^+$ and (b) $TEAH^+$ at various MSA eluent concentrations and flow rates. 164

Figure B-6: A chromatogram from an extracted $PM_{2.5}$ sample collected during a biomass-burning event in British Columbia at the Burnaby Kensington Park site. 164

List of Symbols, Nomenclature, and Abbreviations

•	Radical
°	Degrees
μ	Flow rate
ν	Frequency
ρ	Spearman's coefficient
σ	Standard deviation
Σ	Sum of
h	Planck's constant
k	Rate constant
n_x	Moles of compound x
r^2	Coefficient of determination
t_r	Retention time
w	Peak width at base
C_x	Concentration of compound x
D	Diffusion
F	Flux
H	Theoretical plate height
K_H	Henry's law constant
N_r	Reactive nitrogen
R	Ideal gas constant
V_d	Deposition velocity
R_a	Aerodynamic resistance
R_b	Quasi-laminar resistance
R_c	Surface resistance
R_{ads}	Rate of adsorption
R_s	Peak to peak resolution
V_x	Volume of compound x
μg	Microgram
ng	Nanogram
pg	Picogram
nm	Nanometer
yr	Year
mM	Millimolar
mA	Milliamp
psi	Pounds-per-square inch
kPa	Kilopascals
Hz	Hertz
ppmv	Parts per million by volume
ppbv	Parts per billion by volume
pptv	Parts per trillion by volume
ppqv	Parts per quadrillion by volume

ABS	Acrylonitrile butadiene styrene
BB	Biomass burning
BKP	Burnaby/Kensington Park
CCN	Cloud condensation nuclei
CLOUD	Cosmics Leaving OUtdoor Droplets chamber
DAB	Diaminobutane
DAP	Diaminopentane
DEA	Diethylamine
DMA	Dimethylamine
DIW	Deionized water
DON	Dissolved organic nitrogen
ER	Eagle River
GC	Grand Codroy
GDAS	Global Data Assimilation System
HR	Humber River
HX	Acid
HYSPLIT	Hybrid Single Particle LaGrangian Integraded Trajectory model
IC	Ion chromatography
iMPA	Monoisopropylamine
LC	Liquid chromatography
LOD	Limit of detection
LOQ	Limit of quantitation
MBA	Monobutylamine
MEA	Monethylamine
MMA	Monomethylamine
MPA	Monopropylamine
MOUDI	Micro-orifice uniform-deposit impactor
MS	Mass spectrometry
MSA	Methanesulfonic acid
NL-BELT	Newfoundland and Labrador – Boreal Ecosystem Latitudinal Transect
NO_x	Sum of $NO_{(g)}$ and $NO_{2(g)}$
NOAA	National Oceanographic and Atmospheric Association
NR_3	Alkylamines
NVSN	North Vancouver/Second Narrows
PAN	Peroxyacetyl nitrates
PM_x	Particulate matter having a diameter less than or equal to x
PTFE	Polytetrafluoroethylene
QA/QC	Quality assurance/quality control
RH	Relative humidity
SR	Salmon River
TEA	Triethylamine
TMA	Trimethylamine
USEPA	United States Environmental Protection Agency

List of Appendices

Appendix A – Supporting Information for Chapter Two

Appendix B – Supporting Information for Chapter Three

Co-authorship Statement

This thesis is composed of a set of manuscripts that have been published or are in preparation for publication in peer-reviewed journals. As a result, the repetition of methodology, data presentation, and discussion of data was unavoidable. Bryan K. Place prepared all manuscripts, and all published manuscripts presented in this thesis were reproduced with permission from the respective peer-reviewed journal. Trevor C. VandenBoer, Cora J. Young and Susan E. Ziegler provided critical feedback and comments for each chapter. The contributions of each co-author is provided in more detail below:

Chapter One: Introduction
Author List – Bryan K. Place
Contributions – Prepared by Bryan K. Place with feedback and comments provided by Trevor C. VandenBoer, Cora J. Young and Susan E. Ziegler.

Chapter Two: Passive sampling of gaseous nitric acid along the Newfoundland and Labrador Boreal Ecosystem Latitudinal Transect (NL-BELT)
Author List – Bryan K. Place, Kate A. Edwards, Cora J. Young, Susan E. Ziegler and Trevor C. VandenBoer.
Contributions – Bryan K. Place prepared the chapter with contributions from Trevor C. VandenBoer, Cora J. Young, and Susan E. Ziegler. Trevor C. VandenBoer designed the experiments and Bryan K. Place carried them out. The deployment and collection of the $HNO_{3(g)}$ passive samplers across the NL-BELT from 2015-2016 was done as a team effort between Bryan K. Place and Trevor C. VandenBoer. Kate A. Edwards organized and provided resources for the implementation and collection of the nitric acid passive samplers.

Chapter Three: Quantitation of 11 alkylamines in atmospheric samples: separating structural isomers by ion chromatography
Published in – Atmos. Meas. Tech., 10, 1061-1078, doi:10.5194/amt-10-1061-2017, 2017.
Reproduced with permission by – Atmos. Meas. Tech.
Author List – Bryan K. Place, Aleya T. Quilty, Robert A. Di Lorenzo, Susan E. Ziegler and Trevor C. VandenBoer.

Contributions – Trevor C. VandenBoer designed the experiments. Bryan K. Place carried out the method development, standard injections, biomass-burning sample injections, and data analysis. Aleya T. Quilty contributed to method development, standard preparation and injection, and data analysis. Robert A. Di Lorenzo collected and performed the extractions on all biomass-burning samples. Bryan K. Place prepared the chapter with contributions from all coauthors.

Chapter Four: Conclusions
Author List – Bryan K. Place
Contributions – Prepared by Bryan K. Place with feedback and comments provided by Trevor C. VandenBoer, Cora J. Young and Susan E. Ziegler.

Chapter 1. Introduction

1.1 Introduction to the Atmospheric System

Earth's atmosphere is composed of four different altitude regions relative to the Earth's surface, which are delineated by four distinct temperature inversions that limit the exchange of gas molecules between them. The two highest regions in the atmosphere are known as the thermosphere and mesosphere and are present within the altitude range of approximately 50 – 100 km. The lower atmosphere consists of the troposphere (0 – 15 km) and the stratosphere (15 – 50 km), which contain the majority of the mass of the atmosphere and as a result are the main two regions studied by atmospheric chemists because they have the most significant impact on the physical and chemical processes occurring at the Earth's surface. At the tropopause, the region where the troposphere and stratosphere meet, a temperature inversion occurs where air temperatures begin to increase with altitude. This temperature inversion limits the convective transport of gas between the layers and separates the chemical kinetics and transport of chemicals in the stratosphere from those occurring in the troposphere. Another important region of the atmosphere to note is the planetary boundary layer, which is the first 1-2 km of the atmosphere and is the part of the troposphere in direct contact with the Earth's surface. The planetary boundary layer is a complex region of the atmosphere to characterize since it is heavily influenced by changes in Earth's topography and surface temperatures. It is also the global interface where all humans exist and interact most with the atmosphere.

The atmospheric chemistry and physics of the tropospheric and stratospheric systems are regulated by the emission, transport and fate of biogenic and anthropogenic chemicals. A chemical may be introduced to the atmosphere either via a physical or reactive source and then removed through a chemical or physical sink. An e-folding

lifetime is indicative of how long-lived a chemical is in the atmosphere and describes the time it takes until ≈37% of the initial concentration of the chemical remains. The concentrations of gases in the atmosphere are typically expressed as mixing ratios, which are used to express the volume (or moles) of the given gas per volume (or mole) of air. Abundant atmospheric gases such as $N_{2(g)}$ and $O_{2(g)}$ have mixing ratios of 0.78 and 0.21, respectively, and thus together represent 99% of the atmosphere's volume (Jacob, 1999). As a result, most other atmospheric gases are considered trace gases. Reactive nitrogen (N_r) species, such as those identified in the abstract above and discussed in detail below, are often measured at mixing ratios of 10^{-6} – 10^{-12} and thus represent at most one millionth of the atmosphere's total volume (Jacob, 1999). Thus atmospheric trace gases are often expressed in units of either parts per million, billion, trillion, or quadrillion by volume (ppmv, ppbv, pptv, or ppqv).

1.2 Motivation and Challenges for Characterizing Reactive Nitrogen Species in Remote Ecosystems

1.2.1 Anthropogenic Influence on the Global Nitrogen Cycle

As a result of the industrial and agricultural revolutions the global nitrogen (N) cycle has been severely impacted by human activity (Foley et al., 2005; Gruber and Galloway, 2008). In fact, increases in anthropogenic nitrogen inputs to the environment since the 19th century have been so great that the scientific community has proposed that vital biophysical subsystems or processes at the global scale may be at risk (Rockström et al., 2009). The dispersion of nitrogen across global terrestrial, aquatic and atmospheric interfaces has been shown to be keeping pace with increased anthropogenic inputs

(Galloway et al., 2004), suggesting that all ecosystems, no matter how remote, will continue to be impacted by any future emissions.

A schematic of the modern-day nitrogen cycle is presented in Figure 1-1. More than 99% of the nitrogen on Earth's surface is contained within the atmosphere in the form of unreactive molecular dinitrogen (N_2). Since N_2 exhibits very low chemical and biological reactivity due to its strong triple bond (≈ 950 kJ mol^{-1}; Darwent, 1970), in most cases it must be oxidized or reduced into N_r before it can be cycled through the aquatic and terrestrial environments. Before the 19th century, N_2 was converted to N_r species solely through the natural processes of biological fixation and lightning.

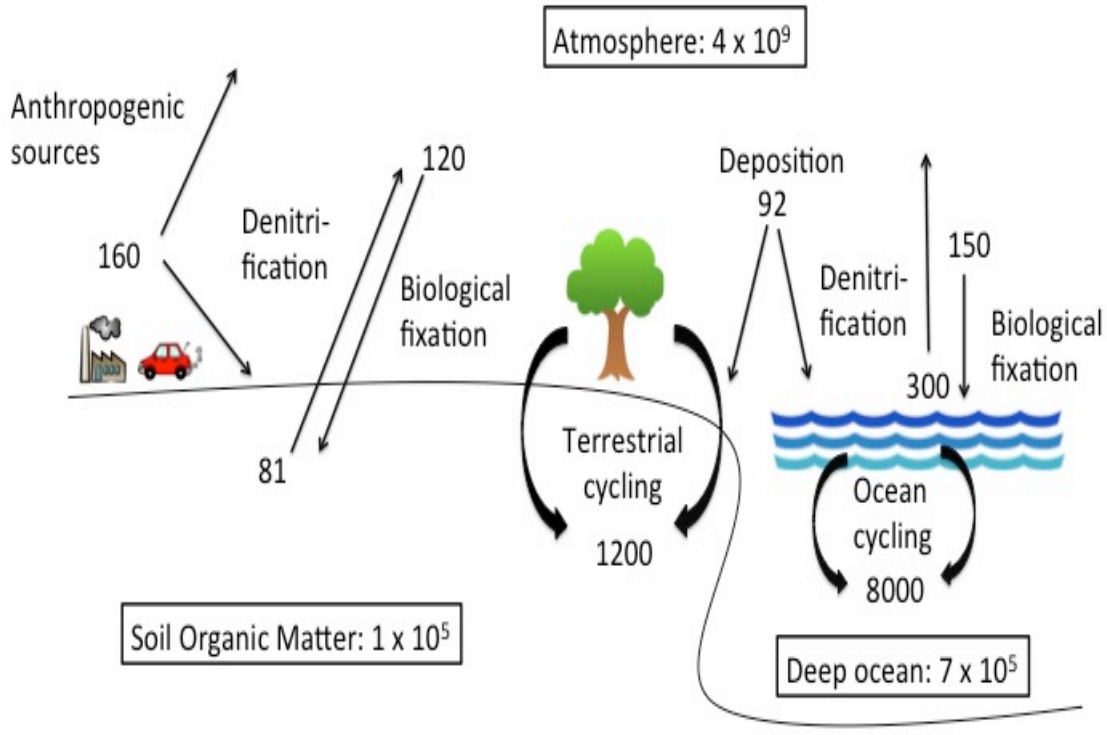

Figure 1-1. Fluxes (Tg N yr^{-1}; arrows) and reservoirs (Tg N; boxes) of the modern day global nitrogen cycle (Adapted from Schlesinger and Bernhardt, 2013).

The process of biological fixation is conducted by specialized aquatic and terrestrial bacteria that are able to reduce N_2 to ammonia (NH_3) catalyzed with molybdenum, vanadium or iron in the active site (Kim and Rees, 1994; Rehder, 2000). Lightning, on the other hand, generates enough energy to break the N_2 triple bond, which leads to the subsequent reaction of a nitrogen atom with molecular oxygen. These net reactions are shown below (R1-1 and R1-2).

(R1-1) $N_2 + 8H^+ + 8e^- \rightarrow 2NH_3 + H_2$

(R1-2) $N_2 + O_2 + \text{lightning} \rightarrow 2NO$

Today the Haber-Bosch reaction and other industrial processes have resulted in anthropogenic inputs of N_r to the environment of approximately 160 Tg N yr^{-1}, representing more than half of the total N_r inputs to the environment at the global scale (Galloway et al., 2004). This has led to an increase in global atmospheric deposition of nearly 200% since the pre-industrial era (Dentener et al., 2006; Galloway et al., 2004; Schlezinger and Bernhardt, 2013). This can have drastic effects on the natural environment. Bobbink et al. (2010) found that nitrogen accumulation can cause terrestrial ecosystem shifts to lower biodiversity, which reduces their adaptability towards changing future conditions. Increases in nitrogen inputs to terrestrial environments can also result in soil acidification and affect plant toxicity (Bobbink et al., 2010). Conversely, nitrogen is an essential element needed for growth of living tissues, such that increased inputs of nitrogen to N-limited ecosystems may stimulate growth. For example, in colder, high-latitude regions where nitrogen fixation dominates N cycling, and the availability of N is

low due to limiting N fixation rates at lower temperatures, these inputs may play a large role in influencing primary production in these regions (Houlton et al., 2008) Further, stimulation of primary production can have positive implications for carbon sequestration and thus climate change mitigation (Ollinger et al., 2008; Sokolov et al., 2008). For example, Ollinger et al. (2008) linked forest canopy nitrogen concentrations in temperate and boreal forests directly to carbon dioxide uptake capacity. Overall, the impact of increased N_r inputs to the environment is still not well understood (Sutton et al., 2011), and thus understanding the cycling of these new inputs is essential for determining the overall fate of global ecosystems faced with a changing global climate.

1.2.2 Analytical Challenges when Sampling and Analyzing Atmospheric Reactive Nitrogen Species in Remote Ecosystems

Nitrogen has nine oxidation states and as a result can be found in a variety of oxidized and reduced forms (Table 1-1) in the atmosphere. Nitric oxide ($NO_{(g)}$), nitrous oxide ($N_2O_{(g)}$), nitrogen dioxide ($NO_{2(g)}$), nitrous acid ($HNO_{2(g)}$), nitric acid ($HNO_{3(g)}$) and ammonia ($NH_{3(g)}$) are some of the N_r species that are commonly detected and quantified in the atmosphere.

Table 1-1. Most abundant oxidized and reduced N_r compounds in the atmosphere.

N_r Species	$NR_3/NH_3/NH_4^+$	N_2O	NO	HNO_2/NO_2^-	NO_2	HNO_3/NO_3^-
Oxidation number	-3	+1	+2	+3	+4	+5

Typical atmospheric mixing ratios of these N_r species are at, or below, a trace ppbv-level and therefore sensitive sampling and analysis techniques are needed to quantify these species (Finlayson-Pitts and Pitts, 2000). In remote ecosystems, N_r mixing ratios can reach ultra-trace pptv and ppqv mixing ratios, making quantitation even more difficult (Flechard et al., 2011; Wentworth et al., 2016). Flechard et al. (2011) measured $NH_{3(g)}$ and $HNO_{3(g)}$ at average mixing ratios of 350 pptv and 80 pptv, respectively, at remote boreal forest sites in Sweden. For this reason, real-time analysis of N_r compounds in remote ecosystems presents a challenge as instrumental detection limits need to be sensitive enough to measure these species at such low concentrations. Additionally, real-time analysis of the atmosphere is often considered an active technique meaning that it requires electrical power, which is not typically available at remote sites without significant investment in dedicated generation or transmission infrastructure.

Contamination and chemical loss are also of concern when sampling atmospheric gases and particles at such low concentrations. Contamination introduced to a sample during handling, transportation, preparation, and/or analysis can easily lead to a false positive, especially at ultra-trace concentration levels. Simultaneously, losses occurring during these processes may lead to the non-detection of analytes that may have been present in the collected samples. Therefore, the experimental design and necessary controls for quantifying sub-ppbv concentrations of N_r species must be established before attempting measurements of these species in remote ecosystems.

An effective way to combat both these issues is to employ an unpowered passive sampling strategy coupled with rigorous sample handling protocols, blanks, and a sensitive analytical measurement technique to analyze remote atmospheric N_r species. For

example, a cheap sorptive or reactive media to sample the remote atmosphere, coupled with a pre-concentration step prior to analysis will improve overall detection limits and negate the use of powered infrastructure, at the expense of time-integrated observational results. Further, by validating the measurements following strict quality assurance and quality control (QA/QC) protocols, data can be considered reliable against sample contamination and loss.

1.3 Passive Sampling of Gaseous Nitric Acid in Canadian Boreal Ecosystems

1.3.1 Motivation for Quantifying Nitric Acid Deposition in Remote Ecosystems

Gaseous nitric acid ($HNO_{3(g)}$) has been identified as a major N_r input to forest ecosystems across the Northern hemisphere (Flechard et al., 2011; Zhang et al., 2009). Deposition models indicate that $HNO_{3(g)}$ may deposit in substantial quantities hundreds of kilometers away from anthropogenic source regions (Verbeke et al., 2015; Lamarque et al., 2013). The deposition of $HNO_{3(g)}$ globally and to remote ecosystems has been shown to mainly occur through the formation and transport of atmospheric peroxyacetyl nitrates (PANs) (R1-3).

(R1-3) $C_xH_yNO_{z(g)} \rightleftharpoons NO_{2(g)} + C_xH_yO_{z-2(g)}$

PANs formed downwind of nitrogen oxide sources can be mixed to high altitudes (> 2 km) during the day due to convective mixing and cooling with upward transport. These PANs then become trapped above the mixed surface layer of air at night as the Earth's

surface cools, creating a thermal inversion. PANs are thermally stable for months in this high altitude region termed the upper troposphere (Atkinson et al., 1997; Singh and Hanst, 1981). They can then undergo long-range transport to remote ecosystems before thermally decomposing back to nitrogen dioxide ($NO_{2(g)}$) in descending air masses, which oxidizes to form $HNO_{3(g)}$. At a temperature of 298 K, PANs will thermally decompose back to $NO_{2(g)}$ in less than an hour (Atkinson et al., 1997).

Short-range transport of nitrogen oxide (NO_x) precursor gases from local anthropogenic emissions can also represent a new source of nitrogen into remote ecosystems. As stated in Sect 1.1.1, these inputs could have either a negative or positive impacts on sensitive remote ecosystems, depending on the nutrient limitation status with respect to nitrogen. In remote high-latitude regions it is anticipated that anthropogenically formed $HNO_{3(g)}$ will stimulate growth and primary production since the introduction of N through microbial fixation occurs at a low rate (Houlton et al., 2008). For these reasons, monitoring $HNO_{3(g)}$ inputs to remote ecosystems is important for understanding the impacts of increased global N_r.

Local biogenic soil emissions of NO_x have also shown to play an important role in $HNO_{3(g)}$ formation in remote regions (Butterbach-Bahl et al., 2009; Molina-Herrera et al., 2017; Müller et al., 1992).Yet, these soil emissions were excluded from the most recent $HNO_{3(g)}$ deposition model (Lamarque et al., 2010; Verbeke et al., 2015), and the variability in inter-site biogenic NO_x emissions makes them very difficult to constrain (Butterbach-Bahl et al., 2009). Therefore, teasing apart local biogenic sources of NO_x from anthropogenic sources will also aid in understanding whether remote ecosystems are

primarily influenced by anthropogenic N emissions or if primary production is driven by local N cycling.

Typically, field measurements of $HNO_{3(g)}$ are performed using either acid-coated denuders (devices used to separate gases from aerosols) or more expensive instrumentation such as chemical-ionization mass spectrometers (Flechard et al., 2011; Le Breton et al., 2014; Zhang et al., 2009). These techniques, although sensitive to low $HNO_{3(g)}$ mixing ratios, require powered infrastructure and are therefore non-trivial to implement in remote locations. In particular, these techniques are unable to achieve large temporal and spatial resolution across a remote ecosystem, which is required to fully constrain $HNO_{3(g)}$ deposition to remote ecosystems (e.g. as in Bytnerowicz et al., 2005). For example, across the NitroEurope network $HNO_{3(g)}$ deposition was shown to have high spatial variability across the European boreal forests (Flechard et al., 2011). Ideally, extending a passive monitoring approach to quantifying ultra-trace levels of $HNO_{3(g)}$, with rigorous analytical characterization, could provide a significant step forward in measurements of this gaseous N_r component.

1.3.2 Properties of Atmospheric Nitric Acid

Due to the properties of $HNO_{3(g)}$ a sensitive atmospheric measurement technique capable of exploiting either its adsorption or solubility properties is desired for its sampling and analysis. Nitric acid is a strong atmospheric acid with a pK_a of -1.2 (Perrin, 1982). It is also very water-soluble ($k_H = 2.1 \times 10^5$ mol L^{-1} atm^{-1}) and partitions rapidly into the aqueous phase (e.g. rainwater, cloud water or fog droplets; Finlayson-Pitts and Pitts, 2000; Schwartz and White 1983). $HNO_{3(g)}$ is also a very "sticky" molecule because

of its polar bond characteristics and it will readily adsorb to polar-group containing surfaces in contact with the atmosphere. At mixing ratios above 1 ppmv, $HNO_{3(g)}$ can be toxic to humans (Wood et al., 2013). However, with respect to remote ecosystems, $HNO_{3(g)}$ is usually measured at ppbv and pptv mixing ratios in the atmosphere in polluted urban regions and rural/remote regions, respectively (Finlayson-Pitts and Pitts, 2000).

1.3.3 Reactive Sources and Sinks of Atmospheric Nitric Acid

Gaseous nitric acid ($HNO_{3(g)}$) is an oxidation product of the precursor gases nitric oxide ($NO_{(g)}$) and nitrogen dioxide ($NO_{2(g)}$). These precursors are emitted into the atmosphere from both biogenic and anthropogenic sources. Out of these two nitrogen oxide species, $NO_{(g)}$ is often emitted in greater amounts, and depending on the source, may account for more than 90% of total NO_x ($\equiv NO_{(g)} + NO_{2(g)}$) emissions (e.g., Lenner, 1987). However, the NO_x species are rapidly cycled between each other through the oxidation of $NO_{(g)}$ by ozone ($O_{3(g)}$) and photolysis of $NO_{2(g)}$ (Jacob, 1999) during the daytime (R1-4 and R1-5). In R1-5, a third body (M), which in the case of R1-5 is represented as $O_{2(g)}$, is needed to mediate the energy transfer/stabilization of the photolysis products.

(R1-4) $NO_{(g)} + O_{3(g)} \rightarrow NO_{2(g)} + O_{2(g)}$

(R1-5) $NO_{2(g)} + h\upsilon(\lambda < 420\ nm) + M \rightarrow NO_{(g)} + O_{3(g)}$

The two main anthropogenic sources of NO_x to the atmosphere are fuel combustion for power generation and automobiles. In total, anthropogenic emissions account for

approximately 60% of global NO_x emissions (Müller, 1992; Finlayson-Pitts and Pitts, 2000). Lightning and biomass burning are the dominant natural and biogenic sources of NO_x to the atmosphere, respectively. Each of these sources emits approximately 20 Tg $NO_{2(g)}$ yr^{-1} (Müller, 1992).

Once $NO_{2(g)}$ has been emitted, created by reaction of $NO_{(g)}$ in the atmosphere, or has been produced through the thermal decomposition of PANs it can undergo a variety of reactions that ultimately lead to the formation of $HNO_{3(g)}$ (Figure 1-2).

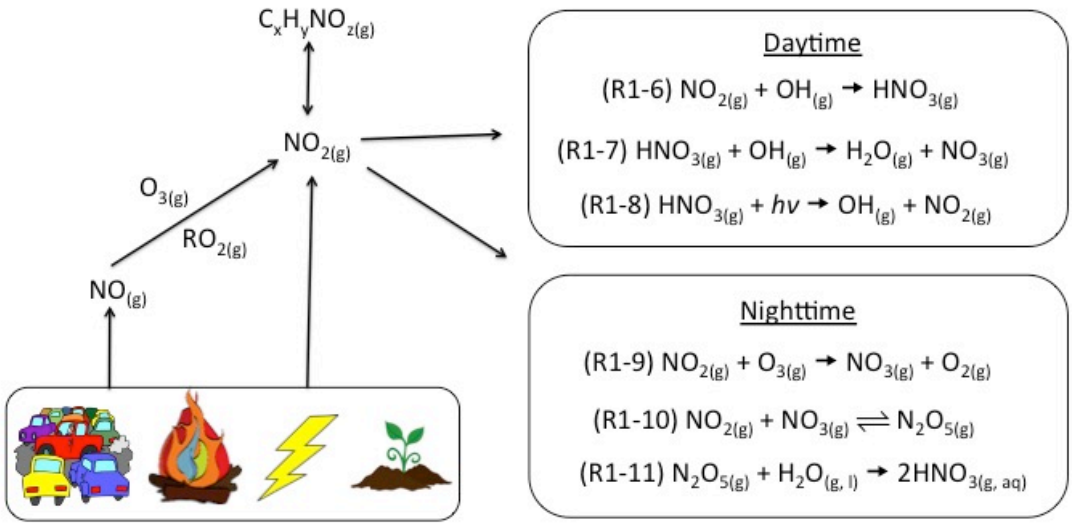

Figure 1-2. Chemical formation and loss processes of $HNO_{3(g)}$ in the atmosphere.

In the daytime, $HNO_{3(g)}$ is formed via its reaction with the hydroxyl radical ($OH_{(g)}$), the dominant oxidant in the atmosphere (R1-6). At a typical global $OH_{(g)}$ number density of 2 x 10^6 molecules cm^{-3} (Finlayson-Pitts and Pitts, 2000) $NO_{2(g)}$ has an e-folding lifetime (referred to henceforth as lifetime) of 16 hours with respect to this reaction (De More et

al., 1997). At night, $NO_{2(g)}$ can react with ozone to form the nitrate radical ($NO_{3(g)}$) (R1-9). $NO_{3(g)}$ can subsequently react with $NO_{2(g)}$ in an equilibrium reaction that forms dinitrogen pentoxide ($N_2O_{5(g)}$), which reacts with unit efficiency with gaseous or liquid water to form two molecules of $HNO_{3(g, aq)}$ (R1-10 and R1-11). These reactions do not occur during the daytime because the nitrate radical photolyses within seconds under actinic conditions (Wayne et al., 1991). In polluted regions, nocturnal $HNO_{3(g, aq)}$ can be formed at an hourly timescale (Mentel et al., 1996; Wahner et al., 1998). However, in remote regions, where $O_{3(g)}$ concentrations are typically less than 20 ppbv (Verbeke et al., 2015), nighttime $HNO_{3(g, aq)}$ formation occurs more slowly.

Although the daytime atmospheric formation of $HNO_{3(g)}$ is not rapid, its loss processes through photolysis (R1-8) and oxidation with the hydroxyl radical (R1-7) have lifetimes on the order of tens of days (Figure 1-2; De More et al., 1997). Thus, $HNO_{3(g)}$ is a long-lived species in the atmosphere with respect to reactive loss. Other sinks of $HNO_{3(g)}$ include its reaction and partitioning into the condensed phase. In the presence of an atmospheric base such as ammonia, an acid-base cluster will form via a hydrogen bonding interaction as shown in R1-12 (Nguyen et al., 1997), with the salt of ammonium nitrate formed in equilibrium with the gas phase. This reaction is not expected to be a major loss process for $HNO_{3(g)}$ however because it will only occur once all the $H_2SO_{4(aq)}$ in the condensed phase has been neutralized (Seinfeld and Pandis, 2006).

(R1-12) $NH_{3(g)} + HNO_{3(g)} \rightleftharpoons NH_4NO_{3(s, aq)}$

In areas with a large influence from the marine environment or mineral dust, $HNO_{3(g)}$ can undergo a double displacement reaction (e.g., Laux et al., 1994). For example, the reaction with $NaCl_{(s)}$ in sea salt particles is:

(R1-13) $NaCl_{(s)} + HNO_{3(g)} \rightleftharpoons NaNO_{3(s)} + HCl_{(g)}$

Similar reactions generating thermodynamically favored nitrate salts and releasing corresponding gaseous acids from the condensed phase are well established (Tang et al., 2017). The particulate nitrate salts formed in R1-12 and R1-13 may then be removed from the atmosphere via dry or wet deposition (i.e. precipitation) into an ecosystem. This process can occur rapidly once $HNO_{3(g)}$ has reacted into the condensed phase. The physical deposition of $HNO_{3(g)}$ to surfaces, however, is the dominant atmospheric sink for gaseous nitric acid.

1.3.4 Deposition of Nitric Acid to Earth's surfaces

$HNO_{3(g)}$ mainly deposits to the Earth's surface, including remote ecosystems, via dry or wet deposition due to its 'stickiness' as a gas, as well as its high water solubility. The dry deposition of $HNO_{3(g)}$ occurs in much greater quantities than other N_r species because its surface sorption properties result in a high value for the calculation of the dry deposition velocity (V_d; cm s^{-1}) for $HNO_{3(g)}$ (Finlayson-Pitts and Pitts, 2000). The V_d of an atmospheric gas describes the rate at which the gas deposits to a surface and this is often modeled using a sum of deposition resistances that represent a combination of

chemical and physical processes (Wesely and Hicks, 2000). Equation 1-1 below describes the V_d at a reference height above the Earth's surface (z) for a gaseous species as a sum of three resistances ($R_a(z)$, R_b, and R_c).

(E1-1) $V_d(z) = [R_a(z) + R_b + R_c]^{-1}$

The $R_a(z)$ term in Equation 1 describes the aerodynamic resistance above Earth's surface at a given reference height and R_b describes the quasi-laminar resistance experienced by the gas in the thin layer of air between the surface and overlying atmospheric gas. Both $R_a(z)$ and R_b are well characterized in the literature, and are mainly affected by wind speed and vegetation (Seinfeld and Pandis, 2006; Wesely and Hicks, 2000). For example, in regions with high wind speeds and tall forests, the dry deposition velocity of a gas is expected to increase due to decreases in $R_a(z) + R_b$. For most gases $R_a(z) + R_b$ tends to be small, and thus they are not the rate-limiting terms for calculating V_d. However, due to the ability of $HNO_{3(g)}$ to deposit efficiently on multiple surfaces, $R_a(z) + R_b$ is important in calculating the overall V_d (Seinfeld and Pandis, 2006). The final dry deposition resistance term, R_c, describes the surface resistance, and is often difficult to characterize when modeling V_d. It is difficult to characterize R_c because information about the surface and vegetation characteristics is needed to fully describe this term. The difficulty in determining the R_c value also underpins the large variability in reported $HNO_{3(g)}$ V_d. For example the reported V_d for $HNO_{3(g)}$ over ice/snow, oceans, and continents is 0.5, 1, and 4 cm s^{-1}, respectively, leading to a range spanning nearly one order of magnitude (Hauglustaine et al., 1994). Even over terrestrial environments, slight differences in

surface characteristics can lead to a wide range of V_d values for $HNO_{3(g)}$ (i.e. 1 cm s^{-1} over shorter vegetation and 4 cm s^{-1} over trees) (Flechard et al., 2011).

The wet deposition of $HNO_{3(g)}$ from the atmosphere occurs during precipitation events through the rapid partitioning and scavenging of $HNO_{3(g)}$ into the aqueous phase (Finlayson-Pitts and Pitts, 2000; Schwartz and White 1983). In the presence of fog and/or clouds, $HNO_{3(g)}$ will also readily partition into the available water before being deposited by rain or fog droplets to the surface. Although the process of wet deposition is dependent on a precipitation event, it is so effective at scavenging $HNO_{3(g)}$ that during an event the atmosphere is completely depleted of this gas. Capturing $HNO_{3(g)}$ surface deposition by both mechanisms is therefore essential when total N_r budgets are desired for a given ecosystem or other atmospheric observatory.

1.3.5 The Atmospheric Passive Sampling Approach

Passive sampling of the atmosphere has become a popular technique in the last few decades because of the breadth of information on temporal and spatial scales it can provide without the need of electricity (Pozo et al., 2006; Mukerjee et al., 2004; Palmes, 1981, Bytnerowicz et al., 2005). In a review of one of the first diffusion based $NO_{2(g)}$ samplers, the main advantages of passive sampling that persist to this day are: low cost, lack of maintenance, minimal space requirements and lack of explosion or fire hazard (Palmes, 1981). Passive samplers often employ diffusion-sorption or reactive uptake techniques to sample the atmosphere. In many cases, passive samplers have been validated via comparison with an active measurement technique (e.g. Mukerjee et al. 2004; Hagenbjörk-Gustafsson et al., 2010). For example, one field study found that

measured $NO_{2(g)}$ values from reactive passive samplers was within 10% of the 'true' value measured by a chemiluminescence detector at the same site (Hagenbjörk-Gustafsson et al., 2010). The same study reported a replicate precision (n = 6) of 6% for the passive samplers (Hagenbjörk-Gustafsson et al., 2010).

The passive sampling of $HNO_{3(g)}$ through physi-sorption and reactive processes has gained a lot of interest in the atmospheric chemistry community within the last two decades (Adon et al., 2010; Bytnerowicz et al., 2001, Bytnerowicz et al., 2005; De Santis et al., 2003; Lan et al., 2004). Using custom-built diffusion-based passive samplers, $HNO_{3(g)}$ has been sampled either through reactive uptake using a filter impregnated with a base (Adon et al., 2010; Lan et al., 2004), or through physisorption using a nylon membrane filter (Bytnerowicz et al., 2001; Bytnerowicz et al., 2005; De Santis et al., 2003). In particular, the use of nylon as a sampling media has been demonstrated to be robust as it has been shown to have favorable interactions with $HNO_{3(g)}$ and has been deemed the perfect sink for $HNO_{3(g)}$ (Durham and Stockburger, 1986). A standard operating procedure for the cleaning, handling and analysis of nylon filters has been developed by the US Environmental Protection Agency to ensure that the gathering of $HNO_{3(g)}$ concentrations across North America is quality assured and quality controlled (Chow and Watson, 1998). The passive sampling of $HNO_{3(g)}$ with nylon filters has thus far been conducted in polluted North American regions (Bytnerowicz et al., 2001; Bytnerowicz et al., 2010) or indoors (De Santis et al., 2003), but their applicability to remote ecosystems is yet to be demonstrated. Further, controlled calibrations of the custom-built samplers, used to determine real-world quantities of $HNO_{3(g)}$, have not investigated the effects of temperature and relative humidity on $HNO_{3(g)}$ uptake. The

effects of temperature on $HNO_{3(g)}$ uptake must be elucidated in order to fully describe the passive samplers since diffusion and sorption are both temperature-dependent processes. Therefore, although the use of nylon membrane filters has been shown to be robust, more work is still needed to characterize the filters' utility for sampling the atmosphere.

1.3.6 Employing a Passive Sampling Technique to Quantify Nitric Acid in Remote Ecosystems

The main objective of the work in this portion of this thesis was to determine the applicability of nylon membrane filter passive samplers coupled with ion chromatography analysis to quantify $HNO_{3(g)}$ mixing ratios in remote boreal forest ecosystems. Secondary objectives of this project included i) assessing the reusability of nylon membrane filters for passive sampling, ii) using determined $HNO_{3(g)}$ concentrations to estimate the annual flux of $HNO_{3(g)}$ across a latitudinal transect of boreal forest sites in Newfoundland and Labrador and iii) using air mass back-trajectory analysis and atmospheric steady-state chemical box model approximations to decouple long- and short-range transport of $HNO_{3(g)}$ from local production.

1.4 Quantitation of Atmospheric Alkylamines in Remote Ecosystems

1.4.1 Motivations for Measuring Atmospheric Alkylamines

Atmospheric alkylamines ($NR_{3(g)}$) have been shown to be potent particle nucleators in the atmosphere. Atmospheric particles and particle-forming species have both direct and indirect effects on Earth's energy balance and, thus, climate (Figure 1-3; Boucher et al., 2013; Lohmann and Feichter, 2005). Particles directly affect the climate through the

scattering, or absorption and re-emission of incident solar radiation. The indirect effect of particles occurs through the formation of cloud condensation nuclei (CCN), which reflect sunlight away from Earth's surface. Increased particle numbers as CCN make them both more reflective and longer-lived in the atmosphere, compounding the indirect effect. $NR_{3(g)}$ are thus imperative to speciate and quantify to understand their global impact on Earth's climate.

Laboratory studies have shown that $NR_{3(g)}$ form molecular clusters in the presence of a variety of gaseous acids, where an acid-base equilibrium between the gas and condensed phase is established (Almeida et al., 2013; Angelino et al., 2001; Berndt et al., 2010, 2014; Bzdek et al., 2010, 2011; Erupe et al., 2011; Jen et al., 2016a, b; Lloyd et al., 2009; Murphy et al., 2007; Qiu et al., 2011; Silva et al., 2008; Smith et al., 2010; Wang et al., 2010a, b; Yu et al., 2012; Zhao et al., 2011; Zollner et al., 2012). Almeida et al. (2013) measured particle formation rates using the Cosmics Leaving OUtdoor Droplets (CLOUD) chamber and determined that dimethylamine in the presence of sulfuric acid enhances particle formation rates 1000 times greater than that of an equivalent molar quantity of $NH_{3(g)}$, which is the dominant atmospheric base (Holland et al., 1999). Furthermore, the study concluded that $NR_{3(g)}$ can compete with $NH_{3(g)}$ in particle formation at relevant ppqv-level atmospheric mixing ratios. These were significant discoveries because alkylamines are often detected in quantities 100 – 1000 times less than ammonia in the atmosphere (Chang et al., 2003; Ge et al., 2011; Schade and Crutzen, 1995). Recent laboratory studies have determined that alkyl diamines are even more potent nucleators than the alkyl monoamines (Jen et al., 2016a, b). Theoretical *ab initio* analysis of these acid-base molecular clusters has further confirmed that particle

formation will occur under ambient atmospheric conditions and concentrations (Barsanti et al., 2009; Kurtén et al., 2008; Loukonen et al., 2010, 2014; Nadykto et al., 2015; Ortega et al., 2012). $NR_{3(g)}$ and their oxidation products, such as amides and imines, can also partition into atmospheric particles to enhance particle growth (Figure 1-3; Malloy et al., 2009; Silva et al., 2008).

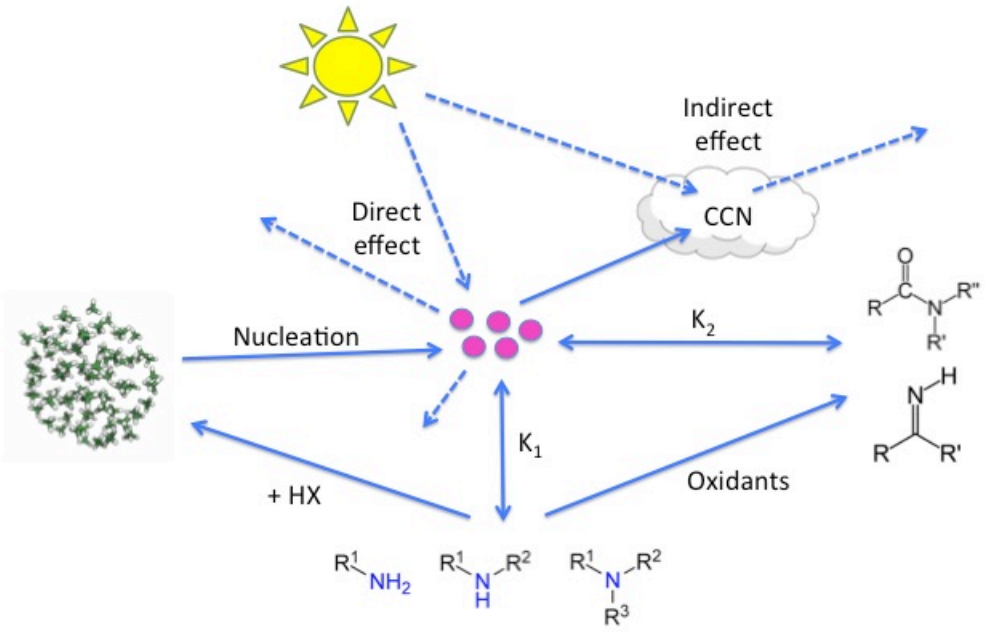

Figure 1-3. Atmospheric chemistry and climate effects of alkylamines. The K_1 pathway represents equilibrium thermodynamic partitioning between the gas and condensed of alkylamines and the K_2 pathway represents the phase partitioning of amides/imines.

Developing a sensitive method that can quantify and speciate atmospheric $NR_{3(g)}$ is also necessary for determining the contribution of reduced organic nitrogen deposition, a potential important component total N_r inputs, particularly in remote locations. Thus far

the deposition of organic nitrogen to ecosystems is still poorly understood and is not included in most models of global nitrogen deposition (Sutton et al., 2011). This is alarming, because multiple studies have reported that dissolved organic nitrogen (DON) in precipitation samples can constitute anywhere from 30 – 60% of the total dissolved nitrogen (TDN) entering an ecosystem (Cape et al., 2011, Cornell et al., 2003; Neff et al., 2002; Yan and Kim, 2015). Yan and Kim (2015) show that most of the DON measured is not recycled from within the ecosystem and likely represents a new source of nitrogen to their sampling sites after an air mass back-trajectory analysis. Another study conducted in Singapore determined that the flux of particulate organic nitrogen to the island was higher than the ammonium and nitrate particulate flux, which are the dominant inorganic N_r species (He et al., 2011). It is likely that alkylamines are contributing to these total organic N fluxes given the ubiquitous nature of these species in the atmosphere (Ge et al., 2011). Further, oceans and forest fires have been shown to emit gaseous methyl and ethylamines in high quantities, and remote ecosystems impacted directly by these emissions have the potential to receive large N inputs from alkylamines (Gibb et al., 1999b; Schade and Crutzen, 1995; Van Neste et al., 1987;). Therefore, developing a method that can quantify $NR_{3(g)}$ in precipitation, particle and gaseous matrices is critically required to determine their contribution towards total organic nitrogen and the total N_r input of an ecosystem.

1.4.2 Properties of Atmospheric Alkylamines

$NR_{3(g)}$ are derivatives of $NH_{3(g)}$ where 1, 2 or 3 of the hydrogen atoms attached to the central nitrogen atom have been replaced by an alkyl group (-R). Due to the electron-

donating properties of the alkane chain, most alkylamines have a higher basicity than ammonia (pKa ≈ 10 vs pKa ≈ 9; Perrin, 1982). $NR_{3(g)}$ are volatile and readily partition into the gas phase from pure solutions. $NR_{3(g)}$ with fewer than 4 carbon atoms in the R-group have vapor pressures greater than 10 kPa at room temperature (Christie and Crisp, 1967). As the alkyl side chain grows in length however the alkylamine becomes less volatile because of greater van der Waals interactions. Alkylamines tend to have high solubilities in water ($K_H \approx 1$ mol m^{-3} Pa^{-1}) because of their ability to participate in hydrogen bonding and dipole-dipole interactions (Christie and Crisp, 1967). The solubility of alkylamines in water also decreases with an increasing R-group chain length due to increasing steric effects. Due to the nature of the condensed phase in the atmosphere as well as the properties of Earth's surface, the aqueous solubility properties of $NR_{3(g)}$ are the best predictors of the behavior of these species in the environment. R1-14 shows the equilibrium partitioning of amines from the gas to the aqueous phase governed by the specific value of K_H. R1-15 then shows their subsequent equilibrium reaction with water once partitioned into the aqueous phase. The degree to which protonation occurs is dependent on pKa of the amine and effective pH of the particle water (Pankow, 2003).

(R1-14) $NR_{3(g)} \rightleftharpoons NR_{3(aq)}$

(R1-15) $NR_{3(aq)} + H_2O_{(l)} \rightleftharpoons NR_3H^+_{(aq)} + OH^-_{(aq)}$

The basicity properties of $NR_{3(g)}$ allows these species to participate in a variety of chemical reactions in the atmosphere as well. $NR_{3(g)}$ react with atmospheric acids (HX) to form atmospheric particles via R1-16 shown below.

(R1-16) $NR_{3(g)} + HX_{(g)} \rightleftharpoons HNR_3X_{(s)}$

The basic nitrogen atom also allows the alkylamine to act as a nucleophile, and react with atmospheric carbonyls to form imines (R1-17).

(R1-17) $RNH_{2(g)} + O{=}CR_{2(g)} \rightarrow RN{=}CR_{2(g)} + H_2O_{(g)}$

Both alkylamines and imine products can partition into pre-existing particles due to their solubility and basicity, causing particle growth. Furthermore, due to their higher basicity, uptake of amines to pre-existing particles can lead to the displacement of ammonia from already formed acid-base clusters (R1-18)

(R1-18) $NR_{3(g)} + NH_4X_{(s)} \rightleftharpoons NR_3HX_{(s)} + NH_{3(g)}$

Further details of the multiphase chemistry of atmospheric alkylamines is reviewed in Qiu and Zhang (2013). Overall, these properties of alkylamines indicate that they will be present in both the gas and particle-phase in the atmosphere. Hence, to understand their

chemistry and transport in the environment, easily and rapidly quantifying the most abundant alkylamines should be seen as a pressing issue to resolve.

1.4.3 Sources and Sinks of Atmospheric Alkylamines

Alkylamines are emitted into the atmosphere by multiple biogenic, natural, and anthropogenic sources (Ge et al., 2011). The largest biogenic source of $NR_{3(g)}$ to the atmosphere is the world's oceans, where $NR_{3(g)}$ are volatilized through the degradation of organic matter (Van Neste et al., 1987; Schade and Crutzen, 1995; Gibb et al., 1999b). It is estimated that these emissions total 80 Gg N yr^{-1} and account for approximately 50% of total biogenic methylamine emissions to the atmosphere (Ge et al., 2011). Measurements of ethylamines in marine aerosols are also commonly reported and suggest that marine environments may be a large source of ethylamines (Facchini et al., 2008; Gibb et al., 1999a; Müller et al., 2009; Sorooshian et al., 2009; van Pinxteren et al., 2015; Youn et al, 2015). Emissions from the natural process of biomass burning (60 ± 28 Gg N yr^{-1}) represent the second largest source of alkylamines to the atmosphere (Lobert et al., 1990, Ge et al., 2011). Estimates suggest that global methylamine emissions from biomass burning may represent up to 50% of the summed biogenic and natural methylamine emissions (Lobert et al., 1990, Ge et al., 2011). Vegetation and volcanic amine sources have also been identified in the literature (Schade and Crutzen, 1995; Mukhin et al., 1978), however their relative contribution to the overall atmospheric $NR_{3(g)}$ budget remains unconstrained. Animal husbandry operations represent the largest known and quantified source of anthropogenic $NR_{3(g)}$ emissions (Kuhn et al., 2011; Lunn and Van de Vyver, 1977; Rabaud et al., 2003; Schade and Crutzen, 1995; Sorooshian et al., 2008),

followed by fisheries (Seo et al., 2011) and sewage-waste treatment facilities (Leach et al., 1999). Tobacco smoke, automobiles and cooking have also been identified as anthropogenic sources of $NR_{3(g)}$ to the atmosphere (Cadle and Mulawa, 1980; Rogge et al., 1991; Schauer et al., 1999; Schmeltz and Hoffmann, 1977).

Once emitted into the atmosphere, small-chain alkylamines are rapidly oxidized in the presence of the hydroxyl radical within a few hours (R1-19; $k \approx 6 \times 10^{-11}$ cm^3 $molecule^{-1}$ s^{-1}) and thus as gases they have a low-propensity to undergo long-range transport (Atkinson et al., 1978; Carl and Crowley, 1998; Ge et al., 2011).

(R1-19) $NH_2CH_{3(g)} + OH_{(g)}\bullet \rightarrow NH_2CH_{2(g)} + H_2O_{(g)}$

However, as stated previously, in the presence of particles or gaseous acids alkylamine species have a high likelihood of partitioning into the particle-phase. If the alkylamines form stable particle-phase salts or reaction products, which are more resistant towards degradation, they can undergo long-range transport to remote environments.

1.4.4 Analytical Characterization of Atmospheric Alkylamines

Interferences from common atmospheric species have presented a constant challenge when analyzing gas- or particle-phase $NR_{3(g)}$. For example, gaseous ammonia, a functional analogue of alkylamines, is always present in greater atmospheric quantities, and has the potential to bias alkylamine measurements if the analytical technique is not selective (Chang et al., 2003; Ge et al., 2011; Schade and Crutzen, 1995). The atmospheric particle-phase is even more complex than the gas-phase and often contains

interferences from ionic and complex organic species (Ault et al., 2013; Di Lorenzo and Young, 2016; Kovač et al., 2013; Saleh et al., 2014; Sobanska et al., 2012; Sun et al., 2006).

Direct mass spectrometry (MS) analysis of an atmospheric sample has been frequently used in field campaigns to overcome common matrix effects of the atmosphere (Aiken et al., 2009; Denkenberger et al., 2007; Silva et al., 2008; Yao et al., 2016). However, since separation of alkylamines was not performed prior to analysis, alkylamine structural isomers were unable to be identified, limiting insight into both sources and chemistry. Further, accurate quantitation of particles is not possible with direct MS analysis since ionization efficiencies cannot be quantified for real atmospheric particles, due to matrix suppression or enhancement effects (Murphy et al., 2007). Derivatization of atmospheric methyl- and ethylamines followed by GC-MS or LC-MS analysis is perhaps the most commonly employed technique for quantifying these compounds (Akyüz, 2007; Fournier et al., 2008; Huang et al., 2009; Key et al., 2011; Possanzini and Di Palo, 1990). These derivatization methods have achieved successful speciation and quantitation of methyl- and ethylamines through the removal of interferences by utilizing extraction and derivatization steps. The drawbacks of derivatization methods are that they require multi-step method optimization, utilize large amounts of reagents and organic solvent, and are difficult, if not impossible, to interface with real-time sampling of the atmosphere.

Ion chromatography (IC) has shown recent promise as a $NR_{3(g)}$ separation and quantitation technique, and has been deployed in the field for the real-time analysis of the atmosphere (Chang et al., 2003; Dawson et al., 2014; Erupe et al., 2010; Huang et al.,

2014; Li et al., 2009; Murphy et al., 2007; Verriele et al., 2012; VandenBoer et al., 2011; VandenBoer et al., 2012). IC analysis has been demonstrated to overcome limitations of MS analysis by separating alkylamine structural isomers, as well as limitations of GC-MS and LC-MS analysis by analyzing atmospheric samples in less than 30 minutes without utilizing large volumes of solvent (VandenBoer et al., 2012). However current IC separation methods in the literature still struggle with the full separation of the full suite of methyl- and ethylamines from common atmospheric cations (Chang et al., 2003; Dawson et al., 2014; Erupe et al., 2010; Huang et al., 2014; Li et al., 2009; Murphy et al., 2007; VandenBoer et al., 2012). This presents a problem for the analysis of the remote atmosphere where alkylamines may be present at molar quantities more than 1000 times less than other cationic species. This can lead to false negatives when detecting atmospheric alkylamines as well as the suppression of potential detection limits where IC peaks are not fully resolved. Therefore for an IC method to be compatible for use in analyzing samples taken from remote atmospheric environments, the full suite of abundant alkylamines must be resolved from potential cationic matrix constituents.

1.4.5 Development and Characterization of an Ion Chromatography Method for Measuring Atmospheric Alkylamines in Remote Ecosystems

The objective of the work in this portion of this thesis was to develop and characterize a sensitive analytical technique that was able to quantify and speciate the most abundant atmospheric alkylamines in samples collected from remote ecosystems, where alkylamine mixing ratios can reach sub-pptv levels. Ion chromatography, employing analyte preconcentration, was used as the separation and quantitation

technique in order to overcome limitations of direct MS analysis and derivatization analysis techniques. The goals of the method were to i) separate nine alkylamines (monomethylamine (MMA), dimethylamine (DMA), trimethylamine (TMA), monoethylamine (MEA), diethylamine (DEA), triethylamine (TEA), monopropylamine (MPA), monoisopropylamine (iMPA), and monobutylamine (MBA)) from five common atmospheric inorganic cations (Na^+, NH_4^+, K^+, Mg^{2+}, and Ca^{2+}), in a runtime of approximately 30 minutes or less, ii) Assess the method precision, accuracy and detection limits, and iii) test the applicability of the method to real-world atmospheric samples through the analysis of biomass burning samples, which contain a complex matrix of organics and inorganic cations.

1.5 References

Adon, M., Galy-Lacaux, C., Yoboué, V., Delon, C., Lacaux, J. P., Castera, P., Gardrat, E., Pienaar, J., Al Ourabi, H., Laouali, D., Diop, B., Sigha-Nkamdjou, L., Akpo, A., Tathy, J. P., Lavenu, F. and Mougin, E.: Long term measurements of sulfur dioxide, nitrogen dioxide, ammonia, nitric acid and ozone in Africa using passive samplers, Atmos. Chem. Phys., 10(15), 7467–7487, doi:10.5194/acp-10-7467-2010, 2010.

Aiken, A. C., Salcedo, D., Cubison, M. J., Huffman, J. a., DeCarlo, P. F., Ulbrich, I. M., Docherty, K. S., Sueper, D., Kimmel, J. R., Worsnop, D. R., Trimborn, a., Northway, M., Stone, E. a., Schauer, J. J., Volkamer, R., Fortner, E., de Foy, B., Wang, J., Laskin, a., Shutthanandan, V., Zheng, J., Zhang, R., Gaffney, J., Marley, N. a., Paredes-Miranda, G., Arnott, W. P., Molina, L. T., Sosa, G. and Jimenez, J. L.: Mexico City aerosol analysis during MILAGRO using high resolution aerosol mass spectrometry at the urban supersite (T0) – Part 1: Fine particle composition and organic source apportionment, Atmos. Chem. Phys., 9, 6633–6653, doi:10.5194/acpd-9-8377-2009, 2009.

Akyüz, M.: Simultaneous determination of aliphatic and aromatic amines in indoor and outdoor air samples by gas chromatography-mass spectrometry, Talanta, 71(1), 486–492, doi:10.1016/j.talanta.2006.10.028, 2007.

Almeida, J., Schobesberger, S., Kürten, A., Ortega, I. K., Kupiainen-Määttä, O., Praplan, A. P., Adamov, A., Amorim, A., Bianchi, F., Breitenlechner, M., David, A., Dommen, J., Donahue, N. M., Downard, A., Dunne, E., Duplissy, J., Ehrhart, S., Flagan, R. C., Franchin, A., Guida, R., Hakala, J., Hansel, A., Heinritzi, M., Henschel, H., Jokinen, T., Junninen, H., Kajos, M., Kangasluoma, J., Keskinen, H., Kupc, A., Kurtén, T., Kvashin, A. N., Laaksonen, A., Lehtipalo, K., Leiminger, M., Leppä, J., Loukonen, V., Makhmutov, V., Mathot, S., McGrath, M. J., Nieminen, T., Olenius, T., Onnela, A., Petäjä, T., Riccobono, F., Riipinen, I., Rissanen, M., Rondo, L., Ruuskanen, T., Santos, F. D., Sarnela, N., Schallhart, S., Schnitzhofer, R., Seinfeld, J. H., Simon, M., Sipilä, M., Stozhkov, Y., Stratmann, F., Tomé, A., Tröstl, J., Tsagkogeorgas, G., Vaattovaara, P., Viisanen, Y., Virtanen, A., Vrtala, A., Wagner, P. E., Weingartner, E., Wex, H., Williamson, C., Wimmer, D., Ye, P., Yli-Juuti, T., Carslaw, K. S., Kulmala, M., Curtius, J., Baltensperger, U., Worsnop, D. R., Vehkamäki, H. and Kirkby, J.: Molecular understanding of sulphuric acid-amine particle nucleation in the atmosphere., Nature, 502(7471), 359–63, doi:10.1038/nature12663, 2013.

Angelino, S., Suess, D. T. and Prather, K. A.: Formation of aerosol particles from reactions of secondary and tertiary alkylamines: Characterization by aerosol time-of-flight mass spectrometry, Environ. Sci. Technol., 35(15), 3130–3138, doi:10.1021/es0015444, 2001.

Atkinson, R., Perry, R. A. and Pitts, J. N.: Rate constants for the reaction of the OH radical with $(CH_3)_2NH$, $(CH_3)_3N$ and $C_2H_5NH_2$ over the temperature range 298-426 K, J. Chem. Phys., 68(4), 1850–1853, 1978.

Atkinson, R.: Gas-phase tropospheric chemistry of volatile organic compounds: 1. Alkanes and alkenes, J. Phys. Chem. Ref. Data, 26, 215-290, 1997.

Ault, A. P., Moffet, R. C., Baltrusaitis, J., Collins, D. B., Ruppel, M. J., Cuadra-Rodriguez, L. A., Zhao, D., Guasco, T. L., Ebben, C. J., Geiger, F. M., Bertram, T. H., Prather, K. A. and Grassian, V. H.: Size-dependent changes in sea spray aerosol composition and properties with different seawater conditions, Environ. Sci. Technol., 47(11), 5603–5612, doi:10.1021/es400416g, 2013.

Barsanti, K. C., McMurry, P. H. and Smith, J. N.: The potential contribution of organic salts to new particle growth, Atmos. Chem. Phys., 9(9), 2949–2957, doi:10.5194/acp-9-2949-2009, 2009.

Berndt, T., Stratmann, F., Sipilä, M., Vanhanen, J., Petäjä, T., Mikkilä, J., Grüner, A., Spindler, G., Lee Mauldin III, R., Curtius, J., Kulmala, M. and Heintzenberg, J.: Laboratory study on new particle formation from the reaction OH + SO_2: influence of experimental conditions, H_2O vapour, NH_3 and the amine tert-butylamine on the overall process, Atmos. Chem. Phys., 10, 7101–7116, doi:10.5194/acp-10-7101-2010, 2010.

Berndt, T., Sipilä, M., Stratmann, F., Petäjä, T., Vanhanen, J., Mikkilä, J., Patokoski, J., Taipale, R., Mauldin, R. L. and Kulmala, M.: Enhancement of atmospheric H2SO4/H2O nucleation: Organic oxidation products versus amines, Atmos. Chem. Phys., 14(2), 751–764, doi:10.5194/acp-14-751-2014, 2014.

Bobbink, R., Hicks, K., Galloway, J., Spranger, T., Alkemade, R., Ashmore, M., Bustamante, M., Cinderby, S., Davidson, E., Dentener, F., Emmett, B., Erisman, J. -W., Fenn, M., Gilliam, F., Nordin, A., Pardo, L. and De Vries, W.: Global assessment of nitrogen deposition effects on terrestrial plant diversity: A synthesis, Ecological Applications, 20(1), 30-59, 2010.

Boucher, O., Randall. D., Artaxo, P., Bretherton, C., Feingold, G., Forster, P., Kerminen, V.-M., Kondo, Y., Liao, H., Lohmann, U., Rasch, P., Satheesh, S. K., Sherwood, S., Stevens, B. and Zhang, X. Y.: Clouds and Aerosols. In: Climate Change 2013: The Physical Science Basis. Contribution of Working Group I to the Fifth Assessment Report of the Intergovernmental Panel on Climate Change, Cambridge, United Kingdom and New York, NY, USA, 87 pp., 2013.

Butterbach-bahl, K., Kahl, M., Mykhayliv, L., Werner, C., Kiese, R. and Li, C.: A European-wide inventory of soil NO emissions using the biogeochemical models DNDC/Forest-DNDC, Atmos. Environ., 43(7), 1392–1402, doi:10.1016/j.atmosenv.2008.02.008, 2009.

Bytnerowicz, A., Padgett, P. E., Arbaugh, M. J., David, R. and Jones, D. P.: Passive

sampler for measurements of atmospheric nitric acid vapor (HNO_3) concentrations, The Scientific World, 1, 815–822, doi:10.1100/tsw.2001.323, 2001.

Bytnerowicz, A., Sanz, M. J., Arbaugh, M. J., Padgett, P. E., Jones, D. P. and Davila, A.: Passive sampler for monitoring ambient nitric acid (HNO_3) and nitrous acid (HNO_2) concentrations, Atmos. Environ., 39(14), 2655–2660, doi:10.1016/j.atmosenv.2005.01.018, 2005.

Bytnerowicz, A., Fraczek, W., Schilling, S. and Alexander, D.: Spatial and temporal distribution of ambient nitric acid and ammonia in the Athabasca Oil Sands Region , Alberta, , 69, 11–21, doi:10.3274/JL10-69-S1-03, 2010.

Bzdek, B. R., Ridge, D. P. and Johnston, M. V.: Amine exchange into ammonium bisulfate and ammonium nitrate nuclei, Atmos. Chem. Phys., 10, 3495–3503, doi:10.5194/acp-3495-2010, 2010.

Bzdek, B. R., Ridge, D. P. and Johnston, M. V.: Amine reactivity with charged sulfuric acid clusters, Atmos. Chem. Phys., 11(16), 8735–8743, doi:10.5194/acp-11-8735-2011, 2011.

Cadle, S. H. and Mulawa, P. A.: Low-molecular-weight aliphatic amines in exhaust from catalyst-equipped cars., Environ. Sci. Technol., 14(6), 718–723, doi:10.1021/es60166a011, 1980.

Cape, J. N., Cornell, S. E., Jickells, T. D. and Nemitz, E.: Organic nitrogen in the atmosphere - Where does it come from? A review of sources and methods, Atmos. Res., 102, 30–48, doi:10.1016/j.atmosres.2011.07.009, 2011.

Carl, S. A. and Crowley, J. N.: Sequential two (blue) photon absorption by NO_2 in the presence of H_2 as a Source of OH in pulsed photolysis kinetic studies: Rate constants for reaction of OH with CH_3NH_2, $(CH_3)_2NH$, $(CH_3)_3N$, and $C_2H_5NH_2$ at 295 K, J. Phys. Chem. A, 102(42), 8131–8141, doi:10.1021/jp9821937, 1998.

Chang, I.-H., Lee, C.-G. and Lee, D. S.: Development of an automated method for simultaneous determination of low molecular weight aliphatic amines and ammonia in ambient air by diffusion scrubber coupled to ion chromatography, Anal. Chem., 75(22), 6141–6146, doi:10.1021/ac0347314, 2003.

Chow, J. C. and Watson, J. G.: Guideline on Speciated Particulate Monitoring, U. S. Environmental Protection Agency, Research Triangle Park, NC, 1998.

Christie, A. O. and Crisp, D. J.: Activity coefficients of the n-primary, secondary and tertiary aliphatic amines in aqueous solution, J. Appl. Chem., 17, 1967.

Cornell, S. E., Jickells, T. D., Cape, J. N., Rowland, A. P. and Duce, R. A.: Organic nitrogen deposition on land and coastal environments: A review of methods and data, Atmos. Environ., 37(16), 2173–2191, doi:10.1016/S1352-2310(03)00133-X, 2003.

Darwent, B. B.: Bond dissociation energies in simple molecules, National Bureau of Standards, Washington, D. C., 52 pp., 1970.

Dawson, M. L., Perraud, V., Gomez, A., Arquero, K. D., Ezell, M. J. and Finlayson-Pitts, B. J.: Measurement of gas-phase ammonia and amines in air by collection onto an ion exchange resin and analysis by ion chromatography, Atmos. Meas. Tech., 7(2), 1573–1602, doi:10.5194/amt-7-2733-2014, 2014.

De More, W. B., Sander, S. P., Golden, D. M., Hampson, R. F., Kurylo, M. J., Howard, C. J., Ravishankara, A. R., Kolb, C. E. and Molina, M. J.: Chemical kinetics and photochemical data for use in stratospheric modeling, Evaluation No. 12, JPL, 97-4, 1997.

Denkenberger, K. A., Moffet, R. C., Holecek, J. C., Rebotier, T. P. and Prather, K. A.: Real-time, single-particle measurements of oligomers in aged ambient aerosol particles, Environ. Sci. Technol., 41(15), 5439–5446, doi:10.1021/es070329l, 2007.

Dentener, F., Drevet, J., Lamarque, J. F., Bey, I., Eickhout, B., Fiore, A. M., Hauglustaine, D., Horowitz, L. W., Krol, M., Kulshrestha, U. C., Lawrence, M., Galy-Lacaux, C., Rast, S., Shindell, D., Stevenson, D., Van Noije, T., Atherton, C., Bell, N., Bergman, D., Butler, T., Cofala, J., Collins, B., Doherty, R., Ellingsen, K., Galloway, J., Gauss, M., Montanaro, V., Müller, J. F., Pitari, G., Rodriguez, J., Sanderson, M., Solmon, F., Strahan, S., Schultz, M., Sudo, K., Szopa, S. and Wild, O.: Nitrogen and sulfur deposition on regional and global scales: A multimodel evaluation, Global Biogeochem. Cycles, 20(4), doi:10.1029/2005GB002672, 2006.

De Santis, F., Vazzana, C., Miniqielli, S. and Allegrini, I.: The measurement of atmospheric pollutants by passive sampling at the Uffizi Gallery, Florence. Annali di Chimica, 93, 45–53, 2003.

Di Lorenzo, R. A. and Young, C. J.: Size separation method for absorption characterization in brown carbon: Application to an aged biomass burning sample, Geophys. Res. Lett., 43(1), 458–465, doi:10.1002/2015GL066954, 2016.

Durham, J. L. and Stockburger, L.: Nitric acid—air diffusion coefficient: experimental determination, Atmos. Environ., 20, 633–637, 1986.

Erupe, M. E., Liberman-Martin, A., Silva, P. J., Malloy, Q. G. J., Yonis, N., Cocker, D. R. and Purvis-Roberts, K. L.: Determination of methylamines and trimethylamine-N-oxide in particulate matter by non-suppressed ion chromatography, J. Chromatogr. A, 1217(13), 2070–2073, doi:10.1016/j.chroma.2010.01.066, 2010.

Erupe, M. E., Viggiano, A. A. and Lee, S. H.: The effect of trimethylamine on atmospheric nucleation involving H_2SO_4, Atmos. Chem. Phys., 11(10), 4767–4775, doi:10.5194/acp-11-4767-2011, 2011.

Facchini, M. C., Decesari, S., Rinaldi, M., Carbone, C., Finessi, E., Mircea, M., Fuzzi, S., Moretti, F., Tagliavini, E., Ceburnis, D. and O'Dowd, C. D.: Important source of marine secondary organic aerosol from biogenic amines., Environ. Sci. Technol., 42(24), 9116–9121, doi:10.1021/es8018385, 2008.

Finlayson-Pitts, B. J. and Pitts, J. N. Chemistry of the Upper and Lower Atmosphere: Theory, Experiments and Applications, Elsevier Inc., 2000.

Flechard, C. R., Nemitz, E., Smith, R. I., Fowler, D., Vermeulen, A. T., Bleeker, A., Erisman, J. W., Simpson, D., Zhang, L., Tang, Y. S. and Sutton, M. A.: Dry deposition of reactive nitrogen to European ecosystems: A comparison of inferential models across the NitroEurope network, Atmos. Chem. Phys., 11(6), 2703–2728, doi:10.5194/acp-11-2703-2011, 2011.

Foley, J. A, DeFries, R., Asner, G. P., Barford, C., Bonan, G., Carpenter, S. R., Chapin, F. S., Coe, M. T., Daily, G. C., Gibbs, H. K., Helkowski, J. H., Holloway, T., Howard, E. A., Kucharik, C. J., Monfreda, C., Patz, J. A., Prentice, I. C., Ramankutty, N. and Snyder, P. K.: Global consequences of land use, Science, 309(5734), 570–574, doi:10.1126/science.1111772, 2005.

Fournier, M., Lesage, J., Ostiguy, C. and Tra, H. Van: Sampling and analytical methodology development for the determination of primary and secondary low molecular weight amines in ambient air, J Env. Monit, 10(3), 379–386, doi:10.1039/b719091n, 2008.

Galloway, J. N., Dentener, F. J., Capone, D. G., Boyer, E. W., Howarth, R. W., Seitzinger, S. P., Asner, G. P., Cleveland, C. C., Green, P. A., Holland, E. A., Karl, D. M., Michaels, A. F., Porter, J. H., Townsend, A. R. and Vörösmarty, C. J.: Nitrogen cycles: past , present , and future., Biogeochemistry, 70, 153-226, doi: 10.1007/s10533-004-0370-0, 2004.

Ge, X., Wexler, A. S. and Clegg, S. L.: Atmospheric amines - Part I. A review, Atmos. Environ., 45(3), 524–546, doi:10.1016/j.atmosenv.2010.10.012, 2011.

Gibb, S. W., Mantoura, R. F. C., Liss, P. S. and Barlow, R. G.: Distributions and biogeochemistries of methylamines and ammonium in the Arabian Sea, Deep. Res. Part II Top. Stud. Oceanogr., 46(3–4), 593–615, doi:10.1016/S0967-0645(98)00119-2, 1999a.

Gibb, S. W., Mantoura, R. F. C. and Liss, P. S.: Ocean-atmosphere exchange and atmospheric speciation of ammonia and methylamines in the region of the NW Arabian

Sea, Global Biogeochem. Cycles, 13(1), 161–178, doi:10.1029/98GB00743, 1999b.

Gruber, N. and Galloway, J. N.: An Earth-system perspective of the global nitrogen cycle., Nature, 451(7176), 293–296, doi:10.1038/nature06592, 2008.

Hagenbjörk-Gustafsson, A., Tornevi, A., Forsberg, B. and Eriksson, K.: Field validation of the Ogawa diffusive sampler for NO_2 and NO_x in a cold climate, J. Environ. Monit., 12(6), 1315–1324, doi:10.1039/b924615k, 2010.

Hauglustaine, D. A., Granier, C, Brasseur, G. P., and Megie, G.: The importance of atmospheric chemistry in the calculation of radiative forcing on the climate system, J. Geophys. Res., 99, 1173-1186, 1994.

He, J., Balasubramanian, R., Burger, D. F., Hicks, K., Kuylenstierna, J. C. I. and Palani, S.: Dry and wet atmospheric deposition of nitrogen and phosphorus in Singapore, Atmos. Environ., 45(16), 2760–2768, doi:10.1016/j.atmosenv.2011.02.036, 2011.

Holland, E. A., Dentener, F. J., Braswell, B. H. and Sulzman, J. M.: Contemporary and pre-industrial global reactive nitrogen budgets, Biogeochemistry, 46, 7–43, doi:10.1007/BF01007572, 1999.

Houlton, B. Z., Wang, Y-P., Vitousek, P. M. and Field, C. B.: A unifying framework for dinitrogen fixation in the terrestrial biosphere, Nature, 454, 327-330, doi: 10.1038/nature/07028, 2008.

Huang, G., Hou, J. and Zhou, X.: A measurement method for atmospheric ammonia and primary amines based on aqueous sampling, OPA derivatization and HPLC analysis, Environ. Sci. Technol., 43(15), 5851–5856, doi:10.1021/es900988q, 2009.

Huang, R. J., Li, W. B., Wang, Y. R., Wang, Q. Y., Jia, W. T., Ho, K. F., Cao, J. J., Wang, G. H., Chen, X., Ei Haddad, I., Zhuang, Z. X., Wang, X. R., Prèvôt, A. S. H., O'Dowd, C. D. and Hoffmann, T.: Determination of alkylamines in atmospheric aerosol particles: A comparison of gas chromatography-mass spectrometry and ion chromatography approaches, Atmos. Meas. Tech., 7(7), 2027–2035, doi:10.5194/amt-7-2027-2014, 2014.

Jacob, D. J. Introduction to Atmospheric Chemistry, Princeton University Press, 1999.

Jen, C. N., Zhao, J., McMurry, P. H. and Hanson, D. R.: Chemical ionization of clusters formed from sulfuric acid and dimethylamine or diamines, Atmos. Chem. Phys., 16, 12513–12529, doi:10.5194/acp-2016-492, 2016a.

Jen, C. N., Bachman, R., Zhao, J., Mcmurry, P. H. and Hanson, D. R.: Diamine-sulfuric acid reactions are a potent source of new particle formation, Geophys. Res. Lett., 43(2), 867–873, doi:10.1002/2015GL066958, 2016b.

Key, D., Stihle, J., Petit, J.-E., Bonnet, C., Depernon, L., Liu, O., Kennedy, S., Latimer, R., Burgoyne, M., Wanger, D., Webster, A., Casunuran, S., Hidalgo, S., Thomas, M., Moss, J. A. and Baum, M. M.: Integrated method for the measurement of trace nitrogenous atmospheric bases, Atmos. Meas. Tech., 4(12), 2795–2807, doi:10.5194/amt-4-2795-2011, 2011.

Kim, J. and Rees, D. C.: Nitrogenase and biological nitrogen fixation, Biochemistry, 33, 3477-3485, 1994.

Kovač, N., Glavaš, N., Dolenec, M., Šmuc, N. R. and Šlejkovec, Z.: Chemical Composition of Natural Sea Salt from the Secovlje Salina (Gulf of Trieste, northern Adriatic), Acta Chim. Slov., 60(3), 706–714, 2013.

Kuhn, U., Sintermann, J., Spirig, C., Jocher, M., Ammann, C. and Neftel, A.: Basic biogenic aerosol precursors: Agricultural source attribution of volatile amines revised, Geophys. Res. Lett., 38(16), 1–8, doi:10.1029/2011GL047958, 2011.

Kurtén, T., Loukonen, V., Vehkamäki, H. and Kulmala, M.: Amines are likely to enhance neutral and ion-induced sulfuric acid-water nucleation in the atmosphere more effectively than ammonia, Atmos. Chem. Phys., 8, 4095–4103, doi:10.5194/acp-8-4095-2008, 2008.

Lamarque, J.-F., Bond, T. C., Eyring, V., Granier, C., Heil, A., Klimont, Z., Lee, D., Liousse, C., Mieville, A., Owen, B., Schultz, M. G., Shindell, D., Smith, S. J., Stehfest, E., Van Aardenne, J., Cooper, O. R., Kainuma, M., Mahowald, N., McConnell, J. R., Naik, V., Riahi, K., and van Vuuren, D. P.: Historical (1850–2000) gridded anthropogenic and biomass burning emissions of reactive gases and aerosols: methodology and application, Atmos. Chem. Phys., 10, 7017–7039, doi:10.5194/acp-10-7017-2010, 2010.

Lamarque, J. F., Dentener, F., McConnell, J., Ro, C. U., Shaw, M., Vet, R., Bergmann, D., Cameron-Smith, P., Dalsoren, S., Doherty, R., Faluvegi, G., Ghan, S. J., Josse, B., Lee, Y. H., Mackenzie, I. A., Plummer, D., Shindell, D. T., Skeie, R. B., Stevenson, D. S., Strode, S., Zeng, G., Curran, M., Dahl-Jensen, D., Das, S., Fritzsche, D. and Nolan, M.: Multi-model mean nitrogen and sulfur deposition from the atmospheric chemistry and climate model intercomparison project (ACCMIP): Evaluation of historical and projected future changes, Atmos. Chem. Phys., 13(16), 7997–8018, doi:10.5194/acp-13-7997-2013, 2013.

Lan, T. T. N., Nishimura, R., Tsujino, Y., Imamura, K., Warashina, M., Hoang, N. T. and Maeda, Y.: Atmospheric concentrations of sulfur dioxide, nitrogen oxides, ammonia, hydrogen chloride, nitric acid, formic and acetic acids in the south of Vietnam measured by the passive sampling method., Anal. Sci., 20(1), 213–7, doi:10.2116/analsci.20.213, 2004.

Laux, J. M., Hemminger, J. C. and Finlayson-Pitts, B. J.: X-Ray photoelectron spectroscopic studies of the heterogeneous reaction of gaseous nitric acid with sodium chloride: Kinetics and contribution to the chemistry of the marine troposphere, Geophys. Res. Lett., 21, 1623-1626, 1994.

Leach, J., Blanch, A. and Bianchi, A. C.: Volatile organic compounds in an urban airborne environment adjacent to a municipal incinerator, waste collection centre and sewage treatment plant, Atmos. Environ., 33(26), 4309–4325, doi:10.1016/S1352-2310(99)00115-6, 1999.

Le Breton, M., Bacak, A., Muller, J. B. A., Xiao, P., Shallcross, B. M. A., Batt, R., Cooke, M. C., Shallcross, D. E., Bauguitte, S. J. B. and Percival, C. J.: Simultaneous airborne nitric acid and formic acid measurements using a chemical ionization mass spectrometer around the UK: Analysis of primary and secondary production pathways, Atmos. Environ., 83(3), 166–175, doi:10.1016/j.atmosenv.2013.10.008, 2014.

Lenner, M.: Nitrogen dioxide in exhaust emissions from motor vehicles, Atmos. Environ., 21, 37-43, 1987.

Li, F., Liu, H., Xue, C., Xin, X., Xu, J., Chang, Y., Xue, Y. and Yin, L.: Simultaneous determination of dimethylamine, trimethylamine and trimethylamine-n-oxide in aquatic products extracts by ion chromatography with non-suppressed conductivity detection, J. Chromatogr. A, 1216(31), 5924–5926, doi:10.1016/j.chroma.2009.06.038, 2009.

Lloyd, J. A., Heaton, K. J. and Johnston, M. V.: Reactive uptake of trimethylamine into ammonium nitrate particles, J. Phys. Chem. A, 113(17), 4840–4843, doi:10.1021/jp900634d, 2009.

Lobert, J. M., Scharffe, D. H., Hao, W. M. and Crutzen, P. J.: Importance of biomass burning in the atmospheric budgets of nitrogen-containing gases, Nature, 346(6284), 552–554, doi:10.1038/346552a0, 1990.

Lohmann, U. and Feichter, J.: Global indirect aerosol effects: a review, Atmos. Chem. Phys., 5, 715–737, doi:10.5194/acp-5-715-2005, 2005.

Loukonen, V., Kurtén, T., Ortega, I. K., Vehkamäki, H., Pádua, A. A. H., Sellegri, K. and Kulmala, M.: Enhancing effect of dimethylamine in sulfuric acid nucleation in the presence of water – a computational study, Atmos. Chem. Phys., 10, 4961–4974, doi:10.5194/acp-10-4961-2010, 2010.

Loukonen, V., Kuo, I. F. W., McGrath, M. J. and Vehkamäki, H.: On the stability and dynamics of (sulfuric acid)(ammonia) and (sulfuric acid)(dimethylamine) clusters: A first-principles molecular dynamics investigation, Chem. Phys., 428, 164–174, doi:10.1016/j.chemphys.2013.11.014, 2014.

Lunn, F. and Van de Vyver, J.: Sampling and analysis of air in pig houses, Agric. Environ., 3, 159–169, doi:10.1016/0304-1131(77)90007-8, 1977.

Malloy, Q. G. J., Qi, L., Warren, B., Crocer III, D. R., Erupe, M. E. and Silva, P. J.: Secondary organic aerosol formation from primary aliphatic amines with NO_3 radical, Atmos. Chem. Phys., 9, 2051 – 2060, 2009.

Mentel, T. F., Bleilebens, D. and Wahner, A.: A Study of nighttime nitrogen oxide oxidation in a large reaction chamber the fate of NO_2 , N_2O_5, HNO_3, and O_3 at different humidities, Atmos. Environ., 30, 4007-4020,1996.

Molina-Herrera, S., Haas, E., Grote, R., Kiese, R., Klatt, S., Kraus, D., Butterbach-Bahl, K., Kampffmeyer, T., Friedrich, R., Andreae, H., Loubet, B., Ammann, C., Horváth, L., Larsen, K., Gruening, C., Frumau, A. and Butterbach-Bahl, K.: Importance of soil NO emissions for the total atmospheric NO_x budget of Saxony, Germany, Atmos. Environ., 152, doi:10.1016/j.atmosenv.2016.12.022, 2017.

Mukerjee, S., Smith, L. A., Norris, G. A., Morandi, M. T., Gonzales, M., Noble, C. A., Neas, L. M. and Özkaynak, A. H.: Field method comparison between passive air samplers and continuous monitors for VOCs and NO_2 in El Paso, Texas, Journal of the Air & Waste Management Association, 54(3), 307-319*,* 2004.

Mukhin, L. M., Bondarev, V. B. and Safonova, E. N.: The role of volcanic processes in the evolution of organic compounds on the primitive earth, Modern Geology, 6, 119-122, 1978.

Müller, J. .: Geographical Distribution and Seasonal Variation of Surface Emissions and Deposition Velocities of Atmospheric Trace Gases, J. Geophys. Res., 97(91), 3787–3804, 1992.

Müller, C., Iinuma, Y., Karstensen, J., van Pinxteren, D., Lehmann, S., Gnauk, T. and Herrmann, H.: Seasonal variation of aliphatic amines in marine sub-micrometer particles at the Cape Verde islands, Atmos. Chem. Phys., 9, 14825–14855, doi:10.5194/acp-9-9587-2009, 2009.

Murphy, S. M., Sorooshian, A., Kroll, J. H., Ng, N. L., Chhabra, P., Tong, C., Surratt, J. D., Knipping, E., Flagan, R. C. and Seinfeld, J. H.: Secondary aerosol formation from atmospheric reactions of aliphatic amines, Atmos. Chem. Phys., 7, 2313–2337, doi:10.5194/acp-7-2313-2007, 2007.

Nadykto, A., Herb, J., Yu, F., Xu, Y. and Nazarenko, E.: Estimating the lower limit of the impact of amines on nucleation in the Earth's atmosphere, Entropy, 17(5), 2764–2780, doi:10.3390/e17052764, 2015.

Neff, J. C., Holland, E. A., Dentener, F. J., McDowell, W. H. and Russell, K. M.: The origin, composition and rates of organic nitrogen deposition: A missing piece of the nitrogen cycle?, Biogeochemistry, 57/58, 99–136, doi:10.1023/A:1015791622742, 2002.

Nguyen, M.-T., Jamka, A. J., Cazar, R. A. and Tao, F.-M.: Structure and stability of the nitric acid–ammonia complex in the gas phase and in water, J. Chem. Phys., 106(21), 8710, doi:10.1063/1.473925, 1997.

Ollinger, S. V, Richardson, A. D., Martin, M. E., Hollinger, D. Y., Frolking, S. E., Reich, P. B., Plourde, L. C., Katul, G. G., Munger, J. W., Oren, R., Smith, M.-L., Paw U, K. T., Bolstad, P. V, Cook, B. D., Day, M. C., Martin, T. A., Monson, R. K. and Schmid, H. P.: Canopy nitrogen, carbon assimilation, and albedo in temperate and boreal forests: Functional relations and potential climate feedbacks., Proc. Natl. Acad. Sci. U. S. A., 105(49), 19336–19341, doi:10.1073/pnas.0810021105, 2008.

Ortega, I. K., Kupiainen, O., Kurtén, T., Olenius, T., Wilkman, O., McGrath, M. J., Loukonen, V. and Vehkamäki, H.: From quantum chemical formation free energies to evaporation rates, Atmos. Chem. Phys., 12(1), 225–235, doi:10.5194/acp-12-225-2012, 2012.

Palmes, E. D.: Development and application of a diffusional sampler for NO_2, Environ. Int., 5(2), 97–100, doi:10.1016/0160-4120(81)90128-8, 1981.

Pankow, J. F.: Gas/particle partitioning of neutral and ionizing compounds to single and multi-phase aerosol particles. 1. Unified modeling framework, Atmos. Environ., 37(24), 3323–3333, doi:10.1016/S1352-2310(03)00346-7, 2003.

Perrin, D. D., Ionisation constants of inorganic acids and bases in aqueous solution, Pergamon Press, 1982.

Possanzini, M. and Di Palo, V.: Improved HPLC determination of aliphatic amines in air by diffusion and derivatization techniques, Chromatographia, 29(3–4), 151–154, doi:10.1007/BF02268702, 1990.

Pozo, K., Harner, T., Wania, F., Muir, D. C. G., Jones, K. C. and Barrie, L. A.: Toward a global network for persistent organic pollutants in air:Results from the GAPS study, Environ. Sci. Technol., 40(16), 4867–4873, doi:10.1021/es060447t, 2006.

Qiu, C., Wang, L., Lal, V., Khalizov, A. F. and Zhang, R.: Heterogeneous reactions of alkylamines with ammonium sulfate and ammonium bisulfate, Environ. Sci. Technol., 45(11), 4748–4755, doi:10.1021/es1043112, 2011.

Qiu, C. and Zhang, R.: Multiphase chemistry of atmospheric amines., Phys. Chem. Chem. Phys., 15(16), 5738–52, doi:10.1039/c3cp43446j, 2013.

Rabaud, N. E., Ebeler, S. E., Ashbaugh, L. L. and Flocchini, R. G.: Characterization and quantification of odorous and non-odorous volatile organic compounds near a commercial dairy in California, Atmos. Environ., 37(7), 933–940, doi:10.1016/S1352-2310(02)00970-6, 2003.

Rehder, D.: Vanadium nitrogenase, Journal of Inorganic Biochemistry, 80, 133-136, 2008.

Rockström, J., Steffen, W., Noone, K., Persson, Å., Chapin, F. S., Lambin, E., Lenton, T. M., Scheffer, M., Folke, C., Schellnhuber, H. J., Nykvist, B., de Wit, C. A., Hughes, T., van der Leeuw, S., Rodhe, H., Sörlin, S., Snyder, P. K., Costanza, R., Svedin, U., Falkenmark, M., Karlberg, L., Corell, R. W., Fabry, V. J., Hansen, J., Walker, B., Liverman, D., Richardson, K., Crutzen, P. and Foley, J.: Planetary boundaries: Exploring the safe operating space for humanity, Ecol. Soc., 14(2), doi:10.1038/461472a, 2009.

Rogge, W. F., Hildemann, L. M., Mazurek, M. A., Cass, G. R. and Simonelt, B. R. T.: Sources of fine organic aerosol. 1. Charbroilers and Meat Cooking Operations, Environ. Sci. Technol., 25(6), 1112–1125, doi:10.1021/es00018a015, 1991.

Saleh, R., Robinson, E. S., Tkacik, D. S., Ahern, A. T., Liu, S., Aiken, A. C., Sullivan, R. C., Presto, A. A., Dubey, M. K., Yokelson, R. J., Donahue, N. M. and Robinson, A. L.: Brownness of organics in aerosols from biomass burning linked to their black carbon content, Nat. Geosci., 7, 1–4, doi:10.1038/ngeo2220, 2014.

Schade, G. W. and Crutzen, P. J.: Emission of aliphatic amines from animal husbandry and their reactions: Potential source of N_2O and HCN, J. Atmos. Chem., 22(3), 319–346, doi:10.1007/BF00696641, 1995.

Schauer, J. J., Kleeman, M. J., Cass, G. R. and Simoneit, B. R. T.: Measurement of emissions from air pollution sources. 1. C1 through C29 organic compounds from meat charbroiling, Environ. Sci. Technol., 33(10), 1566–1577, doi:10.1021/es980076j, 1999.

Schlesinger, W. H. and Bernhardt, E. S. Biogeochemistry: An Analysis of Global Change, Elsevier Inc., 2013.

Schmeltz, I., and Hoffmann, D.: Nitrogen-containing compounds in tobacco and tobacco smoke, Chemical Review, 77(3), 295-311, doi: 10.1021/cr60307a001, 1977.

Schwartz, S. E., and White, W. H.: Kinetics of reactive dissolution of nitrogen oxides into aqueous solution, Ad. Environ. Sci. Technol., 12, 1-116, 1983.

Seinfeld, J. H. and Pandis, S. N., Atmospheric Chemistry: From Air Pollution to Climate Change, John Wiley & Sons, Inc., 2006.

Seo, S. G., Ma, Z. K., Jeon, J. M., Jung, S. C. and Lee, W. B.: Measurements of key offensive odorants in a fishery industrial complex in Korea, Atmos. Environ., 45(17), 2929–2936, doi:10.1016/j.atmosenv.2011.01.032, 2011.

Silva, P. J., Erupe, M. E., Price, D., Elias, J., Malloy, Q. G. J., Li, Q., Warren, B. and Cocker, D. R.: Trimethylamine as precursor to secondary organic aerosol formation via nitrate radical reaction in the atmosphere, Environ. Sci. Technol., 42(13), 4689–4696, doi:10.1021/es703016v, 2008.

Singh, H. B. and Hanst, P. L.: Peroxyacetyl nitrate (PAN) in the unpolluted atmosphere: An important reservoir for nitrogen oxides, Geophys. Res. Lett., 8(8), 941–944, doi:10.1029/GL008i008p00941, 1981.

Smith, J. N., Barsanti, K. C., Friedli, H. R., Ehn, M., Kulmala, M., Collins, D. R., Scheckman, J. H., Williams, B. J. and McMurry, P. H.: Observations of aminium salts in atmospheric nanoparticles and possible climatic implications., Proc. Natl. Acad. Sci. U. S. A., 107(15), 6634–6639, doi:10.1073/pnas.0912127107, 2010.

Sobanska, S., Hwang, H., Choël, M., Jung, H. J., Eom, H. J., Kim, H., Barbillat, J. and Ro, C. U.: Investigation of the chemical mixing state of individual asian dust particles by the combined use of electron probe X-ray microanalysis and raman microspectrometry, Anal. Chem., 84(7), 3145–3154, doi:10.1021/ac2029584, 2012.

Sokolov, A. P., Kicklighter, D. W., Melillo, J. M., Felzer, B. S., Schlosser, A. C. and Cronin, T. W.: Consequences of considering carbon-nitrogen interactions on the feedbacks between climate and the terrestrial carbon cycle, Journal of Climate, 21(15), 3776-3796, doi: 10.1108/17506200710779521, 2008.

Sorooshian, A., Murphy, S. M., Hersey, S., Gates, H., Padro, L. T., Nenes, a., Brechtel, F. J., Jonsson, H., Flagan, R. C. and Seinfeld, J. H.: Comprehensive airborne characterization of aerosol from a major bovine source, Atmos. Chem. Phys., 8, 5489–5520, doi:10.5194/acp-8-5489-2008, 2008.

Sorooshian, A., Padro, L. T., Nenes, A., Feingold, G., McComiskey, A., Hersey, S. P., Gates, H., Jonsson, H. H., Miller, S. D., Stephens, G. L., Flagan, R. C. and Seinfeld, J. H.: On the link between ocean biota emissions, aerosol, and maritime clouds: Airborne, ground, and satellite measurements off the coast of California, Global Biogeochem. Cycles, 23(4), 1–15, doi:10.1029/2009GB003464, 2009.

Sun, Y., Zhuang, G., Tang, A., Wang, Y. and An, Z.: Chemical Characteristics of $PM_{2.5}$ and PM_{10} in Haze−Fog Episodes in Beijing, Environ. Sci. Technol., 40(10), 3148–3155, doi:10.1021/es051533g, 2006.

Sutton, M. A., Howard, C. M., Erisman, J. W., Billen, G., Bleeker, A., Grennfelt, P., van

Grinsven, H. and Grizzetti, B.: European Nitrogen Assessment, Cambridge University Press, 2011.

Tang, M., Huang, X., Lu, K., Ge, M., Li, Y., Cheng, P., Zhu, T., Ding, A., Zhang, Y., Gligorovski, S., Song, W., Ding, X., Bi, X. and Wang, X.: Heterogeneous reactions of mineral dust aerosol: implications for tropospheric oxidation capacity, Atmos. Chem. Phys. Discuss., submitted, 1–124, doi:10.5194/acp-2017-458, 2017.

Vandenboer, T. C., Petroff, A., Markovic, M. Z. and Murphy, J. G.: Size distribution of alkyl amines in continental particulate matter and their online detection in the gas and particle phase, Atmos. Chem. Phys., 11(9), 4319–4332, doi:10.5194/acp-11-4319-2011, 2011.

VandenBoer, T. C., Markovic, M. Z., Petroff, A., Czar, M. F., Borduas, N. and Murphy, J. G.: Ion chromatographic separation and quantitation of alkyl methylamines and ethylamines in atmospheric gas and particulate matter using preconcentration and suppressed conductivity detection, J. Chromatogr. A, 1252(3), 74–83, doi:10.1016/j.chroma.2012.06.062, 2012.

Van Neste, A., Duce, R. A. and Lee, C.: Methylamines in the marine atmosphere, Geophys. Res. Lett., 14(7), 711-714, 1987.

van Pinxteren, M., Fiedler, B., van Pinxteren, D., Iinuma, Y., Körtzinger, A. and Herrmann, H.: Chemical characterization of sub-micrometer aerosol particles in the tropical Atlantic Ocean: marine and biomass burning influences, J. Atmos. Chem., 105–125, doi:10.1007/s10874-015-9307-3, 2015.

Verbeke, T., Lathière, J., Szopa, S. and De Noblet-Ducoudré, N.: Impact of future land-cover changes on HNO3 and O3 surface dry deposition, Atmos. Chem. Phys., 15(23), 13555–13568, doi:10.5194/acp-15-13555-2015, 2015.

Verriele, M., Plaisance, H., Depelchin, L., Benchabane, S., Locoge, N. and Meunier, G.: Determination of 14 amines in air samples using midget impingers sampling followed by analysis with ion chromatography in tandem with mass spectrometry., J. Environ. Monit., 14(2), 402–8, doi:10.1039/c2em10636a, 2012.

Wahner, A., Mentel, T. F. and Sohn, M.: Gas-phase reaction of N_2O_5 with water vapor: Importance of heterogeneous hydrolysis of N_2O_5 and surface desorption of HNO_3 in a large Teflon chamber, Geophys. Res. Lett., 25, 2169-2172, 1998.

Wang, L., Khalizov, A. F., Zheng, J., Xu, W., Ma, Y., Lal, V. and Zhang, R.: Atmospheric nanoparticles formed from heterogeneous reactions of organics, Nat. Geosci., 3(4), 238–242, doi:10.1038/ngeo778, 2010a.

Wang, L., Vinita, L., Khalizov, A. F. and Zhang, R.: Heterogeneous chemistry of

alkylamines with sulfuric acid: Implications for atmospheric formation of alkylaminium sulfates, Environ. Sci. Technol., 44(7), 2461–2465, doi:10.1021/es9036868, 2010b.

Wayne, R. P., Barnes, I., Biggs, P., Burrows, J. P., Canosa-Mas, C. E., Hjorth, J., Lebras, G., Moortgat, G. K., Perner, D., Poulet, G., Restelli, G. and Sidebottom, H.: The nitrate radical: Physics, chemistry, and the atmosphere, Atmos. Environ., 25, 1-203, 1991.

Wentworth, G. R., Murphy, J. G., Croft, B., Martin, R. V., Pierce, J. R., Côté, J. S., Courchesne, I., Tremblay, J. É., Gagnon, J., Thomas, J. L., Sharma, S., Toom-Sauntry, D., Chivulescu, A., Levasseur, M. and Abbatt, J. P. D.: Ammonia in the summertime Arctic marine boundary layer: Sources, sinks, and implications, Atmos. Chem. Phys., 16(4), 1937–1953, doi:10.5194/acp-16-1937-2016, 2016.

Wesely, M. L. and Hicks, B.B.: A review of the current status of knowledge on dry deposition, Atmos. Environ., 34(12–14), 2261–2282, doi:10.1016/S1352-2310(99)00467-7, 2000.

Wood, C., Diamond, G., Koller, L., Woodall, G. and Falke, E. V.: Nitric acid acute exposure guideline levels, in: Acute exposure guideline levels for selected airborne chemicals volume 14, National Academy of Sciences, United States of America, 139 – 176, 2013.

Yan, G. and Kim, G.: Sources and fluxes of organic nitrogen in precipitation over the southern East Sea/Sea of Japan, Atmos. Chem. Phys., 15(5), 2761–2774, doi:10.5194/acp-15-2761-2015, 2015.

Yao, L., Wang, M.-Y., Wang, X.-K., Liu, Y.-J., Chen, H.-F., Zheng, J., Nie, W., Ding, A.-J., Geng, F.-H., Wang, D.-F., Chen, J.-M., Worsnop, D. R. and Wang, L.: Detection of atmospheric gaseous amines and amides by a high resolution time-of-flight chemical ionization mass spectrometer with protonated ethanol reagent ions, Atmos. Chem. Phys. Discuss., 1–32, doi:10.5194/acp-2016-484, 2016.

Youn, J. S., Crosbie, E., Maudlin, L. C., Wang, Z. and Sorooshian, A.: Dimethylamine as a major alkyl amine species in particles and cloud water: Observations in semi-arid and coastal regions, Atmos. Environ., 122, 250–258, doi:10.1016/j.atmosenv.2015.09.061, 2015.

Yu, H., McGraw, R. and Lee, S. H.: Effects of amines on formation of sub-3 nm particles and their subsequent growth, Geophys. Res. Lett., 39(2), 2–7, doi:10.1029/2011GL050099, 2012.

Zhang, L., Vet, R., O'Brien, J. M., Mihele, C., Liang, Z. and Wiebe, A.: Dry deposition of individual nitrogen species at eight Canadian rural sites, J. Geophys. Res. Atmos., 114(2), 1–13, doi:10.1029/2008JD010640, 2009.

Zhao, J., Smith, J. N., Eisele, F. L., Chen, M., Kuang, C. and McMurry, P. H.: Observation of neutral sulfuric acid-amine containing clusters in laboratory and ambient measurements, Atmos. Chem. Phys., 11(21), 10823–10836, doi:10.5194/acp-11-10823-2011, 2011.

Zollner, J. H., Glasoe, W. A., Panta, B., Carlson, K. K., McMurry, P. H. and Hanson, D. R.: Sulfuric acid nucleation: Power dependencies, variation with relative humidity, and effect of bases, Atmos. Chem. Phys., 12(10), 4399–4411, doi:10.5194/acp-12-4399-2012, 2012.

Chapter 2: Passive Sampling of Gaseous Nitric Acid Along the Newfoundland and Labrador Boreal Ecosystem Latitudinal Transect (NL-BELT)

2.1 Abstract

Atmospheric nitric acid ($HNO_{3(g)}$) has been shown to deposit in high amounts in rural and remote environments and thus has the capability to influence the productivity and function of these ecosystems. Potential interactive effects of $HNO_{3(g)}$ deposition and climate change in more remote arctic and boreal regions, where N limitation can be significant, require the quantification of $HNO_{3(g)}$ inputs to better constrain sources and controls on these inputs and their role in climate responses of high-latitude ecosystems. Custom-built $HNO_{3(g)}$ passive diffusion-based samplers employing nylon membrane filters as the $HNO_{3(g)}$ collection media were installed along the Newfoundland and Labrador – Boreal Ecosystem Latitudinal Transect (NL-BELT) to estimate the mixing ratios and flux of $HNO_{3(g)}$ across this boreal forest climate transect. The quality assurance and quality control procedures used enabled the quantification of time-weighted average mixing ratios as low as 2 parts per trillion by volume (pptv) over a monthly sampling period or 72 pptv over a 24-hour sampling period using these custom-built samplers. The nylon membrane filters were tested for their reusability in these relatively remote ecosystems where no statistical difference between the measured mean value of reused and new filters were observed, suggesting that the filters can be reused as long as replicates are employed.

The average mixing ratios at the NL-BELT field sites from the summer of 2015 through to the fall of 2016 were in the tens of pptv level, with a range of 4 – 214 pptv. The annual dry deposition fluxes of $HNO_{3(g)}$ as nitrogen were estimated to be 3 - 16 mg m^{-2} yr^{-1} across the transect. An air mass back trajectory analysis showed that the deposition of $HNO_{3(g)}$ to the NL-BELT sites was correlated with winds originating from

the east, suggesting the short-range transport of $HNO_{3(g)}$ derived from precursor anthropogenic nitrogen oxides emitted in the central and eastern regions of the island of Newfoundland. By assuming a steady-state between $HNO_{3(g)}$ formation and loss processes in the atmosphere, it was possible to determine that local biogenic nitrogen oxide production and oxidation may have accounted for 50% or more of the measured $HNO_{3(g)}$. The seasonal downwelling of peroxyacetyl nitrates (PANs) from the upper troposphere in the spring and early summer may have also contributed to the $HNO_{3(g)}$ observed in excess of the calculated local production potential.

2.2 Introduction

As a result of the start of anthropogenic industrial-scale combustion processes, nitric acid ($HNO_{3(g)}$) concentrations in the atmosphere have increased greatly in the last century. Field measurements and chemistry-climate models have shown that $HNO_{3(g)}$ deposits in high amounts to rural and remote ecosystems, and in some studies it has been the dominant atmospheric nitrogen (N) input to these environments (Flechard et al., 2011; Verbeke et al., 2015; Zhang et al., 2009;). Large inputs of N can be toxic to vegetation, lead to soil acidification and cause ecosystem shifts to lower biodiversity (Cisneros et al., 2010; Bobbink et al., 2010). In terrestrial ecosystems that are N-limited, such as those in high-latitude regions, nitrogen inputs may stimulate vegetation and forest growth (Bedison and McNeil 2009; Bobbink et al., 2010). This fertilization effect will impact the carbon cycle and Earth's climate (Bedison and McNeil, 2009, Ollinger et al., 2008; Sokolov et al., 2008), but will depend upon its magnitude in relationship to climate change impacts on rates of N cycling, the major source of available N in N-limited

ecosystems (Cleveland et al., 1999). Thus the quantitation of $HNO_{3(g)}$ in conjunction with ongoing biogeochemical and ecosystem ecological research enables the linkage of these inputs to ecosystem responses to climate change.

Constraining $HNO_{3(g)}$ inputs to remote ecosystems remains a challenge. Global atmospheric $HNO_{3(g)}$ concentrations have been modeled by Verbeke et al. (2015), but emission inventories of its precursor nitrogen oxide gases (NO_x) used in the model do not include soil emissions or any inter-annual variability in emission factors (Lamarque et al. 2010). This is a concern because soil NO_x emissions are estimated to contribute up to 25% of global NO_x emissions, and have been shown to be an important source of NO_x in rural and remote ecosystems (Butterbach-Bahl et al., 2009; Müller, 1992; Molina-Herra et al., 2017). As a result, measurements of $HNO_{3(g)}$ in remote environments are needed to validate model outputs. Obtaining $HNO_{3(g)}$ measurements in remote ecosystems is difficult, however, because most atmospheric sampling techniques used to monitor $HNO_{3(g)}$ are active and thus require expensive equipment and powered infrastructure (Flechard et al., 2011; Le Breton et al., 2014; Zhang et al., 2009). Therefore, developing a cheap passive technique that is capable of monitoring $HNO_{3(g)}$ inputs to rural and remote ecosystems is essential to fully understanding the role of this increased global anthropogenic nitrogen input to the atmosphere.

$HNO_{3(g)}$ is formed in the atmosphere from various reactions of its precursor gas nitrogen dioxide ($NO_{2(g)}$). In the daytime $HNO_{3(g)}$ is formed through the oxidation of $NO_{2(g)}$ with the hydroxyl radical ($OH_{(g)}$) via R2-1. While during the night $NO_{2(g)}$ undergoes a series of reactions (R2-2 to R2-4) to form $HNO_{3(g)}$.

(R2-1) $NO_{2(g)} + OH_{(g)} \rightarrow HNO_{3\,(g)}$

(R2-2) $NO_{2(g)} + O_{3(g)} \rightarrow NO_{3(g)} + O_{2(g)}$

(R2-3) $NO_{2(g)} + NO_{3(g)} \rightleftharpoons N_2O_{5(g)}$

(R2-4) $N_2O_{5(g)} + H_2O_{(g)} \rightarrow 2HNO_{3(g)}$

$NO_{2(g)}$ can be directly emitted into the atmosphere or form through the oxidation of nitric oxide ($NO_{(g)}$) via R2-5. These two species make up the NO_x family (i.e. the sum of $NO_{(g)}$ and $NO_{2(g)}$) and they rapidly cycle between one another in the daytime atmosphere via R2-5 and R2-6.

(R2-5) $NO_{(g)} + O_{3(g)} \rightarrow NO_{2(g)} + O_{2(g)}$

(R2-6) $NO_{2(g)} + h\upsilon + M \rightarrow NO_{(g)} + O_{3(g)} + M$

Precursor NO_x species are emitted into the atmosphere primarily through anthropogenic fuel combustion processes, which account for approximately 60% of global NO_x emissions (Müller, 1992; Finlayson-Pitts and Pitts, 2000). The other major sources of atmospheric NO_x include biomass burning and lightning (Müller, 1992), with lesser contributions from denitrifying bacteria (Denman et al., 2007). Therefore, it is largely assumed that $HNO_{3(g)}$ is a marker of anthropogenic pollution given the relative contribution of anthropogenic NO_x to the atmosphere.

$HNO_{3(g)}$ is rapidly wet and dry deposited from the atmosphere due to its high solubility and ‘stickiness’ (Finlayson-Pitts and Pitts, 2000; Schwartz and White 1983),

and thus it is often deposited in high quantities in proximity to its source location. However, its precursor gas $NO_{2(g)}$ can undergo long-range transportation to remote ecosystems through the formation of peroxyacetyl nitrates (PANs). $NO_{2(g)}$ can react with volatile organics in the urban atmosphere to form PANs that are thermally stable in the upper troposphere (R2-7; Singh and Hanst, 1981). When PANs are formed under cold conditions or transported rapidly to cold regions (e.g. lofted air masses into the upper troposphere, high latitudes) they can remain stable in the atmosphere for months.

(R2-7) $NO_{2\,(g)} + C_xH_yO_{z(g)} \rightleftharpoons C_xH_yNO_{z\,(g)}$

When these PAN species down well from the upper troposphere they thermally decompose in less than an hour as they reach temperatures of 298 K or greater (Atkinson et al., 1997). Thus PANs are capable of transporting long distances aloft before decomposing to $NO_{2(g)}$.

In rural and remote ecosystems $HNO_{3(g)}$ mixing ratios in air can be as low as 10 parts per trillion by volume (pptv), requiring a sensitive atmospheric measurement technique to quantify this acid (Finlayson-Pitts and Pitts, 2000; Flechard et al., 2011; Zhang et al., 2009). Typical atmospheric sampling of $HNO_{3(g)}$ is active, and thus requires power, and often times expensive instrumentation. For example, Flechard et al. (2011) and Zhang et al. (2009) sample $HNO_{3(g)}$ at rural and remote forests by actively pulling air through denuders coated with a reactive basic solution (Flechard et al., 2011; Zhang et al., 2009). Chemical ionization mass spectrometers have also been used to obtain large spatial

scale rural measurements via aircraft campaigns (Le Breton et al., 2014) but are very costly, require highly trained and dedicated personnel, and are unable to probe within 100 m of the surface (Young et al., 2012). Active sampling techniques such as these may also be biased high since there is typically an anthropogenic point source (e.g. a generator, or small town) collocated with people using vehicles near the active sampler that could be emitting NO_x.

Passive sampling of $HNO_{3(g)}$ overcomes these limitations of active sampling and has been performed using nylon membrane filters as sorption media for $HNO_{3(g)}$ in polluted forests in California, U.S.A. and Alberta, Canada (Bytnerowicz et al., 2001; Bytnerowicz et al., 2010). This passive sampling strategy has the advantages of low costs, low maintenance, reduced personnel training, and the potential to obtain large spatial scale measurements, but has never been deployed for use in remote ecosystems where $HNO_{3(g)}$ mixing ratios are expected to be below 100 pptv (Bytnerowicz et al., 2001). Complications in quantitation from temperature (T) and relative humidity (RH) may create additional uncertainty from the previously reported calibrations if they are highly variable over the sampling period. Further, the effect of T and RH on $HNO_{3(g)}$ passive sampling with nylon membrane filters is still largely uncharacterized. The utility of these samplers in such environments is highly desirable, but still requires rigorous analytical field methodology development.

In this work we pursued an ultra-trace $HNO_{3(g)}$-capable methodology for the passive sampling of this gas by i) developing a quality assurance and control procedure for quantifying trace quantities of $HNO_{3(g)}$ from nylon membranes using ion chromatography, ii) assessing the reusability of nylon membrane filters for passive

sampling, iii) determining the ability of sorption-based nylon membrane samplers to quantify $HNO_{3(g)}$ in remote ecosystems, iv) estimating the annual flux of $HNO_{3(g)}$ across a latitudinal transect of similar forest sites in Newfoundland and Labrador, and v) decoupling long- and short-range transport of $HNO_{3(g)}$ from local production through the use of comprehensive air mass back-trajectory statistical analysis and steady-state approximations.

2.3 Methods

2.3.1 Custom Built Nitric Acid Passive Samplers

Nitric acid passive gas samplers were custom-built by adaptation (Figure 2-1) from the design detailed in Bytnerowicz et al. (2005). The filter pack sampler assembly is composed of one nylon membrane filter (47 mm, 1.0 μm, Nylasorb™, Pall Corporation, P/N 66509), one supported polytetrafluoroethylene (PTFE) filter (47 mm, 1.0 μm, Zefluor™, Pall Corporation, P/N P5PJ047), a petri dish (60 x 15 mm, VWR), two PTFE rings (50 x 2 mm, McMaster Carr, P/N 8547K41), and one polycarbonate ring (50 x 5 mm, McMaster Carr, P/N 8585K18). The nylon filter, which samples $HNO_{3(g)}$ through a sorption mechanism, is housed inside the petri dish between two PTFE rings. A PTFE filter, supported underneath by a PTFE ring and above by a polycarbonate ring prevents intrusion of atmospheric particles. A tight-fitting polycarbonate ring holds the filter assembly securely in the petri dish.

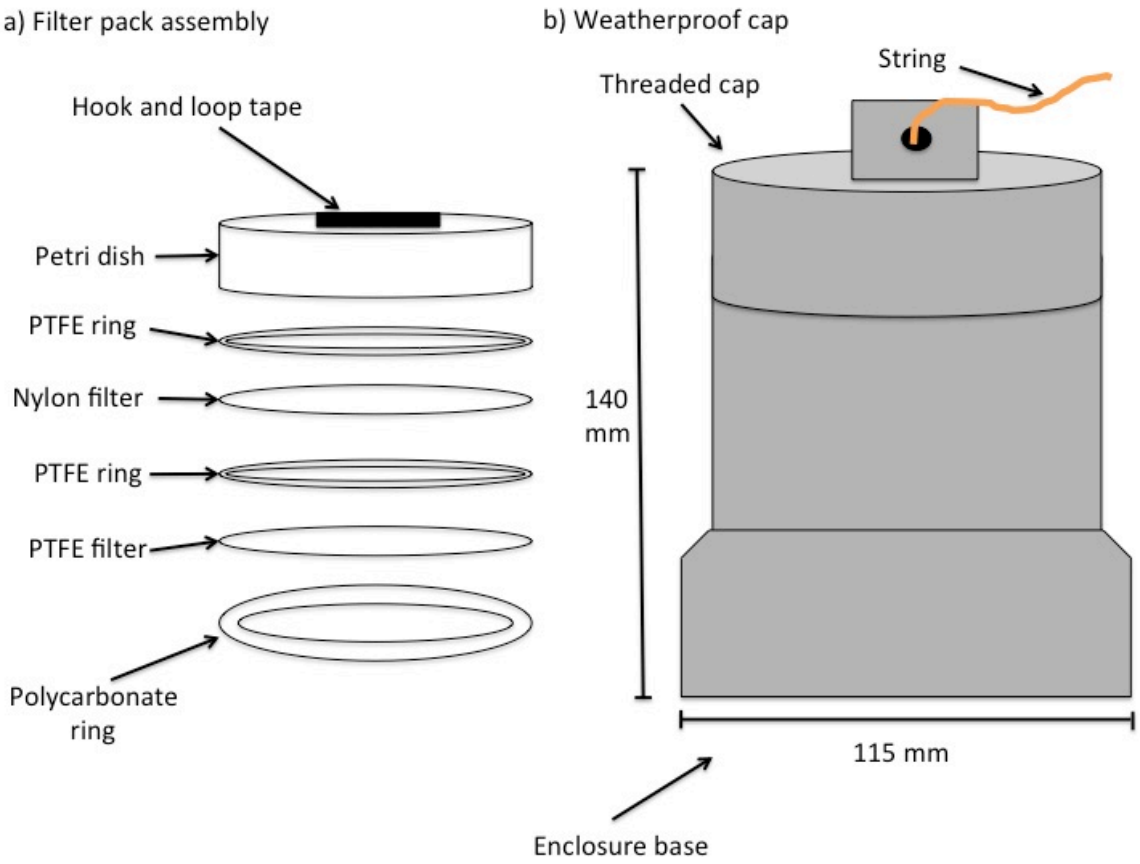

Figure 2-1. Schematic of the custom-built $HNO_{3(g)}$ passive samplers. The filter pack assembly (a) consists of a petri dish (60 x 15 mm), a nylon membrane filter (47 mm, 1.0 µm), a supported PTFE filter (47 mm, 1.0 µm), two PTFE rings (50 x 2 mm) and a polycarbonate ring (50 x 5 mm). The weatherproof enclosure (b) consists of an ABS enclosure base and an ABS screw cap with a drilled hole to loop string through for mounting in situ.

Weatherproof enclosures were constructed from two ABS fittings to protect the samplers from wind and rain. One fitting was used as the enclosure base and a threaded fitting as the cap. The filter pack assembly was fastened inside the cap with hook and loop adhesive tape. The weatherproof enclosures were painted silver to reflect incident light and reduce heating of the weatherproof enclosures.

2.3.2 Passive Sampler Deployment Along the Newfoundland and Labrador – Boreal Ecosystem Latitudinal Transect (NL-BELT)

The $HNO_{3(g)}$ passive gas samplers were installed in August 2015 across four watersheds in western Newfoundland and southern Labrador, which comprise the NL-BELT (Figure 2-2).

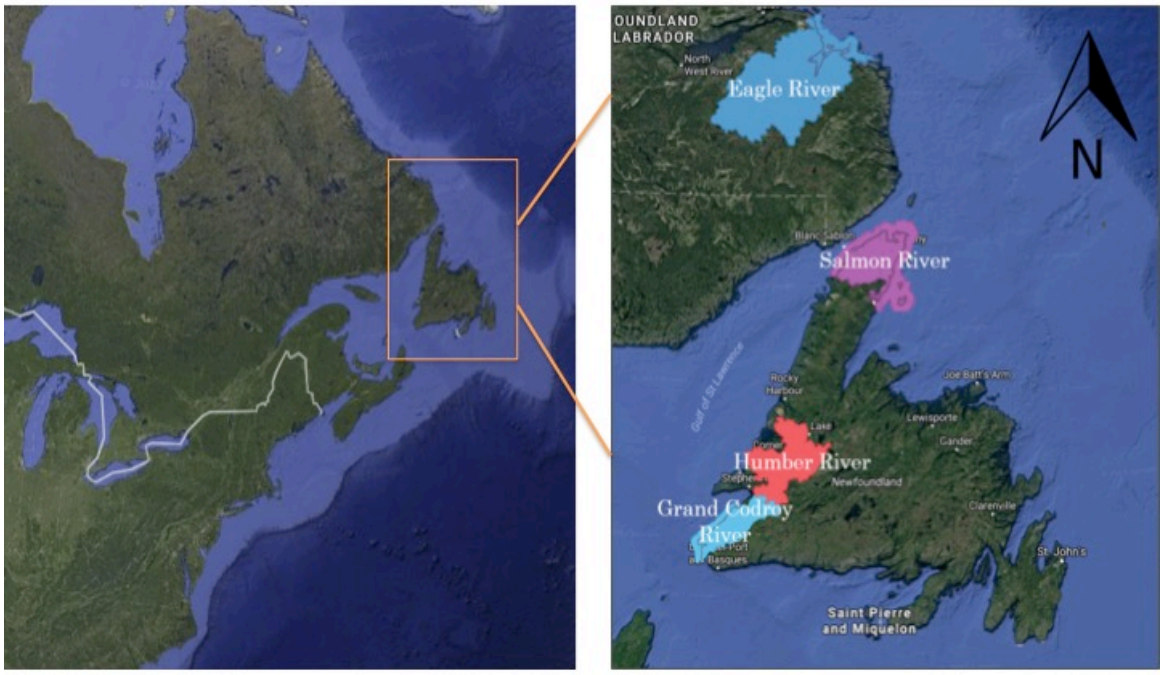

Figure 2-2. Map of North America (left) highlighting the geographical location of Newfoundland and Labrador and map of the NL-BELT (right) showing the four watershed regions (Grand Codroy (GC), Humber River (HR), Salmon River (SR), and Eagle River (ER)) that comprise the NL-BELT.

In each watershed three balsam fir-dominated forest experimental sites exist, with one utilized for atmospheric sampling. These were the field sites providing supporting measurements of soil moisture, relative humidity, and air temperature in each watershed region (see Section 2.3.3). The $HNO_{3(g)}$ samplers were deployed in triplicate at each site in order to capture intra-site variability in atmospheric composition. The samplers were

installed at the following site locations: Grand Codroy O'Regan's site (GC; 47.893° N, 59.174° W), Humber River Camp 10 site (HR; 49.070° N, 57.643° W), Salmon River Hare Bay site (SR; 51.256° N, 56.138° W), and Eagle River Muddy Pond site (ER; 53.550° N, 56.987° W).

The weatherproof enclosures were hung using screw hooks approximately 3 m above ground level on selected trees that were on the edges of forest stands or clearings greater than 15 m in diameter in order to facilitate intrusion of the atmosphere and minimize canopy effects on sample composition. Nylon membrane $HNO_{3(g)}$ sample collection and reinstallation was performed on a monthly basis at the Newfoundland sites (GC, HR and SR) and on a bimonthly basis at the Labrador site (ER) during the summer of 2015 and throughout the summer of 2016. A time-integrated sample was also collected over the 2015-2016 winter at each field site spanning 6 to 8 months. Sampler filter packs for each exchange were assembled in a sealed petri dish in St. John's, Canada and were transported in an insulated box containing ice packs (~ 10 °C) to the Canadian Forestry Service field laboratory located in Pasadena, NL where they were refrigerated until taken again in an insulated box to the field sites. They were then exchanged with the previously deployed sampling filter packs. The samples were transported in the insulated box until they could be stored at 4 °C prior to extraction for analysis. A field blank filter was carried to each sample site and briefly exposed to capture any systematic contamination during the handling and transportation of the filter packs.

2.3.3 Supporting Measurements at the NL-BELT Sites

Temperature (T) and relative humidity (RH) probes (HOBO® U23 pro v2, P/N U23-001) were installed at all the Newfoundland island sites in November 2015 and at the Labrador site in June 2016. Solar radiation shields (HOBO®, P/N RS1) were affixed to a tree at each site at roughly the same height above ground level as the $HNO_{3(g)}$ samplers and the T and RH probes were installed within each shield. Supporting atmospheric measurements of $NO_{x(g)}$, $NO_{2(g)}$, $NH_{3(g)}$ and $O_{3(g)}$ were provided by reactive passive samplers (Ogawa® USA) that were installed in triplicate at all four field sites in the summer of 2014. Briefly, the $NO_{x(g)}$, $NO_{2(g)}$, $NH_{3(g)}$ and $O_{3(g)}$ samplers chemically collected these gases via their reaction with impregnated filters housed within the samplers after the gases had diffused through a diffuser end cap. The filters were extracted in 15 ml of DIW and analyzed via IC using the program described in Sect 2.3.4.2.

2.3.4 Sample Handling, Analysis and Quality Control

2.3.4.1 Handling and Extraction of Nylon and PTFE Filters

The nylon and PTFE filters were handled, extracted and analyzed following procedural recommendations outlined by the U.S. Environmental Protection Agency (USEPA) (Chow and Watson, 1998). The nylon filters were pre-cleaned via the following procedure: i) six times rinse with >18.2 MΩ x cm ultrapure deionized water (DIW; Barnstead Nanopure Infinity, Thermo Scientific, Waltham, MA, USA), ii) minimum of 12 hours soak in 0.015 M Na_2CO_3 (> 99.5%, Sigma-Aldrich), iii) second soak of at least 12 hours in DIW, and iv) six times rinse with DIW. The supported PTFE filters were pre-

cleaned with two six-time rinses and two 12-hour minimum soaks in DIW. The filters were air-dried for approximately 2 hours before being installed in the samplers. The PTFE and nylon membrane filters were rinsed and soaked for an additional day as per the USEPA recommendation in order to achieve lower method detection limits. After sample collection, the nylon filters were gently rolled using clean forceps and placed into 15 ml polypropylene tubes (Falcon®, P/N 352097). The filters were extracted in 10 ml of 1 mM KOH diluted from 1 N KOH (Thermo Fisher Scientific, P/N AC278400010) and were sonicated for 10 minutes at 30 °C (VWR Scientific Products/Aquasonic 150 HT, Ultrasonic Water Bath). The PTFE filters were extracted for particulate analysis using 10 ml of DIW following the same procedure.

2.3.4.2 Analysis of Nylon and PTFE filters by Ion Chromatography

The filter extracts were analyzed for the HNO_3 conjugate base anion (NO_3^-) via ion chromatography (IC). Calibration standards were prepared through serial dilution of a primary mixed anion standard concentrate (Dionex seven-anion II, P/N: 057590, Thermo Scientific, Sunnyvale, CA, USA) with ultrapure DIW to a NO_3^- concentration range of 4 – 300 ng ml^{-1}. The IC calibration standard set consisted of 5 calibration standards, 2 check standards and a calibration reagent blank. The analytes were separated from other common inorganic and organic anions using a KOH mobile phase gradient elution program with a fixed flow rate of 1.5 ml min^{-1}. The gradient program started with a 1 mM KOH hold for the first 7 mins followed by a linear increase to 16 mM KOH over the next 9 mins. The KOH was held at 16 mM for 4 mins then linearly increased to 25 mM from 20 mins to 25 mins. At 25 mins the concentration was linearly increased to 60 mM over a

period of 8 mins, yielding a total run time of 33 mins. The eluent concentration was returned to 1 mM and allowed to equilibrate for 1 minute before the beginning of the next injection. An eluent generator cartridge (ThermoScientific, EGC III, P/N: 074532) used in conjunction with a DIW reservoir supplied the KOH mobile phase. Analytes were separated on ThermoScientific AG11 (4 x 50 mm, P/N: 052962) and AS11-HC (4 x 250 mm, P/N: 052960) guard and analytical columns. All analytes were pre-concentrated on a concentrator column (TAC-ULP1, 5 x 23 mm, P/N: 061400) from 1 ml sample volumes injected using a ThermoScientific AS-DV autosampler and were quantified by suppressed (AERS 500, 4mm, P/N: 082540) conductivity detection (DS6 heated conductivity cell).

2.3.4.3 Washing Procedures and Negative Controls

The 15 ml polypropylene tubes were acid-washed (10% v/v HCl) and pre-sonicated with DIW for 60 minutes before filters were placed in the tubes and sample extractions were performed. IC standards were prepared using Class A Corning polymethylpentene 50 ($\pm$ 0.06) ml volumetric flasks that were rinsed eight times with DIW prior to use. Standards were stored in 60 ml brown Nalgene polypropylene bottles that were pre-cleaned in a 10% HCl bath, followed by eight rinses each with distilled water and then DIW.

The full $HNO_{3(g)}$ filter pack assembly was rinsed 10 times with DIW between sampling deployments. As mentioned previously, a representative field blank filter pack assembly was carried to each sampling site and briefly exposed to capture any systematic contamination during the handling and transportation of the filter packs. The field blank filters were handled and extracted following the same procedure outlined in Sect. 2.3.4.1

and all sample quantities were calculated by accounting for the field blank observations of NO_3^-, where the quantities were above the IC detection limits. Additionally, 10 ml of 1 mM KOH and DIW reagent blanks were taken and analyzed with each set of samples to determine the potential NO_3^- background signal derived from the extract solvents and any contamination in the 15 ml polypropylene tubes.

2.3.4.4 Ion Chromatography Instrumental Performance Evaluation

The IC method precision was determined using calibration standard peak areas from n = 5 calibration curves analyzed over a period of four months. The method precision was calculated as the relative standard deviation in the slope across the five calibrations. The accuracy of the method was assessed using two check standards positioned at the high and low end of the calibration working range. The low check standard was prepared to a NO_3^- concentration of 5.4 ng ml^{-1} and the high check standard to a concentration of 54 ng ml^{-1}. Accuracy was calculated by determining the difference between the calculated values of the check standards (n = 8) and their known concentrations using the corresponding calibration slope on a given IC run. The average instrumental limit of detection (LOD) was calculated as 3 times the analyte signal to noise using peak heights from four separate calibrations. The noise was calculated as the standard deviation in the calibration reagent blank conductivity signal across the NO_3^- retention window, which consisted of approximately 100 – 150 conductance data points depending on the blank chromatogram analyzed.

2.3.5 Reusability of Nylon Membrane Filters

The reusability of the nylon filters was tested by deploying ten passive samplers on the rooftop of the Memorial University Earth Science building in St. John's, Canada (Figure 2-2; 47.574° N, 52.734° W). Five used and re-cleaned filter packs and five new filter packs were installed in the weatherproof enclosures for a two-week period (November 15 – December 14, 2016). The nylon filters were extracted and analyzed to determine the extent to which the nylon filters could be reused. Field blanks consisting of a new nylon filter assembly and a used nylon filter assembly were transported to the roof site and exposed for five seconds to track any systematic contamination. All filter reuse sample data was blank-corrected using their corresponding field blanks.

2.3.6 Calculation of $HNO_{3(g)}$ Mixing Ratios from Filter Extracts

To convert the mass loadings of NO_3^- adsorbed to each filter to an average atmospheric mixing ratio, the response of the passive gas samplers to a given dose of $HNO_{3(g)}$ needed to be known. The calibration of this style of passive sampler has been performed previously in a PTFE chamber (Bytnerowicz et al., 2005), where the linear uptake of $HNO_{3(g)}$ to the samplers (μg) with a known nitric acid dose over time (μg h m^{-3}) was determined. The slope (Units: μg m^{-3} $HNO_{3(g)}$ h (μg $NO_{3\,(filter)}^{-}$)$^{-1}$) of this previously reported response was employed in this work to determine the average atmospheric $HNO_{3(g)}$ mixing ratios during the NL-BELT sampling periods. Equation 2-1 describes the mass loading conversion of $HNO_{3(g)}$ in μg m^{-3} of air using the IC NO_3^- concentrations in μg ml^{-1} (C_x), extract volume in ml (v), calibration slope (m) and sampling period in hours (t).

(E2-1) $[HNO_{3(g)}] = C_x v m t^{-1}$

The mass loading of $HNO_{3(g)}$ in μg m^{-3} was then converted to a volume by volume mixing ratio by converting the mass of $HNO_{3(g)}$ per m^3 of air to volume of $HNO_{3(g)}$ per m^3 of air via the ideal gas law (E2-2).

(E2-2) $V_x = n_x R T P^{-1}$

The volume of $HNO_{3(g)}$ in air (V_x; m^3) was calculated using the moles of $HNO_{3(g)}$ (n_x), and temperature (T) and pressure (P) were assumed to be standard at 1 atm and 298.15 K. The final mixing ratios were determined by taking the ratio of $HNO_{3(g)}$ to the cubic meter of air, multiplied by 10^{12}, resulting in a mixing ratio expressed in units of pptv.

2.3.7 Calculation of $HNO_{3(g)}$ Annual Fluxes Across the NL-BELT

Annual dry deposition fluxes of $HNO_{3(g)}$ for each site were calculated using the calculated average $HNO_{3(g)}$ mass loadings per sampling period (n = 3) for every sample collection between August 2015 and August 2016 via E2-3. The $HNO_{3(g)}$ flux (F; mg N m^{-2}) per sampling period was calculated as the product of the mass loading of $HNO_{3(g)}$ in units of mg N m^{-3} at a reference height (z; m) and the deposition velocity (V_d) in m s^{-1} of the gas modeled for the reference height.

(E2-3) $F = - [HNO_{3(g)}(z)]V_d(z)$

To date, all commonly employed dry deposition models estimate the dry deposition of gases via a sum of deposition resistances (Wesely and Hicks, 2000). These resistance terms are shown in E2-4, where $R_a(z)$ represents the aerodynamic resistance at a reference height, R_b the quasi-laminar resistance and R_c the affinity of pollutant uptake on a surface (Wesely and Hicks, 2000; Seinfeld and Pandis, 2006).

(E2-4) $V_d(z) = [R_a(z) + R_b + R_c]^{-1}$

We utilized a V_d of 3 ± 1 cm s^{-1} in this work to calculate $HNO_{3(g)}$ fluxes based on a literature survey of similar ecosystems. The V_d used was the average modeled V_d for the NitroEurope forested network (Flechard et al., 2011). The implications and assumptions for using this V_d value are discussed in Sect 2.4.3. After $HNO_{3(g)}$ number densities from August 2015 to August 2016, including number densities obtained during the winter sampling period, were converted to fluxes, they were summed to determine an annual flux for this period (365 ± 5 days).

2.3.8 HYSPLIT Model Calculations for Estimating Air Mass Back Trajectories

An air mass back trajectory analysis was performed using the Hybrid Single-Particle LaGrangian Integrated Trajectory model (HYSPLIT) to determine the origin of air masses to all field sites during the sampling periods (Rolph, 2017; Stein et al., 2015). The trajectory analysis was performed using the Global Data Assimilation System (GDAS) meteorology data set with 0.5-degree resolution. Back trajectories were initiated

from ground level at each site location every 3 hours for the duration of the sampling period and each trajectory was run backwards for 120 hours. Frequency plots were generated using the NOAA HYSPLIT online interface to provide qualitative geographic interpretation of air mass history. Quantitative geographic sector assignment was performed in Igor Pro by running a custom-built procedure on raw trajectory endpoint latitude and longitude coordinates (Figure A-1). Back trajectory end points were thus assigned to one of four quadrants (southwest, southeast, northwest, northeast) centered on the sampling site locations provided in Sect 2.3.2.

Raw endpoint output files for entire sampling periods were concatenated and sorted before being imported to Igor Pro for sector assignment. The integrity of the data was qualitatively verified as unchanged and intact after the concatenation and sorting procedure was performed by visually inspecting the re-plotted trajectories using supplemental software designed for importing raw HYPLIT data into Igor Pro (Petit, J. – E et al., 2017). Further, the Igor Pro procedure was tested with multiple variations and combinations of possible data inputs and the procedure was determined to perform its function across this wide range of possible data inputs.

2.4 Results and Discussion

2.4.1 Ion Chromatography Method Performance, Quality Assurance, and Quality Control

The IC method utilized in this work is capable of resolving six organic acids from seven common inorganic anions found in atmospheric samples (Figure A-2). Organic acids are considered common atmospheric matrix components that may potentially

physisorb to the nylon membrane filters. Taking into consideration that succinate, formate, acetate, lactate, propionate, and butyrate as well as fluoride, nitrite, chloride, bromide, sulfate and phosphate do not coelute with NO_3^-, this method is robust for the analysis of a wide variety of atmospheric acids. The IC method precision for NO_3^- was determined to be $\pm$ 3% across n = 5 calibrations, and the calibration linearity across these five calibrations was high ($r^2 \geq 0.998$). These statistics indicate strong instrumental reproducibility with analyte mass injections below 1 μg. The average instrumental low check standard and high check standard accuracy determined from n = 8 standards were 70% and 94%, respectively. The lower accuracy found for the low check standard is derived from the NO_3^- concentration of the standard being only double the instrumental limit of quantitation (LOQ). The higher instrumental accuracy (94%) was used in error propagation for the quantitation of all field samples because all sample NO_3^- peak areas fell in the upper range of the calibration. The average instrumental LOD was determined to be 700 $\pm$ 300 pg ml^{-1}, making the IC method applicable to the ultra-trace analysis of NO_3^- in environmental samples. This translates into a time-integrated passive sampling method detection limit of 2 pptv $HNO_{3(g)}$ when sampling ambient air over a 30-day period or 72 pptv over a 24-hour period. NO_3^- contamination in the field blanks and reagent blanks was consistently below the NO_3^- concentration detected in all NL-BELT samples (Figure A-3). NO_3^- concentrations in the field blanks typically ranged from 5–50 ng ml^{-1}, and reagent blank NO_3^- concentrations ranged from 2–30 ng ml^{-1}. During the autumn and winter sampling periods when $HNO_{3(g)}$ mixing ratios were the lowest, NO_3^- in some of the field blanks represented up to 50% of the NO_3^- detected in the sample filter extracts.

2.4.2 Atmosphere-Biosphere Interactions Through $HNO_{3(g)}$ at the NL-BELT

2.4.2.1 Mixing Ratios and Trends in $HNO_{3(g)}$ Collected by Passive Sampling

The average $HNO_{3(g)}$ mixing ratios across the NL-BELT were in the few to tens of parts per trillion by volume (pptv) range (Figure 2-3). During all months but one, $HNO_{3(g)}$ mixing ratios were below 100 pptv. These observed mixing ratios of $HNO_{3(g)}$ are consistent with concentrations reported in European boreal ecosystems, in particular, those that are part of the NitroEurope network (Flechard et al., 2011). Further, at rural forested sites in Québec and Nova Scotia, mixing ratios of $HNO_{3(g)}$ were also quantified at the pptv-level (Zhang et al., 2009). The $HNO_{3(g)}$ quantities measured across the NL-BELT are also consistent with the output of a chemistry-climate model for the Newfoundland and Labrador region, which estimated that the $HNO_{3(g)}$ mixing ratios for the region would be below 300 pptv (Verbeke et al., 2015).

The comparability between the $HNO_{3(g)}$ mixing ratios determined across the NL-BELT with $HNO_{3(g)}$ quantities determined in similar ecosystems lends credibility to the $HNO_{3(g)}$ passive sampling methodology used in this work, particularly since active techniques were employed by Flechard et al. (2011) and Zhang et al. (2009) to make their $HNO_{3(g)}$ measurements . The consistency between these results suggests that the analyses of the nylon membrane filters, following strict quality assurance and quality control protocols, were sound. Further, given that the NL-BELT $HNO_{3(g)}$ mixing ratios were within the order of magnitude expected, this suggests that the calibration slope determined by Bytnerowicz et al. (2005) was reliable and representative of $HNO_{3(g)}$ quantities adsorbed to the nylon membrane filters across the NL-BELT.

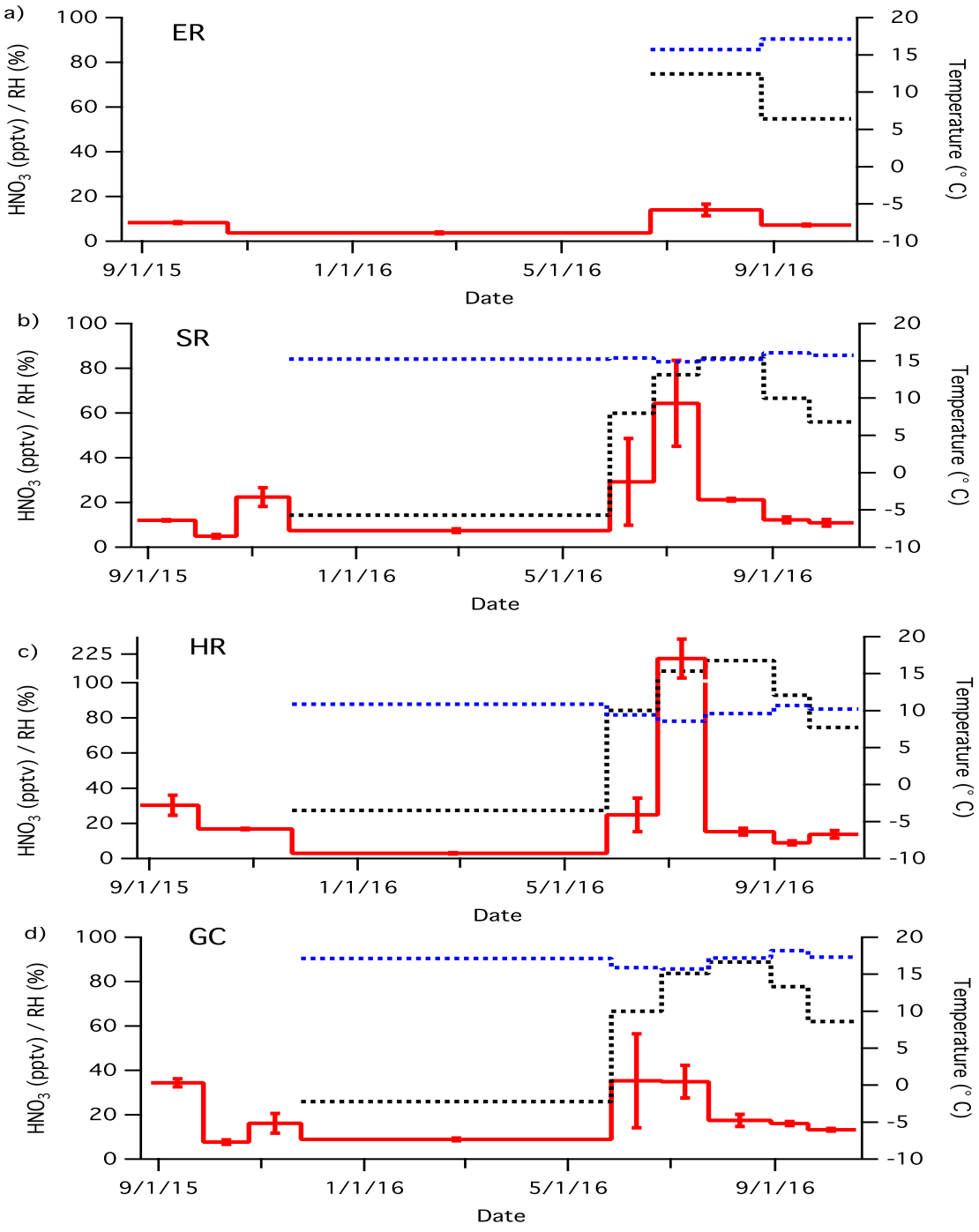

Figure 2-3. Time-weighted average $HNO_{3\,(g)}$ mixing ratios (red trace) and average air temperatures (dotted black trace) per sampling period in a) GC b) HR c) SR and d) ER from August 2015 to October 2016. The width of each bar represents the period over which the sample was collected. Error bars denote the standard error of triplicate samples collected within each site.

If the sensitivity and accuracy of this passive sampling method were indeed well founded, then this method would present a huge step forward in the remote sampling of $HNO_{3(g)}$. This method is capable of achieving the same spatial-scale measurements as the studies listed previously without the use of powered infrastructure and highly trained personnel. Further considerations in the accuracy of the $HNO_{3(g)}$ method and ensuing discussion is presented in Sect. 2.4.2.2.

The $HNO_{3(g)}$ mixing ratios observed at each site show a seasonal trend, with higher amounts and greater within site variation measured during the months of June and July. For example, at the GC site $HNO_{3(g)}$ mixing ratios were approximately 40 pptv in June and July of 2016, and this decreased to between 10 and 20 pptv during August, September and October, consistent with the measurements made in these same months in 2015. This seasonal trend observed in the mixing ratios does not follow the trend in increasing temperatures through the summer. Higher temperatures lead to higher diffusion and adsorption of $HNO_{3(g)}$ to the passive samplers, and would also suggest stronger actinic conditions, which would lead to higher steady-state quantities of the OH radical and thus $HNO_{3(g)}$ formation. Since no temperature-dependent trend is present (i.e. OH is not the limiting reagent) this suggests that the sampled concentrations are more emission or transport source-dependent with respect to precursor NO_x. There is likely still a slight temperature-dependent contribution present during these sampling periods, as diffusion and adsorption rates are slightly higher and OH production has been shown to be the highest in the summer months (Lelieveld et al., 2016), but it does not dominate the formation chemistry. Thus the $HNO_{3(g)}$ seasonality could result from i) differences in local biogenic NO_x production, ii) local transport of NO_x and $HNO_{3(g)}$, and/or iii) long-

range transport of NO_x and $HNO_{3(g)}$. The effect of temperature on the accuracy of passively sampled $HNO_{3(g)}$ concentrations is further discussed in Sect. 2.4.2.2 and the emission and transport hypotheses are discussed in more detail in Sect. 2.4.4.

There is no latitudinal trend of increasing or decreasing $HNO_{3(g)}$ between the three NL-BELT Newfoundland sites, and no monthly trends appeared to be consistent across both time and space. The observed $HNO_{3(g)}$ mixing ratios at the northernmost site in Labrador (ER) were, however, consistently lower than all three of the Newfoundland sites. It is also noteworthy that in the month of July 2016 there was an average mixing ratio of 213 pptv sampled at the HR field site, which is an order of magnitude higher than all other sampling periods. The HR site is the closest field site to a town (Corner Brook, population: 20000 people, density: 80 people per km^2), and during the month of July 2016 tourism in the province is high (Department of Tourism, 2016), which may have had an influence on increasing local commuter traffic, use of fireworks, and campfires near the HR site, which could release precursor NO_x (Müller, 1992). However, it is not possible to assign a definitive cause for this high $HNO_{3(g)}$ measurement since the samples represent a time-integrated monthly average and the available supporting measurements from the atmospheric monitoring program do not provide tracer evidence towards assigning such types of sources.

2.4.2.2 Considerations Regarding the Accuracy of Calculated $HNO_{3(g)}$

Potential limitations of a controlled lab-based calibration in determining real-world atmospheric $HNO_{3(g)}$ mixing ratios include the effects of relative humidity, particulate matter, temperature, and wind on $HNO_{3(g)}$ uptake to the nylon passive sampling filters.

For example, Bytnerowicz et al. (2005) found that calibrations in ambient air were 30 % less efficient and suggested that this was likely due to $HNO_{3(g)}$ uptake on adsorbed water or particulate matter to the PTFE filter mounted over the nylon filter. As a result of these previous observations, the potential limitations of employing a controlled calibration to determine real-world observations were assessed to enable more accurate interpretation of the results from this study.

Firstly, the controlled calibration performed by Bytnerowicz et al. was performed in < 1% RH clean air and therefore the determined uptake rate may not be representative of the $HNO_{3(g)}$ uptake across the NL-BELT, where average RH values were between 80 and 90% (Figure 2-3). Filter packs exposed to high humidity's such as these have been shown to incur $HNO_{3(g)}$ losses to the PTFE filter of up to 60% (Padgett, 2010). Thus, the elevated RH in our study sites may lead to $HNO_{3(g)}$ adsorption to water (or particulate matter entrained in the water) on the PTFE filter and negatively bias the results by up to 60% (Figure 2-4). To test whether $HNO_{3(g)}$ adsorption to the PTFE filters had occurred, the PTFE filters were extracted and analyzed for their NO_3^- content. The PTFE filter extract analysis showed that during most sampling periods across the NL-BELT sample particulate/adsorbed nitrate quantities were not statistically different from the nitrate quantities observed in the PTFE filter field blanks. When the PTFE filter nitrate quantities exceeded those in the field blanks, the nitrate quantities in the extracts were on average ten times less than the quantities measured in the nylon filter extracts for the given month. This indicates that $HNO_{3(g)}$ mixing ratios measured during most sampling periods were likely only negatively biased by 15% or less.

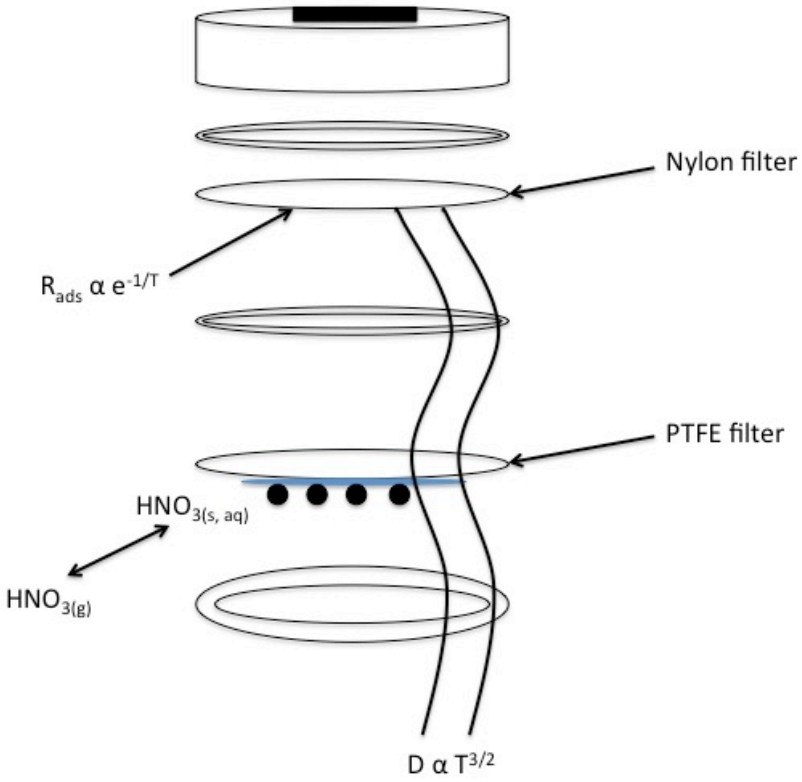

Figure 2-4. Schematic of potential effects of temperature, relative humidity and particulate concentrations on $HNO_{3(g)}$ uptake to the nylon filters.

During the months of November 2015, September 2016, and October 2016, however, nitrate quantities in the PTFE filter extracts were half the amount measured in the nylon filter extracts, indicating that the $HNO_{3(g)}$ quantities measured during these months may have been negatively biased by up to 33%. Taking these biases into account, the $HNO_{3(g)}$ mixing ratios at some sites across the NL-BELT are likely underestimated by about 10 – 33%, however these biases are not large enough to impact the seasonal and latitudinal trends observed within the data.

Another assumption made when calculating the $HNO_{3(g)}$ mixing ratios using the controlled calibration is that no temperature effects exist. The calibration performed by Bytnerowicz et al. (2005) was conducted at a single temperature, and therefore the temperature-dependence of the sampler uptake is unknown. The processes of diffusion (D; $cm^2\ s^{-1}$) and adsorption (R_{ads}; s^{-1}) are known to be temperature-dependent (Figure 2-4). Equation 2-5 shows the temperature dependence of diffusion based on the Chapman-Enskog theory, while E2-6 describes the temperature-dependence of adsorption via its Arrhenius rate constant relationship. According to E2-5, the rate of diffusion of gases will increase by 10% when air temperature rises from 0 to 20 °C, assuming *ceteris paribus* conditions.

(E2-5) $D \alpha T^{3/2}$

(E2-6) $R_{ads} \alpha e^{-1/T}$

Therefore, since the data is not corrected for the varying temperatures across the NL-BELT calculated absolute $HNO_{3(g)}$ mixing ratios and fluxes might have an additional 10% error when making comparisons between the coldest and hottest months. Again, this is expected to be a systematic offset across all the NL-BELT sites since relative temperature differences between the NL-BELT sites were minimal within any sampling period. For example, average temperatures at all the island sites were within 5 °C of one another during each monthly sampling period in 2016 (Figure 2-3). With this 5 °C range, gas diffusion rates will vary only by approximately 2%, which is well-within the replicate

sample standard error for any NL-BELT region and is therefore negligible when making comparisons between sites for the same sampling period.

Controlled calibrations with consistent air turnover also do not reflect wind turbulence experienced in ambient conditions. This may have a considerable impact on the adsorbed $HNO_{3(g)}$ concentrations across the NL-BELT where winds readily exceed 100 km hr^{-1} (Historical Climate Data, 2017), which is atypical for most parts of North America. However, the selection of sampling sites within 15 m clearings within the experimental stands provides a significant reduction in local wind speeds, while maintaining connectivity between the sampling site and atmosphere. Coupled with the sampler weatherproof enclosure, the effects of wind on sampling bias are assumed to be minimal as the combination should keep the air entering the sampler at a diffusion-based regime.

To further confirm whether the determined $HNO_{3(g)}$ mixing ratios using the controlled calibration were reasonable, steady-state $HNO_{3(g)}$ mixing ratio approximations were performed using measured NO_x values and representative parameterizations of local conditions at the field sites that were not explicitly measured. The results of this approximation indicated that the converted $HNO_{3(g)}$ mixing ratios using the controlled calibration were indeed indicative of the potential production of real-world $HNO_{3(g)}$ mixing ratios. The steady-state approximation results are discussed in more detail in Sect 2.4.4.2.

The greatest source of error in our $HNO_{3(g)}$ measurements is, therefore, loss of the analyte to the PTFE filter at high RH. Given the systematic nature of this loss at all sampling locations, and the likely minimal effects of temperature, wind speed, and

particulate matter, the interpretation of the $HNO_{3(g)}$ relative amounts and trends should be considered sound. In the future, in order to get a better representation of absolute $HNO_{3(g)}$ mixing ratios and reduce uncertainties, controlled laboratory calibrations that are more reflective of NL-BELT conditions should be performed in addition to side-by-side comparisons with active $HNO_{3(g)}$ sampling techniques.

2.4.2.3 Reusability of Nylon Membrane Filters for Passive Sampling of $HNO_{3(g)}$

The reusability of the nylon membrane filters has not been reported in previous studies and was tested here to evaluate the potential to decrease cost and waste associated with passive sampling of $HNO_{3(g)}$. Since the filters sample through a sorption based process, and not reactive uptake, it is expected that the nylon membrane filters would be relatively unchanged from their original state after extraction since this process is the same as the filter preparation process (Section 2.3.4.1). The mixing ratios measured by the new and reused filter packs installed for 2 weeks in December 2016 in St. John's, in eastern Newfoundland, were 33 $\pm$ 4 and 34 $\pm$ 7 pptv, respectively. Although the samplers were installed in an urban environment, these low mixing ratios are consistent with what would be expected during the winter when actinic conditions are minimized and OH production in the troposphere is slow. These lower $HNO_{3(g)}$ mixing ratios are also very similar to the magnitude of the remote concentrations sampled along the NL-BELT and are therefore suitable for assessing the reusability of these filters in a remote environment with low levels of $HNO_{3(g)}$. Using a t-test comparison of two means, the measured quantities were determined to have no statistical difference at the 99% confidence interval. The relative standard deviation between the used nylon membrane filter packs,

however, was double that of the new filter packs. Thus, although the used filters showed high accuracy, they were less precise than the new nylon filters. The lower precision in the used filters may result from physical degradation of the nylon filters during the extraction and sonication processes or be within the natural variability of the small population of tested filters (n = 5). In the former case, Liu et al. (2015) found that sonicating polypropylene for more than 5 minutes led to decreases in the polypropylene intrinsic velocity and high-molecular-weight portions. If such shifts in the physical properties of the nylon polymer had also occurred, this could have lead to more heterogeneity in the filters, and thus caused the increased variance in its effective uptake rate. Overall, the finding of this experiment suggests that nylon filters may be re-cleaned and reused for passive sampling in remote ecosystems, so long as replicates are deployed to capture $HNO_{3(g)}$ with analytical precision.

2.4.3 Annual Fluxes of $HNO_{3(g)}$ to the NL-BELT

Determining the dry deposition flux of $HNO_{3(g)}$ to the NL-BELT is essential for constraining the total inputs of nitrogen across these remote ecosystems. Zhang et al. (2009) determined that the dry deposition flux of $HNO_{3(g)}$ in Canada can constitute anywhere between 20 to 80% of the total dry deposition flux of particulate and gaseous nitrogen species to rural and remote forested sites. Further, across the NitroEurope network, $HNO_{3(g)}$ and $NH_{3(g)}$ were identified as the dominant dry deposition inputs, often exceeding the dry deposition of particulate nitrogen.

A wide range of values reported in the literature for the V_d of $HNO_{3(g)}$ make it difficult to constrain annual fluxes across the NL-BELT. The R_a and R_b terms in Equation

2-4 are well characterized for $HNO_{3(g)}$ and few differences in their parameterizations exist between dry deposition models (Flechard et al., 2011; Hicks and Liss, 1976; Wesely and Hicks, 2000;). However, varying parameterizations in the R_c terms from model to model largely explains the variation in deposition velocities for $HNO_{3(g)}$ reported in the literature (Finlayson-Pitts and Pitts, 2000; Flechard et al., 2011; Verbeke et al., 2015; Zhang et al., 2009). In this work we employ a V_d of 3 ± 1 cm s^{-1} to calculate the annual fluxes of $HNO_{3(g)}$ to the NL-BELT sites. This V_d range is the average modeled deposition velocity output from four commonly used modules employed in chemical transport models across Europe and North America. Specifically this modeled value is representative of spruce and pine dominated forests in Europe (Flechard et al., 2011) and should apply well to other coniferous needle forest types including the balsam fir dominated stands of the NL-BELT. These average modeled V_d values were also based upon field-scale measurements of meteorology and turbulence, and did not rely on model predictions for these two parameters. The range of V_d values reported by Flechard et al. (2011) are much higher than those modeled at forested sites across Canada (0.61 – 2.11 cm s^{-1}) and that estimated for Newfoundland and Labrador by Verbeke et al. (2015) using the LMDz-INCA global chemistry-climate model (0.8 – 1.6 cm s^{-1}) (Verbeke et al., 2015; Zhang et al., 2009). The discrepancy in the V_d range reported for Canadian ecosystems likely results from the parameterization of the deposition model used to estimate V_d and not necessarily results from differences in forest surface areas between the Canadian and European sites. This was demonstrated by Flechard et al. (2011) where they show that the deposition model used for the Canadian forest ecosystems systematically estimated V_d values lower than the other models used in their inter-comparison. Therefore, employing a higher V_d range

(ie. 2-4 cm s^{-1}) is likely more representative of the NL-BELT ecosystems because the model analysis used to obtain this range is more robust. To ensure there were also no discrepancies between the surface areas at the NL-BELT and those used to model the V_d for $HNO_{3(g)}$ across the NitroEurope sites, leaf area indices (LAI) were inter-compared. The LAI values at the GC site were previously reported to range from 3-4 m^2 m^{-2} (Xinbiao Zhu, personal communication, April 24, 2017), which is similar to the LAI range for the Spruce and Pine forests (LAI average 3-5 m^2 m^{-2}) modeled in the NitroEurope network (Flechard et al., 2011). Thus, using a V_d of 3 $\pm$ 1 cm s^{-1} to estimate fluxes to the NL-BELT appears suitable based on the current state of knowledge and the error (30%) considered here makes comparison of the calculated fluxes conservative.

The estimates of the $HNO_{3(g)}$ annual fluxes as mass of N to each site further indicate that there were no latitudinal trends in this nitrogen input to these forests. The fluxes of $HNO_{3(g)}$ as N to each site estimated with a V_d of 3 cm s^{-1} were 10 $\pm$ 1, 16 $\pm$ 2, 9 $\pm$ 1, and 3.6 $\pm$ 0.3 mg N m^{-2} yr^{-1} at GC, HR, SR and ER, respectively (Figure 2-5). The error in the fluxes (black error bars) was calculated using the sum of squares approach carrying forward the standard errors from the observed mixing ratios. The largest annual flux at HR was driven by the single high $HNO_{3(g)}$ measurement in July 2016. If the $HNO_{3(g)}$ mixing ratio for the month of July were replaced using the average $HNO_{3(g)}$ mixing ratio between June and August of 2016, the calculated flux would be 10 $\pm$ 1 mg N m^{-2} yr^{-1}. Under such a constraint, where a local source event may have been present, without it there would be no statistical difference between GC, HR and SR at the 95% confidence level using a t-test comparison of means. Treating the July measurement as an outlier under these circumstances allows for a broader understanding of the long-term

biogeochemical cycling of reactive nitrogen across the NL-BELT. These fluxes, like the mixing ratios, are consistent with what has been reported in European boreal ecosystems as well as in rural Canadian forests (Flechard et al., 2011; Korhonen et al., 2013; Zhang et al., 2009). Fluxes of $HNO_{3(g)}$ across the NitroEurope network ranged from 20 to 600 mg N m^{-2} yr^{-1} (Flechard et al., 2011), while fluxes across 8 Canadian rural forests ranged from 20 to 80 mg N m^{-2} yr^{-1} (Zhang et al., 2009). The $HNO_{3(g)}$ fluxes reported in this work were within the same order of magnitude as these previous reports but did not exceed 20 mg N m^{-2} yr^{-1} at any site, which is consistent with the remote location of these forests relative to precursor emission regions.

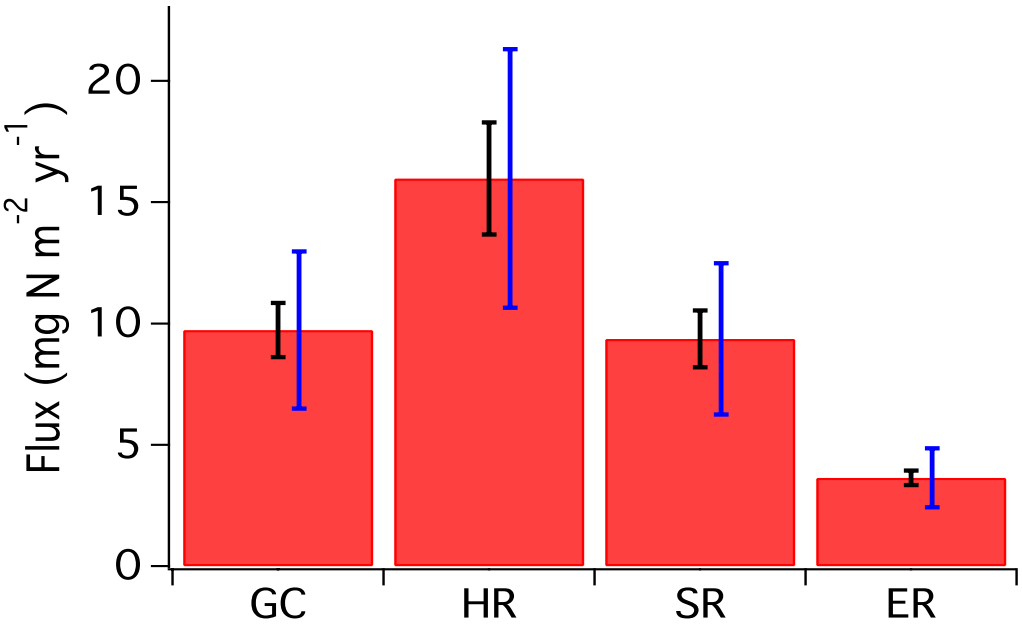

Figure 2-5. Annual flux of $HNO_{3(g)}$ as N to the NL-BELT field sites from August 2015 to August 2016 calculated using a deposition velocity of 3 cm s^{-1}. The black error bars represent sum of squares of the triplicate standard error in mixing ratios and the blue error bars represent the variability in the flux calculated by considering depositional velocity (V_d) may range from 2 – 4 cm s^{-1} in these forests.

The potential range of error in annual fluxes estimated using the upper and lower bounds of V_d range from 2 – 4 cm s^{-1} reported by Flechard et al. (2011) was compared to the observations in order to test the sensitivity of the calculated fluxes with respect to the precision of the measurements (Figure 2-5). The range of potential V_d values is a larger potential uncertainty than the within-site spatial variability suggesting that the range of deposition velocities considered here is indeed likely a conservative approach in quantifying and representing uncertainty in regional fluxes (Figure 2-5). Variability in deposition velocity may contribute to the regional or local error observed in the annual $HNO_{3(g)}$ - fluxes. For example, local-scale differences in turbulence will affect the measured $HNO_{3(g)}$ mixing ratios, as well as the V_d for $HNO_{3(g)}$.

Overall, taking the uncertainty in flux estimates resulting from the variability in V_d, triplicate passive samples standard error, and uncertainty in converting chromatographic values into mixing ratios (Sect 2.4.2.2) into account, the determined $HNO_{3(g)}$ fluxes are within the same order of magnitude as the other N_r fluxes of $NO_{(g)}$, $NO_{2(g)}$, and $NH_{3(g)}$ that have been reported at the NL-BELT sites (Trevor VandenBoer, personal communication, March 1, 2017). This lends credibility to the measurements and suggests that the assumptions made when converting measured NO_3^- concentrations to $HNO_{3(g)}$ fluxes were sound. The $HNO_{3(g)}$ flux into the GC, SR and ER field sites represented 11 – 13% of the total dry deposition N_r flux into these systems, indicating that it is an important source of reactive nitrogen. The largest dry deposition fluxes of N_r into these NL-BELT forest sites, however, were $NO_{(g)}$ followed by $NH_{3(g)}$, which represented

64 – 70% and 17 – 24% of the total N_r dry deposition flux, respectively (Trevor VandenBoer, personal communication, March 1, 2017).

2.4.4 Assigning a Source of Measured $HNO_{3(g)}$

2.4.4.1 Air Mass Back-Trajectory Analysis and Geographical Sector Assignment

The use of air mass transport models in understanding atmospheric observations is a commonly employed interpretation technique and has been reviewed in detail by Fleming et al. (2012). Air mass back trajectories have previously been employed to assign geographical sectors for the origin of air masses for long-term *in situ* ground-level measurements in Ireland (Mace Head), Canada (Alert, Nunavut) and the U.S.A. (Barrow, Alaska) (Sharma et al., 2006; Simmonds et al., 1997). Geographical sector analysis allows one to tease apart whether observed concentrations are influenced by factors such as anthropogenic vs. biogenic or short-range vs. long-range pollutant transport.

The air mass back trajectory parameters employed in this work were carefully selected and tested before the HYSPLIT model was run for the NL-BELT field sites (Fleming et al., 2012; Rolph, 2017; Sharma et al., 2006; Simmonds et al., 1997; Stein et al., 2015). The GDAS meteorological data set was chosen because it was 1 of 2 data sets that encompassed the NL-BELT region, and was the most common data set employed in the literature (Fleming et al., 2012). A sensitivity test was performed to determine whether trajectory arrival height influenced geographical sector assignment to the NW, NE, SE and SW sectors by varying the back trajectory arrival heights to 0, 10 and 100 meters. The test showed that arrival height had no influence on the quantitative back trajectory analysis, and therefore an arrival height of 0 m was chosen based on the

installment location of the $HNO_{3(g)}$ passive samplers. Trajectories were initiated every 3 hours to increase the number of data points and to reduce bias. This parameter was selected based on previous studies where back-trajectories were initiated every 6 hours for the long-term study of pollutant transport (Sharma et al., 2006; Simmonds et al., 1997). Finally, each trajectory that was initiated every 3 hours was run 5 days backwards to determine if there was the potential influence of long-range transport on the $HNO_{3(g)}$ observations. This parameter was set because the HYSPLIT program limited frequency back trajectories to a maximum of 5 days and also because it is known that running a trajectory 7-10 days backwards leads to very high uncertainty in air mass origin (Rolph, 2017; Stein et al., 2015).

The sample frequency plot outputs from the HYSPLIT back-trajectory model (Figure 2-6) suggested that a majority of the air masses arriving at all four sites originated from continental North America. The percentage distribution of air mass back trajectories shown in these frequency plots was calculated by dividing the number of trajectory end point outputs in each 1° x 1° grid square by the total number of trajectories run during the simulation. Although these frequency plots allow for a qualitative geographical sector assignment of where the air masses arriving at each of the NL-BELT sites may be coming from during a given sampling period, it does not quantitatively assess month to month and site to site differences regarding air mass origin. Therefore, assignment of air mass percentages arriving from the NE, NW, SW and SE sectors was performed (Table A-1).

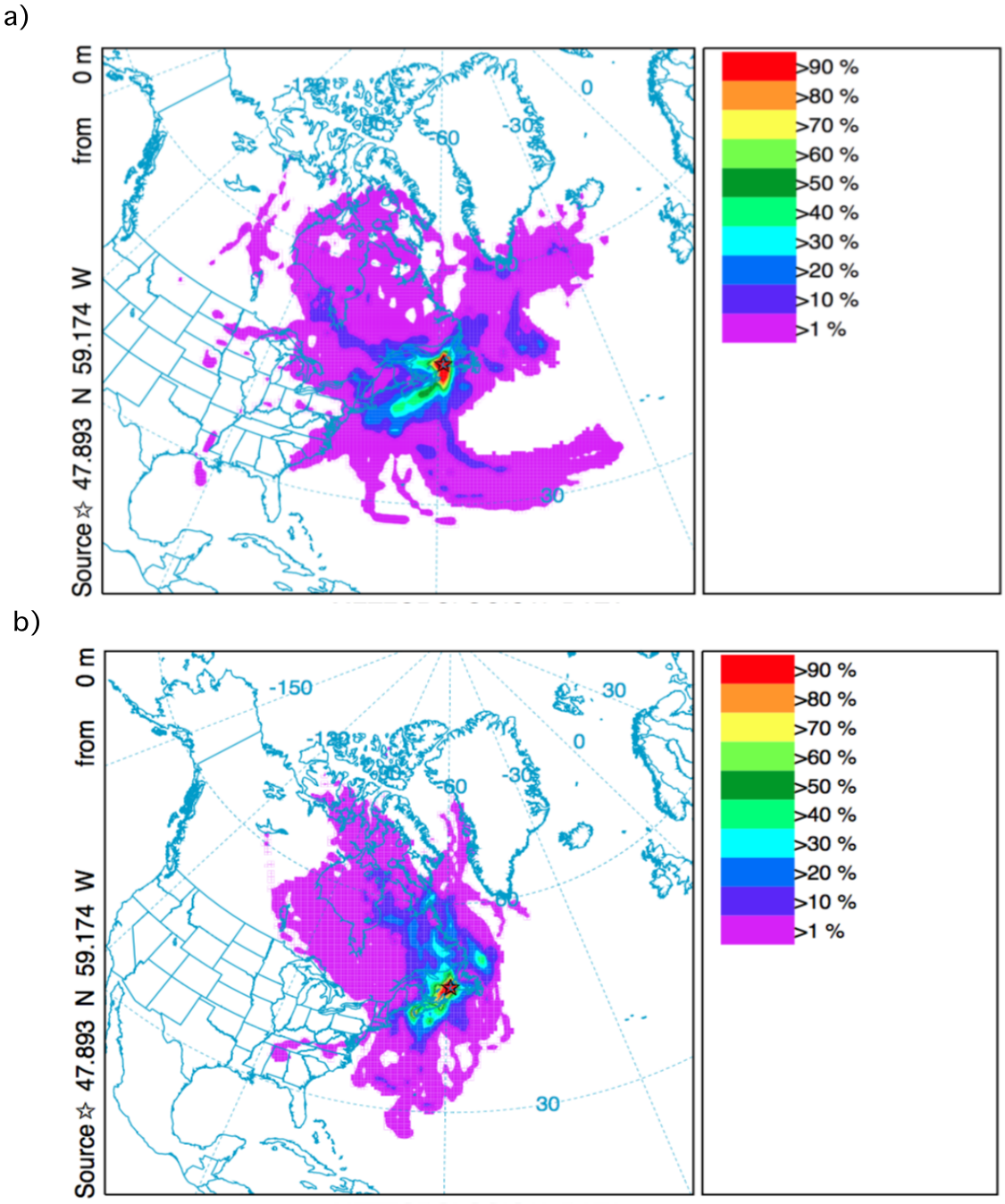

Figure 2-6. Example HYSPLIT model output frequency plots for distribution of air masses arriving at GC during the months of a) July 2016 and b) September 2016. The percentage distribution of air mass back trajectories is calculated by dividing the number of trajectory end point outputs in each 1° x 1° grid square by the total number of trajectories run in the simulation.

For each field site across NL-BELT, on any given month the arriving air masses predominantly originated from the NW and SW sector (Table A-1). This is consistent with what would be expected from the prevailing westerlies, winds with a west to east trajectory across North America. These winds are also known to intensify in the fall (Jacob, 1999), and this seasonal effect is clearly evident (Table A-1) where the percentage of air masses arriving from the NW and SW sectors dominates during the months of October and September in both 2015 and 2016, over earlier months.

For the final step of geographic sector assignment, the $HNO_{3(g)}$ mixing ratios for the Newfoundland island sites were correlated with the geographic sector percentages to determine whether a trend existed between observed $HNO_{3(g)}$ concentrations and the geographic quadrants. In general, a very weak to weak linear correlation between $HNO_{3(g)}$ mixing ratios and air mass history was observed across all Newfoundland island regions ($r^2 = 0.02 – 0.68$; Table 2-1). Even when air mass history was interpreted solely between the East and West sectors, there was still a weak linear correlation ($r^2 = 0.40 – 0.60$).

Table 2-1. Descriptive statistics for correlations between air mass source regions and measured concentrations of $HNO_{3(g)}$ at each site. The coefficient of determination (r^2) describes the strength of fit using a linear regression between two sets of data. The Spearman's rho (ρ) describes the directionality of the correlation and describes the strength of fit when using any appropriate monotonic function to fit the data.

	Grand Codroy				**Humber River**				**Salmon River**			
	NE	**SE**	**SW**	**NW**	**NE**	**SE**	**SW**	**NW**	**NE**	**SE**	**SW**	**NW**
r^2	0.34	0.28	0.18	0.50	0.13	0.02	0.35	0.39	0.68	0.20	0.20	0.57
ρ	0.68	0.61	0.48	-.85	0.18	0.67	0.29	-.61	0.72	0.52	-.07	-.45
r^2	0.40		0.40		0.07		0.07		0.60		0.60	
ρ	0.89		-0.89		0.43		-0.43		0.83		-0.83	

Conversely, the Spearman's rho (ρ) values determined for the correlation between the geographical sectors and sampled mixing ratios shows a stronger relationship between air mass history and atmospheric observations (Table 2-1). This is particularly evident when geographical sectors are divided into East and West, where the value of ρ exceeds 0.8 for Grand Codroy and Salmon River. Furthermore, the Spearman's rho values indicate that there is a negative association between the measured mixing ratios and air masses arriving from the West. This finding suggests that the long-range transport of $HNO_{3(g)}$ and its precursor gases from continental North America is not the dominant source of the observed $HNO_{3(g)}$. This is consistent with $HNO_{3(g)}$ being rapidly dry deposited with a lifetime of < 24 hours once emitted into the atmosphere (Finlayson-Pitts and Pitts, 2000). This suggests that increases in $HNO_{3(g)}$ deposition at these sites is associated either with short-range transport of air masses, local emissions of $NO_{2(g)}$ and $NO_{(g)}$ that are reacting to form the measured quantities of $HNO_{3(g)}$, and/or the down welling and decomposition of PANs. The short-range transport of air masses would be originating from the Central and Avalon Peninsula regions of Newfoundland, where approximately half the provincial population resides (≈250000 people), with anthropogenic emissions of NO_x from fossil fuel use in urban centers, industry, and transport. This would be consistent with the positive correlations between $HNO_{3(g)}$ mixing ratios and the winds originating from the East listed in Table 1. Local emission of NO_x, on the other hand, would likely result from local biogenic emissions from nitrifying and denitrifying bacteria in the soils of the Balsam fir-dominated stands (Sutton et al., 2011). A study conducted in Saxony, Germany found that agricultural and forest soil NO_x emissions on average represented up to 13% of total NO_x emissions in an area heavily

populated with industry (Molina-Herrera, 2017). Furthermore, in rural areas of Saxony soil NO_x contributed up to 98% of the total NO_x emissions (Molina-Herrera, 2017) demonstrating the potentially dominant role of biogenic emission sources of NO_x in explaining observations in remote ecosystems. The down welling of PANs from the upper troposphere may also contribute to the measured $HNO_{3(g)}$ mixing ratios (R2-7). This could represent a new source of nitrogen to the ecosystems from $NO_{2(g)}$ emissions hundreds to thousands of kilometers away, since PANs are thermally stable in the upper troposphere for long periods of time.

The short-range transport, local production, and decomposition of PAN may all contribute to $HNO_{3(g)}$ formation across the NL-BELT, however wind sector analysis alone is unable to assign a distinct source mechanism. To complete the source apportionment of the measured $HNO_{3(g)}$ mixing ratios, one must investigate the known chemistry that occurs in the atmosphere. With the aid of supporting measurements of $NO_{(g)}$, $NO_{2(g)}$ and $O_{3(g)}$ across the NL-BELT, the $HNO_{3(g)}$ sources and their relative contribution may be resolved.

2.4.4.2 Steady-State Approximation of Locally-Derived $HNO_{3(g)}$

To determine if local biogenic emission sources of NO_x could explain the measured $HNO_{3(g)}$ mixing ratios a chemical box model approach was used (Figure 2-7).

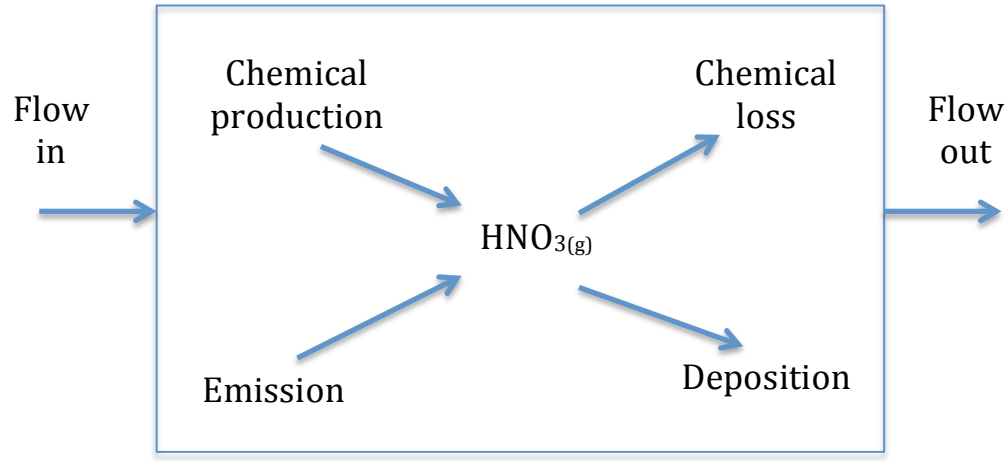

Figure 2-7. Conceptual schematic of the chemical box model employed for calculating abundance of $HNO_{3(g)}$ across the NL-BELT derived from known atmospheric chemical mechanisms of formation and loss.

A steady-state mass balance equation for $HNO_{3(g)}$ can be created assuming that the sum of sources of $HNO_{3(g)}$ to the atmosphere equals that of its sinks (Jacob, 1999). Since the hypothesis being tested is that local NO_x emissions are responsible for observed $HNO_{3(g)}$ mixing ratios, the advection terms in Figure 2-7 are assumed to be zero. Also, since $HNO_{3(g)}$ is formed in the atmosphere from precursor gases, there is no emission term in the steady-state calculation. Under these assumptions, the terms in E2-7 can be solved to estimate a steady-state $HNO_{3(g)}$ mixing ratio.

(E2-7) Σ Chemical production = Σ Chemical loss + Σ Deposition

The chemical production and loss processes in E2-7 are governed by kinetic chemical lifetimes. For first order reactions, lifetimes are calculated as the inverse of the reaction

rate constant (k^{-1}). With higher order rate constants the amount of reactant present as well as the rate constant dictate the chemical's lifetime. Chemical reactions that occur on the shortest timescales will dominate the production and loss processes.

The chemical production of $HNO_{3(g)}$ in the atmosphere occurs via R2-1 to R2-4 (Sect. 2.2). For the purposes of $HNO_{3(g)}$ formation across the NL-BELT it is assumed that R2-1 will be the main formation process. R2-1 occurs during the daytime when $OH_{(g)}$ radical concentrations are highest, while R2-2 to R2-4 proceed during the night due to the rapid photolysis of $NO_{3(g)}$ under actinic (i.e. sunlit) conditions (Wayne et al., 1991). At the NL-BELT sites R2-2 through R2-4 are expected to be negligible due to small mixing ratios of $O_{3(g)}$ and comparably high mixing ratios of $NO_{(g)}$ leading to the loss of $NO_{3(g)}$ (R2-8).

(R2-8) $NO_{(g)} + NO_{3(g)} \rightarrow 2NO_{2(g)}$

$NO_{(g)}$ concentrations are present at mixing ratios from 100 – 500 pptv at the NL-BELT sites (Trevor VandenBoer, personal communication, April 12, 2017). It is well documented that $NO_{(g)}$ and $NO_{3(g)}$ do not coexist at high concentrations (De More et al., 1997). This is because $NO_{3(g)}$ will react with this $NO_{(g)}$ to form $NO_{2(g)}$ in seconds, shutting down R2-3 and R2-4. Furthermore, at $O_{3(g)}$ levels of 14 - 20 ppbv, levels measured across the NL-BELT (Trevor VandenBoer, personal communication, May 24, 2017), $NO_{2(g)}$ would have a lifetime of > 20 hours ($k_2 = 3.2 \times 10^{-17}$ cm^3 $molecule^{-1}$ s^{-1}, De More et al., 1997) with respect to R2-2. Therefore, the assumption that the chemical

production of $HNO_{3(g)}$ will mainly proceed through R2-1 at the four NL-BELT field sites is justified.

The chemical loss of $HNO_{3(g)}$ in the atmosphere occurs through its oxidation and photolysis (R2-9 and R2-10).

(R2-9) $HNO_{3(g)} + OH_{(g)} \rightarrow H_2O_{(g)} + NO_{3(g)}$

(R2-10) $HNO_{3(g)} + h\nu \rightarrow OH_{(g)} + NO_{2(g)}$

These reactions occur very slowly in the troposphere and are not expected to be dominant loss processes across the NL-BELT. $HNO_{3(g)}$ has a lifetime with respect to oxidation and photolysis of over 50 days ($k_9 = 1.1 \times 10^{-13}$ cm^3 molecule^{-1} s^{-1}, $k_{10} = 1 \times 10^{-7}$ s^{-1}) under atmospheric conditions expected across the NL-BELT (De More et al., 1997). This indicates that deposition will be the dominant sink of $HNO_{3(g)}$ from the atmosphere due to its high dry deposition velocity discussed in the previous section, with a lifetime of < 20 hours in the atmospheric boundary layer. Thus, the chemical loss term from E2-7 can be eliminated and the final equation can be rewritten as E2-8 shown below:

(E2-8) $[NO_{2(g)}][OH_{(g)}]k_1 = [HNO_{3(g)}]z^{-1}V_d$

The deposition of $HNO_{3(g)}$ will occur as a function of the atmospheric boundary layer height (z) and V_d, and the formation of $HNO_{3(g)}$ will occur as a function of the number density of $NO_{2(g)}$, $OH_{(g)}$, and a formation rate constant (k_1). By rearranging this equation and substituting in measured values or estimates from the literature the potential upper

and lower limits on locally produced quantities of $HNO_{3(g)}$ can be determined. The value for the mean marine boundary layer height (z) is difficult to constrain, and can vary between 300 and 2000 m on any given day (Carpenter et al., 2010; Norton et al., 2006). The values for the mean boundary layer height across the NL-BELT were estimated to be 1200 $\pm$ 300 based on the typical boundary layer height observed in Mace Head, Ireland, an island that is also located in the marine North Atlantic boundary layer (Norton et al., 2006). The distribution of $OH_{(g)}$ as a function of latitude and season has been extensively modeled by Lelieveld et al., (2016), and based on their work a value of $10 \pm 2 \times 10^5$ molecules cm^{-3} is representative for the months of June, July, and August, and $5 \pm 1 \times 10^5$ molecules cm^{-3} for September and October. The rate k_1 was calculated to be $1.1 + 0.1 \times 10^{-11}$ molecules^{-1} cm^3 s^{-1} using recommended values at 1 atm, and 285 $\pm$ 3 K (De More et al., 1997). Finally, the concurrent measurements of $NO_{2(g)}$ being made at the field sites were used to estimate $HNO_{3(g)}$ formation rates at the field sites (Table 2-2). To test the local emissions hypotheses, it is assumed that the measured $NO_{2(g)}$ mixing ratios at the field sites arise from local NO_x soil emissions and/or local anthropogenic emissions.

Using the 2016 sampling period at GC as a case study, the measured $HNO_{3(g)}$ mixing ratios have been compared against the calculated $HNO_{3(g)}$ values in Figure 2-8.

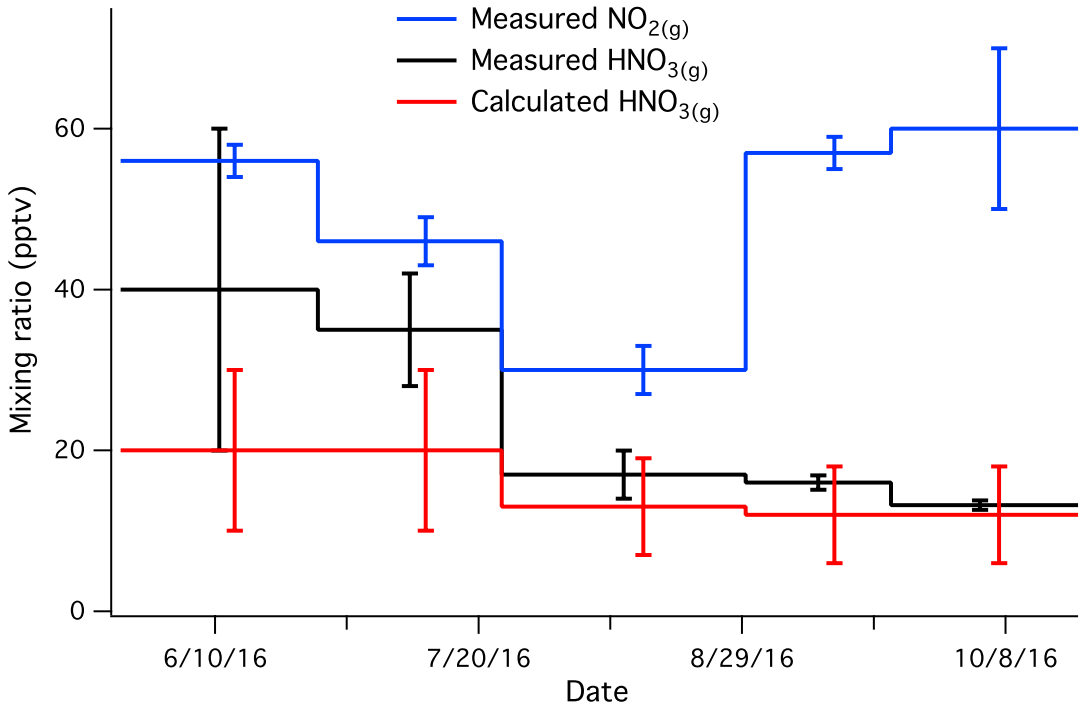

Figure 2-8 Measured $NO_{2(g)}$ (blue trace) and $HNO_{3(g)}$ (black trace) mixing ratios, and calculated $HNO_{3(g)}$ (red trace) mixing ratios using a steady-state approximation, for GC in the summer of 2016. The error bars for the measured $NO_{2(g)}$ and $HNO_{3(g)}$ mixing ratios represent the standard error in triplicate measurements. The error bars for the calculated $HNO_{3(g)}$ mixing ratios represent the propagation of uncertainty when calculating the mixing ratios.

As the months progress from June to October, it seems that the measured $NO_{2(g)}$ concentrations can photochemically generate a greater proportion of the measured $HNO_{3(g)}$ concentrations. This is consistent with the trend observed with the wind sector analysis, where more 'clean' air masses on average are arriving from the west later in the summer, likely resulting in the NL-BELT sites being impacted only by local emissions. Thus, the $HNO_{3(g)}$ concentrations measured in September and October may be attributed mainly to local NO_x emissions, as the winds continue predominantly from the west.

Under the steady-state assumption outlined above it seems as if the calculated $HNO_{3(g)}$ mixing ratios are unable to account for the measured $HNO_{3(g)}$ concentrations during the months of June and July 2016. Therefore, it is possible that $HNO_{3(g)}$ formation is occurring via either short-range or long-range transport of $NO_{2(g)}$ to the GC site. The short-range transport and formation of $HNO_{3(g)}$ is consistent with a greater contribution of air masses arriving from the east in the months of June and July. However, although long-range transport trends of $NO_{2(g)}$ from continental North America are inconsistent with the wind sector analysis, the down welling and decomposition of PAN to $NO_{2(g)}$ cannot be discounted. The transportation of PAN to Newfoundland and Labrador was modeled to be the highest in the springtime, when thermal conditions are optimized for its transport (Fischer et al., 2014). Sources of PAN to the atmosphere from anthropogenic emissions, biomass burning, and lightning have also shown to be greater in the springtime and early summer (Fischer et al., 2014). They modeled PAN mixing ratios in the top 2 km of the Newfoundland and Labrador region during spring and early summer to be 300 – 400 pptv, which with even partial thermal decomposition, could easily account for the missing quantity in our $HNO_{3(g)}$ formation calculations. Further, modeled PAN mixing ratios drop during later summer and fall months (Fischer et al., 2014), consistent with the reduction in discrepancy between our chemical box model and the observations. This lends support to the hypothesis that PAN may be contributing to $HNO_{3(g)}$ formation across NL-BELT during the spring and early summer.

While the calculated steady-state $HNO_{3(g)}$ mixing ratios have allowed for a more accurate source–apportionment of the measured $HNO_{3(g)}$, the approach used contained multiple assumptions, namely a wide range of potential uncertainty in any unmeasured

terms. Thus the steady-state source–apportionment must be interpreted qualitatively relative to the replicate observations. Statistical evaluation of similarity between replicate measures against calculated values with uncertainty derived from broad approximations would be an invalid comparison, and so were not performed. Further, since only data from one field site was used in this case study, it is hard to draw broad conclusions for $HNO_{3(g)}$ seasonal formation across the NL-BELT. Given this, not only did the calculated $HNO_{3(g)}$ mixing ratios fall within the same order of magnitude as the measured values but they also helped explain the observed seasonality despite the many chemical assumptions made. Overall, it can be concluded that most of the observed $HNO_{3(g)}$ at the GC location of the NL-BELT appears to be derived from local NO_x emissions, most likely from soil microbial processes, with contributions from long-range transport of PANs or regional transport of $HNO_{3(g)}$ from central and eastern Newfoundland in the spring and early summer.

2.5 Conclusions

Sorption-based nylon membrane filter passive sampling of $HNO_{3(g)}$ can be implemented in remote ecosystems at a very low cost to achieve large spatial resolution. The passive sampling technique implemented in this work has the capability of detecting $HNO_{3(g)}$ at an average mixing ratio of 2 pptv when sampling over a monthly period, and was demonstrated in a remote ecosystem to measure mixing ratios as low as 4 pptv. IC pre-concentration and suppressed conductivity accompanied by extensive QA/QC procedures allowed for the sensitive analysis of these remote $HNO_{3(g)}$ ultra-trace concentrations. Furthermore, the reusability of the nylon filter sampling media was tested

in the presence of low $HNO_{3(g)}$ mixing ratios and the filters showed promise for reuse in remote ecosystems.

The average mixing ratios determined at remote boreal forested sites across the NL-BELT were in the pptv range, and on average were below 50 pptv. The flux of $HNO_{3(g)}$ determined across the NL-BELT ranged from 3 – 16 mg N m^{-2} yr^{-1}, which was comparable to other rural and remote forest ecosystems in Canada, as well as boreal ecosystems in Europe. $HNO_{3(g)}$ mixing ratios across the NL-BELT in 2015 and 2016 followed a seasonal trend, but showed no consistent latitudinal trend. Source apportionment was performed using an air mass back trajectory analysis and steady-state approximation to explain the seasonal trend in the data. In conclusion, the seasonality in the $HNO_{3(g)}$ data was likely due to short-range transport of $NO_{x(g)}$ emissions from eastern Newfoundland (<1500 km), and the long-range transport and down welling of PAN in the springtime (> 1500 km), but dominantly throughout the year from the oxidation of local biogenic and anthropogenic NO_x emissions.

2.6 References

Atkinson, R.: Gas-phase tropospheric chemistry of volatile organic compounds: 1. Alkanes and alkenes, J. Phys. Chem. Ref. Data, 26, 215-290, 1997.

Bedison, J. E. and McNeil, B. E.: Is the growth of temperate forest trees enhanced along an ambient nitrogen deposition gradient?, Ecology , 90(7), 1736–1742, 2009.

Bobbink, R., Hicks, K., Galloway, J., Spranger, T., Alkemade, R., Ashmore, M., Bustamante, M., Cinderby, S., Davidson, E., Dentener, F., Emmett, B., Erisman, J. -W., Fenn, M., Gilliam, F., Nordin, A., Pardo, L. and De Vries, W.: Global assessment of nitrogen deposition effects on terrestrial plant diversity: a synthesis., Ecological Applications, 20(1), 30-59, 2010.

Butterbach-bahl, K., Kahl, M., Mykhayliv, L., Werner, C., Kiese, R. and Li, C.: A European-wide inventory of soil NO emissions using the biogeochemical models DNDC / Forest-DNDC, Atmos. Environ., 43(7), 1392–1402, doi:10.1016/j.atmosenv.2008.02.008, 2009.

Bytnerowicz, A., Padgett, P. E., Arbaugh, M. J., David, R. and Jones, D. P.: Passive sampler for measurements of atmospheric nitric acid vapor (HNO_3) concentrations, The Scientific World, 1, 815–822, doi:10.1100/tsw.2001.323, 2001.

Bytnerowicz, A., Sanz, M. J., Arbaugh, M. J., Padgett, P. E., Jones, D. P. and Davila, A.: Passive sampler for monitoring ambient nitric acid (HNO_3) and nitrous acid (HNO_2) concentrations, Atmos. Environ., 39(14), 2655–2660, doi:10.1016/j.atmosenv.2005.01.018, 2005.

Bytnerowicz, A., Fraczek, W., Schilling, S. and Alexander, D.: Spatial and temporal distribution of ambient nitric acid and ammonia in the Athabasca Oil Sands Region , Alberta, , 69, 11–21, doi:10.3274/JL10-69-S1-03, 2010.

Carpenter, L. J., Fleming, Z. L., Read, K. A., Lee, J. D., Moller, S. J., Hopkins, J. R., Purvis, R. M., Lewis, A. C., Müller, K., Heinold, B., Herrmann, H., Fomba, K. W., Pinxteren, D., Müller, C., Tegen, I., Wiedensohler, A., Müller, T., Niedermeier, N., Achterberg, E. P., Patey, M. D., Kozlova, E. A., Heimann, M., Heard, D. E., Plane, J. M. C., Mahajan, A., Oetjen, H., Ingham, T., Stone, D., Whalley, L. K., Evans, M. J., Pilling, M. J., Leigh, R. J., Monks, P. S., Karunaharan, A., Vaughan, S., Arnold, S. R., Tschritter, J., Pöhler, D., Frieß, U., Holla, R., Mendes, L. M., Lopez, H., Faria, B., Manning, A. J., and Wallace, D. W. R.: Seasonal characteristics of tropical marine boundary layer air measured at the Cape Verde Atmospheric Observatory, J. Atmos. Chem., 67, 87–140, doi:10.1007/s10874-011-9206-1, 2010.

Chow, J. C. and Watson, J. G.: Guideline on Speciated Particulate Monitoring, U. S. Environmental Protection Agency, Research Triangle Park, NC, 1998.

Cisneros, R., Bytnerowicz, A., Schweizer, D., Zhong, S., Traina, S. and Bennett, D. H.: Ozone , nitric acid , and ammonia air pollution is unhealthy for people and ecosystems in southern Sierra Nevada , California, Environ. Pollut., 158(10), 3261–3271, doi:10.1016/j.envpol.2010.07.025, 2010.

Cleveland, C. C., Townsend, A. R., Schimel, D. S., Fisher, H., Howarth, R. W., Hedin, L. O., Perakis, S. S., Latty, E. F., Von Fischer, J. C., Elseroad, A. and Wasson, M. F.: Global patterns of terrestrial biological nitrogen (N_2) fixation in natural ecosystems, Global Biogeochemical Cycles, 13, 623–645, doi: 10.1029/1999GB900014, 1999.

Denman, K., Brasseur, G., Chidthaisong, A., Ciais, P., Cox, P., Dickinson, R., Hauglustaine, D., Heinze, C., Holland, E., Jacob, D., Lohmann, U., Ramachandran, S., da Silva Dias, P., Wofsy, S. and Zhang, X.: Couplings between changes in the climate system and biogeochemistry, 2007

De More, W. B., Sander, S. P., Golden, D. M., Hampson, R. F., Kurylo, M. J., Howard, C. J., Ravishankara, A. R., Kolb, C. E. and Molina, M. J.: Chemical kinetics and photochemical data for use in stratospheric modeling, Evaluation No. 12, JPL, 97-4, January 15, 1997.

Department of Business, Tourism, Culture and Rural Development Year-To-Date Tourism Highlights December 2016 (Newfoundland and Labrador): http://www.tcii.gov.nl.ca/tourism/tourism_research/pdf/Tourism_performance_2016_YTD_December_2016_March_14_2016.pdf, Last access: 18 April 2017.

Finlayson-Pitts, B. J. and Pitts, J. N. Chemistry of the upper and lower atmosphere: Theory, experiments and applications, Elsevier Inc., 2000.

Fischer, E. V., Jacob, D. J., Yantosca, R. M., Sulprizio, M. P., Millet, D. B., Mao, J., Paulot, F., Singh, H. B., Roiger, A., Ries, L., Talbot, R. W., Dzepina, K. and Pandey Deolal, S.: Atmospheric peroxyacetyl nitrate (PAN): A global budget and source attribution, Atmos. Chem. Phys., 14(5), 2679–2698, doi:10.5194/acp-14-2679-2014, 2014.

Flechard, C. R., Nemitz, E., Smith, R. I., Fowler, D., Vermeulen, A. T., Bleeker, A., Erisman, J. W., Simpson, D., Zhang, L., Tang, Y. S. and Sutton, M. A.: Dry deposition of reactive nitrogen to European ecosystems: A comparison of inferential models across the NitroEurope network, Atmos. Chem. Phys., 11(6), 2703–2728, doi:10.5194/acp-11-2703-2011, 2011.

Fleming, Z. L., Monks, P. S. and Manning, A. J.: Review: Untangling the influence of air-mass history in interpreting observed atmospheric composition, Atmos. Res., 104–

105, 1–39, doi:10.1016/j.atmosres.2011.09.009, 2012.

Hicks, B. B., and Liss, P. S.: Transfer of SO_2 and other reactive gases across the air-sea interface, Tellus, 28(4), 348–354, 1976.

Historical Climate Data (Government of Canada): http://climate.weather.gc.ca/, last access: 17 March 2017.

Jacob, D. J. Introduction to Atmospheric Chemistry, Princeton University Press, 1999.

Korhonen, J. F. J., Pihlatie, M., Pumpanen, J., Aaltonen, H., Hari, P., Levula, J., Kieloaho, A. J., Nikinmaa, E., Vesala, T. and Ilvesniemi, H.: Nitrogen balance of a boreal Scots pine forest, Biogeosciences, 10(2), 1083–1095, doi:10.5194/bg-10-1083-2013, 2013.

Lamarque, J.-F., Bond, T. C., Eyring, V., Granier, C., Heil, A., Klimont, Z., Lee, D., Liousse, C., Mieville, A., Owen, B., Schultz, M. G., Shindell, D., Smith, S. J., Stehfest, E., Van Aardenne, J., Cooper, O. R., Kainuma, M., Mahowald, N., McConnell, J. R., Naik, V., Riahi, K., and van Vuuren, D. P.: Historical (1850–2000) gridded anthropogenic and biomass burning emissions of reactive gases and aerosols: methodology and application, Atmos. Chem. Phys., 10, 7017–7039, doi:10.5194/acp-10-7017-2010, 2010.

Le Breton, M., Bacak, A., Muller, J. B. A., Xiao, P., Shallcross, B. M. A., Batt, R., Cooke, M. C., Shallcross, D. E., Bauguitte, S. J. B. and Percival, C. J.: Simultaneous airborne nitric acid and formic acid measurements using a chemical ionization mass spectrometer around the UK: Analysis of primary and secondary production pathways, Atmos. Environ., 83(3), 166–175, doi:10.1016/j.atmosenv.2013.10.008, 2014.

Lelieveld, J., Gromov, S., Pozzer, A. and Taraborrelli, D.: Global tropospheric hydroxyl distribution, budget and reactivity, Atmos. Chem. Phys., 16(19), 12477–12493, doi:10.5194/acp-16-12477-2016, 2016.

Liu, Y., Xie, L., Ma, Y., Xue, K., Qui, W., Shan, T., and Gao, G.: The effects of sonication time and frequencies on degradation, crystallization behavior, and mechanical properties of polypropylene, Polymer Engineering and Science, 2566 – 2575, doi:10.1002/pen, 2015.

Molina-Herrera, S., Haas, E., Grote, R., Kiese, R., Klatt, S., Kraus, D., Butterbach-Bahl, K., Kampffmeyer, T., Friedrich, R., Andreae, H., Loubet, B., Ammann, C., Horváth, L., Larsen, K., Gruening, C., Frumau, A. and Butterbach-Bahl, K.: Importance of soil NO emissions for the total atmospheric NO_x budget of Saxony, Germany, Atmos. Environ., 152, doi:10.1016/j.atmosenv.2016.12.022, 2017.

Müller, J. .: Geographical Distribution and Seasonal Variation of Surface Emissions and

Deposition Velocities of Atmospheric Trace Gases, J. Geophys. Res., 97(91), 3787–3804, 1992.

Norton, E. G., Vaughan, G., Methven, J., Coe, H., Brooks, B., Gallagher, M. and Longley, I.: Boundary layer structure and decoupling from synoptic scale flow during NAMBLEX, Atmos. Chem. Phys., 6, 433-445, doi: 10.5194/acp-6-433-2006, 2006.

Ollinger, S. V, Richardson, A. D., Martin, M. E., Hollinger, D. Y., Frolking, S. E., Reich, P. B., Plourde, L. C., Katul, G. G., Munger, J. W., Oren, R., Smith, M.-L., Paw U, K. T., Bolstad, P. V, Cook, B. D., Day, M. C., Martin, T. A., Monson, R. K. and Schmid, H. P.: Canopy nitrogen, carbon assimilation, and albedo in temperate and boreal forests: Functional relations and potential climate feedbacks., Proc. Natl. Acad. Sci. U. S. A., 105(49), 19336–19341, doi:10.1073/pnas.0810021105, 2008.

Padgett, P. E.: The effect of ambient ozone and humidity on the performance of nylon and Teflon filters used in ambient air monitoring filter-pack systems, Atmos. Pollut. Res., 1(1), 23–29, doi:10.5094/APR.2010.004, 2010.

Petit, J. E., Favez, O., Albinet, A. and Canonaco, F.: A user-friendly tool for comprehensive evaluation of the geographical origins of atmospheric pollution: Wind and trajectory analyses, Environ. Model. Softw., 88, 183–187, doi:10.1016/j.envsoft.2016.11.022, 2017.

Rolph, G.D.. Real-time Environmental Applications and Display sYstem (READY) Website (http://ready.arl.noaa.gov), NOAA Air Resources Laboratory, Silver Spring, MD., 2017.

Seinfeld, J. H. and Pandis, S. N. Atmospheric chemistry: From air pollution to climate change, John Wiley & Sons, Inc., 2006.

Schwartz, S. E., and White, W. H.: Kinetics of reactive dissolution of nitrogen oxides into aqueous solution, Ad. Environ. Sci. Technol., 12, 1-116, 1983.

Sharma, S., Andrews, E., Barrie, L. A., Ogren, J. A. and Lavoué, D.: Variations and sources of the equivalent black carbon in the high Arctic revealed by long-term observations at Alert and Barrow: 1989-2003, J. Geophys. Res. Atmos., 111(14), 1989–2003, doi:10.1029/2005JD006581, 2006.

Simmonds, P. G., Seuring, S., Nickless, G. and Derwent, R. G.: Segregation and interpretation of ozone and carbon monoxide measurements by air mass origin at the TOR station Mace Head, Ireland from 1987 to 1995, J. Atmos. Chem., 28(1–3), 45–59, doi:10.1023/A:1005817916497, 1997.

Singh, H. B. and Hanst, P. L.: Peroxyacetyl nitrate (PAN) in the unpolluted atmosphere:

An important reservoir for nitrogen oxides, Geophys. Res. Lett., 8(8), 941–944, doi:10.1029/GL008i008p00941, 1981.

Sokolov, A. P., Kicklighter, D. W., Melillo, J. M., Felzer, B. S., Schlosser, A. C. and Cronin, T. W.: Consequences of considering carbon-nitrogen interactions on the feedbacks between climate and the terrestrial carbon cycle, Journal of Climate, 21(15), 3776-3796, doi: 10.1108/17506200710779521, 2008.

Stein, A.F., Draxler, R.R, Rolph, G.D., Stunder, B.J.B., Cohen, M.D., and Ngan, F.: NOAA's HYSPLIT atmospheric transport and dispersion modeling system, Bull. Amer. Meteor. Soc., 96, 2059-2077, doi:10.1175/BAMS-D-14-00220.1, 2015.

Sutton, M. A., Howard, C. M., Erisman, J. W., Billen, G., Bleeker, A., Grennfelt, P., van Grinsven, H. and Grizzetti, B.: European Nitrogen Assessment, Cambridge University Press, 2011.

Verbeke, T., Lathière, J., Szopa, S. and De Noblet-Ducoudré, N.: Impact of future land-cover changes on HNO_3 and O_3 surface dry deposition, Atmos. Chem. Phys., 15(23), 13555–13568, doi:10.5194/acp-15-13555-2015, 2015.

Wayne, R. P., Barnes, I., Biggs, P., Burrows, J. P., Canosa-Mas, C. E., Hjorth, J., Lebras, G., Moortgat, G. K., Perner, D., Poulet, G., Restelli, G. and Sidebottom, H.: The nitrate radical: Physics, chemistry, and the atmosphere, Atmos. Environ., 25, 1-203, 1991.

Wesely, M. L. and Hicks, B.B. A review of the current status of knowledge on dry deposition, Atmos. Environ., 34(12–14), 2261–2282, doi:10.1016/S1352-2310(99)00467-7, 2000.

Young, C.J., Washenfelder, R.A., Roberts, J.M., Mielke, L.H., Osthoff, H.D., Tsai, C., Pikelnaya, O., Stutz, J., Veres, P.R., Cochran, A.K., VandenBoer, T.C., Flynn, J., Grossberg, N., Haman, C.L., Lefer, B., Stark, H., Graus, M., de Gouw, J., Gilman, J.B., Kuster, W.C., and Brown, S.S.: Vertically resolved measurements of nighttime radical reservoirs in Los Angeles and their contribution to the urban radical budget. Environ. Sci. Technol., 46, 10965-10973, 2012.

Zhang, L., Vet, R., O'Brien, J. M., Mihele, C., Liang, Z. and Wiebe, A.: Dry deposition of individual nitrogen species at eight Canadian rural sites, J. Geophys. Res. Atmos., 114(2), 1–13, doi:10.1029/2008JD010640, 2009.

3. Quantitation of Eleven Alkylamines in Atmospheric Samples: Separating Structural Isomers by Ion Chromatography

3.1 Abstract

Amines are important drivers in particle formation and growth, which have implications for Earth's climate. In this work, we developed an ion chromatographic (IC) method using sample cation-exchange preconcentration for separating and quantifying the nine most abundant atmospheric alkylamines (monomethylamine ($MMAH^+$), dimethylamine ($DMAH^+$), trimethylamine ($TMAH^+$), monoethylamine ($MEAH^+$), diethylamine ($DEAH^+$), triethylamine ($TEAH^+$), monopropylamine ($MPAH^+$), monoisopropylamine ($iMPAH^+$), and monobutylamine ($MBAH^+$)) and two alkyl diamines 1, 4-diaminobutane ($DABH^+$) and 1, 5-diaminopentane ($DAPH^+$). Further, the developed method separates the suite of amines from five common atmospheric inorganic cations (Na^+, NH_4^+, K^+, Mg^{2+}, Ca^{2+}). All 16 cations are greater than 95% baseline resolved and elute in a runtime of 35 min. This paper describes the first successful separation of $DEAH^+$ and $TMAH^+$ by IC and achieves separation between three sets of structural isomers, providing specificity not possible by mass spectrometry. The method detection limits for the alkyl amines are in the picogram per injection range and the method precision ($\pm$ 1 σ) analyzed over 3 months was within 16% for all the cations. The performance of the IC method for atmospheric application was tested with biomass-burning (BB) particle extracts collected from two forest fire plumes in Canada. In extracts of a size-resolved BB sample from an aged plume we detected and quantified $MMAH^+$, $DMAH^+$, $TMAH^+$, $MEAH^+$, $DEAH^+$ and $TEAH^+$ in the presence of Na^+, NH_4^+, and K^+ at molar ratios of amine to inorganic cation ranging from 1:2 to 1:1000. Quantities of $DEAH^+$ and $DMAH^+$ of 0.2 – 200 ng m^{-3} and 3 – 1200 ng m^{-3}, respectively, were present

in the extracts and an unprecedented amine-to-ammonium molar ratio greater than 1 was observed in particles with diameters spanning 56 – 180 nm. Extracts of respirable fine-mode particles ($PM_{2.5}$) from a summer forest fire in British Columbia in 2015 were found to contain $iMPAH^+$, $TMAH^+$, $DEAH^+$ and $TEAH^+$ at molar ratios of 1:300 with the dominant cations. The amine-to-ammonium ratio in a time series of samples never exceeded 0.15 during the sampling of the plume. These results and an amines standard addition demonstrate the robustness and sensitivity of the developed method when applied to the complex matrix of BB particle samples. The detection of multiple alkylamines in the analyzed BB samples indicates that this speciation and quantitation approach can be used to constrain BB emission estimates and the biogeochemical cycling of these reduced nitrogen species.

3.2 Introduction

Particles in the atmosphere can modulate climate through their direct and indirect effect on the radiative balance of Earth's atmosphere (Boucher et al., 2013; Lohmann and Feichter, 2005). This potential warming or cooling effect of particles represents the greatest uncertainty in Earth's radiative forcing (Myhre et al., 2013). Additionally, particles with a diameter of 2.5 μm or less ($PM_{2.5}$) have been classified as carcinogens (IARC, 2016) and are estimated to be responsible for 3 million deaths annually worldwide (Stephen et al., 2012). Thus, understanding the quantities and the chemical and physical nature of the species involved in the formation and growth of new particles is of paramount importance.

Recent work has shown that organic compounds may contribute considerably to particle nucleation (Ehn et al., 2014; Ortega et al., 2016; Tröstl et al., 2016; Willis et al., 2016). In particular, the need to measure and quantify gaseous atmospheric alkylamines has gained interest because of their exceptional ability to partake in atmospheric particle formation. Multiple laboratory investigations have shown the nucleation potential of methyl- and ethyl-substituted amines through gaseous acid-base chemistry reactions (Almeida et al., 2013; Angelino et al., 2001; Berndt et al., 2010, 2014; Bzdek et al., 2010, 2011; Erupe et al., 2011; Jen et al., 2016a, b; Lloyd et al., 2009; Murphy et al., 2007; Qiu et al., 2011; Silva et al., 2008; Smith et al., 2010; Wang et al., 2010a, b; Yu et al., 2012; Zhao et al., 2011; Zollner et al., 2012). Theoretical calculations and studies have also found that amines have a high disposition to form atmospheric nanoparticles (Barsanti et al., 2009; Kurtén et al., 2008; Loukonen et al., 2010, 2014; Nadykto et al., 2015; Ortega et al., 2012). From these works, alkylamines have been shown to form clusters via

neutralization reactions at rates up to three orders of magnitude greater than ammonia (Almeida et al., 2013; Berndt et al., 2010; Bzdek et al., 2011; Kurtén et al., 2008; Loukonen et al., 2010; Nadykto et al., 2015), and readily exchange with ammonium in already formed ammonium-bisulfate molecular clusters (Bzdek et al., 2010; Lloyd et al., 2009; Qiu et al., 2011). These studies suggest that alkylamines can compete with ammonia to form particles even though they have been quantified at mixing ratios that are 3 or more orders of magnitude lower in the atmosphere (Chang et al., 2003; Ge et al., 2011; Schade and Crutzen, 1995). Atmospheric measurements made during new particle formation events have further confirmed that alkylamines participate in particle formation at ambient concentrations and that these species may be present in most atmospheric particles (Creamean et al., 2011; Dall'Osto et al., 2012; Hodshire et al., 2016; Kulmala et al., 2013; Kürten et al., 2016; Ruiz-Jimenez et al., 2012; Smith et al., 2010; Tao et al., 2016).

Alkylamine emissions to the atmosphere arise from both natural and anthropogenic sources (Ge et al., 2011). Short-chain alkyl amines such as the methylated and ethylated amines are predominantly reported in emission inventories. Measurements show that atmospheric alkyl amines are prevalent in ambient air across the globe, especially in the particle phase (Ge et al., 2011). For example, methyl- and ethyl- amines were measured by an aerosol time-of-flight mass spectrometer at both rural and urban sites all across Europe (Healy et al., 2015). In particular, these amines have been measured in substantial quantities near animal husbandry operations (Kuhn et al., 2011; Lunn and Van de Vyver, 1977; Rabaud et al., 2003; Schade and Crutzen, 1995; Sorooshian et al., 2008), fisheries (Seo et al., 2011), and sewage-waste treatment facilities (Leach et al., 1999). Other

anthropogenic sources include tobacco smoke (Schmeltz and Hoffmann, 1977), automobiles (Cadle and Mulawa, 1980) and cooking (Rogge et al., 1991; Schauer et al., 1999). The ocean is estimated to be the largest natural source of alkylamines, where they are released as volatile degradation products (Ge et al., 2011; Gibb et al., 1999a, b). Aliphatic amines have also been detected in smoldering stage biomass-burning (BB) plumes. These have been estimated to represent a quarter of global methylated amine emissions (Lobert et al., 1990; Schade and Crutzen, 1995).

Real-time in situ speciation and quantitation of atmospheric amines in the particle and gas phase can be difficult because alkylamines are commonly found at or below parts per trillion by volume (pptv) mixing ratios in the atmosphere (Ge et al., 2011). Furthermore, the atmospheric matrix can be complex and ubiquitous atmospheric species can cause matrix effects for various analytical methods targeting these reduced nitrogen species. Being able to chromatographically resolve alkylamines from the dominant base, ammonium, represents a major challenge when sampling the gas phase (Chang et al., 2003; Ge et al., 2011; Schade and Crutzen, 1995). Quantifying amines in particle samples, for example by ion chromatography (IC), presents a greater challenge due to possible interferences from sodium, potassium, ammonium, magnesium and calcium whose concentrations are dependent on the particle source characteristics and the measurement location (Ault et al., 2013; Kovač et al., 2013; Sobanska et al., 2012; Sun et al., 2006). Particles frequently contain complex organic mixtures, such as high molecular weight organic compounds, which can cause further matrix effects during separation or direct analysis (Di Lorenzo and Young, 2016; Saleh et al., 2014).

Achieving full speciation of alkylamines is important because the nucleation potential of amines has been shown to increase with basicity (Berndt et al., 2014; Kurtén et al., 2008; Yu et al., 2012). For example, although monopropylamine (MPA) and trimethylamine (TMA; pKa = 9.8) are structural isomers of one another, MPA (pKa = 10.7) is likely to be a more potent nucleator due to its stronger basicity. The suite of alkylamines that have been commonly detected in the atmosphere contains multiple structural isomers (e.g. monoethylamine, MEA and dimethylamine, DMA), making it difficult to speciate the amines using mass spectrometry (MS) without prior separation. Multiple field investigations sampling atmospheric particles using MS analysis have reported the detection of amine ion peaks but have been unable to assign them to a specific amine (Aiken et al., 2009; Denkenberger et al., 2007; Silva et al., 2008; Yao et al., 2016). Derivatization of alkyl amines coupled with HPLC or GC separation has been reported to aid in separation and quantitation of amine species (Akyüz, 2007; Huang et al., 2009; Fournier et al., 2008; Key et al., 2011; Possanzini and Di Palo, 1990). However, these approaches are time consuming, require optimization of reaction conditions, and employ phase separations, which use large quantities of consumables, reagents, and solvents. Capillary electrophoresis has also been employed for aqueous amine separation, however in either case derivatization was required (Dabek-Zlotorzynska and Maruszak, 1998) or the separation of atmospherically relevant cations was not addressed (Fekete et al., 2006). The use of ion chromatography to directly separate and quantify atmospheric alkylamines has been demonstrated (Chang et al., 2003; Dawson et al., 2014; Erupe et al., 2010; Huang et al., 2014; Li et al., 2009; Murphy et al., 2007; VandenBoer et al., 2012; Verriele et al., 2012), yet the established IC methods struggle with coeluting cations

(Huang et al., 2014; Murphy et al., 2007; VandenBoer et al., Verriele et al., 2012) or they do not address a full suite of atmospherically relevant alkyl amines and inorganic cations (Chang et al., 2003; Dawson et al., 2014; Erupe et al., 2010; Li et al., 2009).

In this work we demonstrate the separation and quantitation of the nine most abundant atmospheric alkylamines, two alkyl diamines, and six inorganic cations through the use of ion chromatography. We show i) the separation method approach to maximizing peak resolution in the context of real-time atmospheric sampling and analysis; ii) the effects of column temperature on amine coelution; iii) the method precisions, accuracies, sensitivities and limits of detection (LODs) for all alkyl amine and inorganic cations; and iv) application of the method to the complex matrix of atmospheric BB particle extracts to demonstrate method sensitivity and robustness.

3.3 Methods

3.3.1 Chemicals and Materials

Inorganic cation stock solutions were prepared from a primary mixed cation standard concentrate (Dionex six-cation II, Lot no. 150326, Thermo Scientific, Waltham, MA, USA) consisting of Li^+, Na^+, NH_4^+, K^+, Mg^{2+} and Ca^{2+} chloride salts. Alkyl amines (MMA (monomethylamine, 40% w/w), DMA (dimethylamine, 40% w/w), TMA (trimethylamine, 25% w/w), MEA (monoethylamine, 70% w/w), DEA (diethylamine, >99% w/w), TEA (triethylamine, >99% w/w), MPA (monopropylamine, $\geq$ 99% w/w), iMPA (monoisopropylamine, $\geq$ 99% w/w) MBA (monobutylamine, 99.5% w/w), MEtA (monoethanolamine, $\geq$ 98% w/w), DAB (1,4-diaminobutane, > 98.5% w/w) and DAP (1,5-diaminopentane, 95% w/w)) were purchased from Sigma-Aldrich (Oakville, ON,

Canada). Calibration standards were prepared by serial dilution in >18.2 MΩ x cm ultrapure deionized water (Barnstead Nanopure Infinity, Thermo Scientific, Waltham, MA, USA). Since these alkylamine species will largely be protonated in solution we will denote each of these species in their cationic form (i.e. NR_3H^+) henceforth when referring to the condensed phase.

3.3.2 Ion Chromatography

A ThermoScientific ICS-2100 Ion Chromatography System (Thermo Scientific, Mississauga, ON, Canada) utilizing Reagent-Free Ion Chromatography (RFIC^{TM}) components was used to develop the separation of the selected amines and inorganic cations. A ThermoScientific methanesulfonic acid (MSA) eluent generator cartridge (EGC III, P/N: 074535) was used in conjunction with an ultrapure deionized water reservoir to supply the eluent mobile phase with H_3O^+ ions as the competing exchanger. A continuously regenerated trap column (CR-CTC II, P/N: 066262) was attached in series to the eluent cartridge to remove cation contaminants from the eluent, thereby improving instrument detection limits. Samples were preconcentrated on a cation exchange column (TCC-ULP1; 5 x 23 mm, P/N: 063783) using a ThermoScientific AS-DV autosampler to deliver the desired volume. Concentrated analytes were separated using ThermoScientific CG19 (4 x 50 mm, P/N: 076027) and CS19 (4 x 250 mm, P/N: 076026) guard and analytical cation-exchange columns. The column effluent was passed through a suppressor operating in recycle mode (CERS 500, 4 mm) prior to detection of the analytes using a DS6 heated conductivity cell thermostated at 30 °C. The eluent conductance was recorded at 5 Hz and the chromatographic peaks were analyzed using

the Chromeleon™ 7 software package. A ThermoScientific CG15 (4 x 50 mm, P/N: 052200) guard column was added in-line later to attempt further improvement in analyte separation.

3.3.3 CS19 Separation Optimization

The gradient program used for the separation of methylamines, ethylamines, other alkylamines, and six inorganic cations on the CS19 cation-exchange column was optimized by combining analyte separation parameters from multiple isocratic elution runs at varying MSA concentrations (1 - 16 mM) and mobile phase flow rates (0.75 - 1.25 ml min^{-1}) at a column temperature of 30 °C. Maximum peak resolution was optimized using an eluent gradient program and the column temperature was increased to resolve coeluting peaks (see Sect. 3.4.1.1).

Optimal separation of a suite of 15 cations was achieved using a mobile phase flow rate of 1.25 ml min^{-1} and a column temperature of 55 °C. The eluent gradient program is as follows: an initial MSA concentration of 1 mM held for 20 min, a step increase to 4 mM followed immediately by an exponential ramp to 10 mM over 10 minutes (Chromeleon curve factor = 7). The final concentration of 10 mM was held for an additional 5 min, yielding a total run time of 35 min. The IC was returned to initial conditions and re-equilibrated for 10 min as the next 1 ml sample aliquot was prepared for injection by the AS-DV. The suppressor current, optimized for this flow rate and the maximum eluent concentration in accordance with the calculation provided by the manufacturer, was set at 37 mA. The typical backpressure in the system at these

conditions was 2100 psi. The Chromeleon method file for the method described above is detailed in Fig. B-1 in the Appendix.

3.3.4 Quality Assurance and Quality Control

Standards were prepared using Class A Corning polymethylpentene 50 (± 0.06) ml volumetric flasks that were rinsed four times with ethanol and eight times with ultrapure water prior to use. Standards were stored in 60 ml brown Nalgene polypropylene bottles that were pre-cleaned in a 10% HCl bath, followed by eight sequential rinses with distilled and ultrapure water, respectively. The mixed amine standards and mixed inorganic cation standards were prepared separately and each cation standard set was composed of five calibration standards, two check standards and an ultrapure deionized water blank. Ranges and related parameters are denoted by mass injected, as the preconcentration column negates the effect of volume. All amine calibration standards had a mass calibration range of 5-500 ng. The mass range for each inorganic cation calibration is as follows: Li^+ (0.82-16 ng), Na^+ (7.8-160 ng), NH_4^+ (8.4-170 ng), K^+ (26-520 ng), Mg^{2+} (6.4-130 ng), and Ca^{2+} (18-360 ng). All calibration curves contained trace inorganic cation impurities from the ultrapure deionized water source or holding vessels that fell below the lowest calibration standard and were corrected accordingly to allow for inter-day method performance comparison. Trace quantities of amines were not observed. An example of a calibration blank chromatogram is presented in Fig. B-2.

Method precision for each methyl- and ethylamine cation was determined using standard calibration curves (n = 9) injected across 5 different days spanning 3 months. The precision for the propyl- and butylamines was determined using 2 standard

calibration curves analyzed over 1 month. Method precision for Li^+, Na^+, NH_4^+ and K^+ was assessed using calibrations (n = 6) from 3 separate days spanning 2 months. Precision for each cation was calculated using the standard deviation (σ) in the slope of the linear calibration curves. Check standards positioned between the two highest and the two lowest calibration standards for each cation were used to determine method accuracy across the calibration range. The low check standard was 15 times greater than the lowest standard and the high check standard was 150 times higher than the lowest standard. Accuracy was determined by the percent relative error between the known and calculated concentrations of the check standards. The LODs for the singly-charged inorganic cations (n = 4) and methyl- and ethylamines (n = 5) were determined using calibration standard and calibration blank chromatograms from 3 or more separate days. The LODs for the propyl- and butylamines were determined using calibration standard and blank chromatograms from 2 separate days. The LODs are reported as concentrations resulting in a ratio of signal peak height to background noise of 3. The background noise was determined using the standard deviation of the conductance signal that fell within the retention time window for each analyte in their respective calibration blank chromatograms.

To assess the method robustness in the presence of a complex matrix the gradient method standard addition was performed on a subsample of a size-resolved BB particle extract (320 – 560 nm; see Sect 3.3.5). Standard addition was performed by adding known quantities of methyl- and ethylamine solution to a 0.5 ml subsample of the extract followed by dilution to 5 ml. The amount of the methyl- and ethylamines added to the internal calibration matched that of the external calibration. The slope and retention times

for the methyl- and ethylamines from the internal calibration were calculated and compared to those performed externally to quantify matrix effects. Discussion of the analytical performance of the CS19 gradient program is presented in Sect. 3.4.1.

3.3.5 Size-Resolved BB Sample Analysis

A size-resolved particle sample from a BB plume was collected using a nanoMOUDI II (nano micro-orifice uniform-deposit impactor, model 122-R, MSP Corp., Shoreview, MN, USA) in St. John's, Newfoundland on 6 July 2013. Satellite images of the plume smoke, HYSPLIT back trajectories, and measured $PM_{2.5}$ concentrations reported by Environment and Climate Change Canada indicate that these plumes originated from boreal forest fires in northern Québec and Labrador on 4 July 3013 and travelled via Labrador and the Gulf of St. Lawrence to the sampling site (Di Lorenzo and Young, 2016). The nanoMOUDI samples were collected on 13 aluminum substrate stages into size-resolved bins of atmospheric particles with a diameter range spanning 0.010 –18 μm. Air was sampled continuously for 25.5 h at a flow rate of 30 L min^{-1}. A subsample of each aluminum substrate (10% of the total substrate area) was extracted into a glass vial with 5 mL ultrapure deionized water by sonication (VWR Scientific Products/Aquasonic 150HT, Ultrasonic Water Bath) for 40 min. The extracts were filtered using a 0.2 μm polytetrafluoroethylene (PTFE) filter and stored in polypropylene vials at 4 °C prior to analysis by IC within 24 h. Cation analytes within these samples all fell within their respective calibration ranges and did not require any further dilution. An aluminum substrate field blank was also transported and exposed to the ambient atmosphere briefly at the collection site before being stored in a sealed container for the

duration of the sample collection, transported back with the samples, and extracted simultaneously following the same procedure. All calculated quantities were corrected with measurements of the field blank and additional error from this correction propagated into our final reported values. The field blank chromatogram for the size-resolved BB samples is presented in Fig. A-2.

3.3.6 BC Fire Sample Analysis

The full method for the collection and extraction of BB particle samples collected during July wildfires in British Columbia is detailed in Di Lorenzo et al. (2016). Briefly, $PM_{2.5}$ samples were collected at two sites approximately 100 km east of the BB location. The first site was located in Burnaby/Kensington Park (BKP) and the second was in North Vancouver/Second Narrows (NVSN). The particle samples were collected using beta attenuation particle monitors (5030 SHARP Monitor at the BKP site, 5030i SHARP monitor at the NVSN site, Thermo Fisher Scientific, Waltham, MA, USA) at a 16.67 L min^{-1} flow rate in 8 h intervals. Particles were collected on glass microfiber filter tape and stored at -20 °C until extracted. Approximately 37% of each filtered particulate deposit was placed into a polypropylene vial with 10 ml of deionized water and sonicated for 40 min. The extracts were filtered with PTFE syringe filters (3 mm diameter, 0.2 μm pore size, VWR International, Radnor, Pennsylvania, USA) and diluted by a factor of five with ultrapure deionized water so that all analytes were in the IC calibration range. An unexposed area of the glass microfiber filter tape was sampled and extracted for use as a field blank. All calculated quantities and errors were blank-corrected using the field blank.

3.4 Results and Discussion

3.4.1 Analytical Method Performance of CS19 Cation Exchange Column

3.4.1.1 Separation Approach and Optimization of Parameters

Our approach to separation involved injecting the highest mixed inorganic cation and mixed amine standards for the expected working range (0.1 – 2.5 μg ml^{-1}) at static flow rates (0.75, 1, and 1.25 ml min^{-1}) while systematically increasing the isocratic eluent concentration (4 - 16 mM). The quality of each isocratic method was assessed by calculating the peak-to-peak resolution (R_s) using the retention time (t_R; min) and peak width at base (w; min) determined from the highest standard for each pair of cations following E3-1:

(E3-1) $R_S = \frac{2(t_{R2}-t_{R1})}{w_2+w_1}$

Using the upper limit of the expected working range for all analytes provides a lower limit on peak-to-peak resolution between these species. The peak-to-peak resolutions of the isocratic methods run using a 0.75 and 1.25 ml min^{-1} flow rate for the selected inorganic and alkylamine cations are presented in Figs. B-3 and B-4. Peak-to-peak resolution between all peaks increased as the mobile-phase ionic strength was lowered when the flow rate was held constant. This is in agreement with E3-2, the fundamental resolution equation, which describes peak-to-peak resolution (R) in terms of the unit-less efficiency factor (N), retention factor (k), and a selectivity factor (α) terms.

(E3-2) $R = \left(\frac{\sqrt{N}}{4}\right)\left(\frac{k}{k+1}\right)\left(\frac{\alpha-1}{\alpha}\right)$

With low mobile phase ionic strength, the retention factor of the analytes is expected to increase, leading to greater resolution, consistent with our observations. In contrast, the effect of flow rate on peak resolution is nonintuitive and must be obtained empirically. Lower flow rates increase the retention factor, which in turn increases resolution. However, an increase in mobile-phase flow rate has a competing effect on the efficiency factor in Eq. (3-2). The efficiency term is governed by the theoretical plate height (H; mm) as described by the Van Deemter equation (E3-3), which highlights the competing effect of flow rate (μ; ml min^{-1}) on peak resolution:

(E3-3) $H = \mathrm{A} + \frac{B}{\mu} + C\mu$

Figures B-3 and B-4 show no loss in peak resolution when using a higher flow rate (1.25 ml min^{-1} vs 0.75 ml min^{-1}). To confirm that there was no loss in efficiency at higher flows, Van Deemter plots were created, using $MMAH^+$ and $TEAH^+$ as representative early and late-eluting species, by plotting theoretical plate height versus flow rate (Fig. B-5). To do this, the theoretical plate heights described in E3-3 were calculated using E3-4, which relates H to column length (L; mm), t_R and w. The A, B and C terms of E3-3 were then determined by solving a system of equations using the calculated H values for $MMAH^+$ and $TEAH^+$ at three isocratic flow rates as they are located at opposite ends of the elution range of the six most abundant atmospheric alkylamines (Fig. 3-1).

(E3-4) $\frac{L}{H} = 16\left(\frac{t_R}{w}\right)^2$

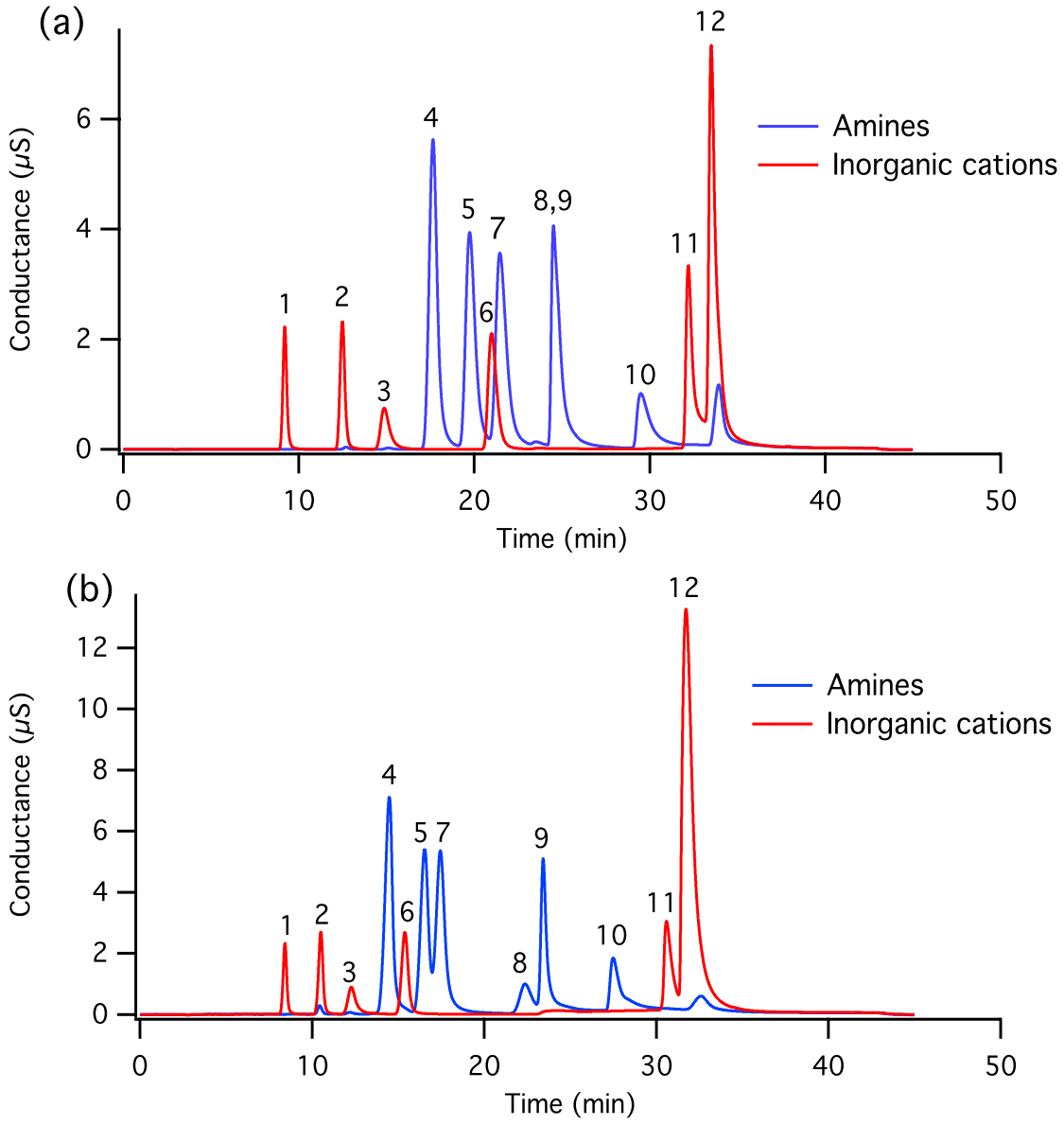

Figure 3-1. Separation of amine and inorganic cation standards with the highest resolution gradient program at (a) 30 and (b) 55°C. The order of elution and mass of cation injected in (a) is as follows: Li^+ (1, 16 ng), Na^+ (2, 158 ng), NH_4^+ (3, 169 ng), $MMAH^+$ (4, 500 ng), $MEAH^+$ (5, 500 ng), K^+ (6, 524 ng), $DMAH^+$ (7, 500 ng), $TMAH^+$ (8, 500 ng), $DEAH^+$ (9, 500 ng), $TEAH^+$ (10, 500 ng), Mg^{2+} (11, 128 ng), and Ca^{2+} (12, 361 ng). Cation peaks represent the same mass injected and are labeled according to the same numeric identities in (b).

The Van-Deemter plots for $MMAH^+$ and $TEAH^+$ show no sacrifice in resolution when operating at higher flow rates and low eluent concentrations. The resolution between Mg^{2+} and Ca^{2+} as well as between $TMAH^+$ and $TEAH^+$ improved at the higher flow rate for all isocratic eluent concentrations. This was due to a decrease in peak width from diffusion band broadening. Furthermore, there was little to no sacrifice in resolution for all other cation peak pairs when operating at a higher flow rate. Of particular note, utilizing a 4 mM MSA isocratic separation at a 1.25 ml min^{-1} flow rate instead of a 0.75 ml min^{-1} flow resulted in a runtime that was 20 min shorter, which improves the applicability of IC for near-real-time analysis of hourly to bi-hourly atmospheric sample collection timescales. A shorter run time also improves the method throughput capacity for offline analyses and reduces total eluent consumption. For these reasons, the faster flow rate was selected in designing and optimizing a gradient program. Further isocratic methods using lower MSA concentrations (1 mM and 2 mM) were run at a 1.25 ml min^{-1} flow rate to quantify values of peak-to-peak resolution for the inorganic cations and alkylamines before approaching a gradient method (Fig. B-3 and B-4). An increase in resolution greater than one was observed for all analyte pairs aside from $DEAH^+/TMAH^+$ when using a 1 mM MSA eluent concentration.

All gradient methods that were tested started with a 1 mM hold, followed by a step-wise increase and/or ramp to higher eluent concentrations at a column temperature of 30 °C. By combining the best isocratic separations for various pairs of cation analytes sequentially, iterative modifications were used to improve resolution based on Equations (3-1)-(3-3) with the best separation method selected from amongst the iterations. Higher column temperature has been used to improve the quality of an IC separation method

(Hatsis and Lucy, 2001; van Pinxteren et al., 2015; Rey and Pohl, 1996, 2003). Therefore, column temperature was systematically increased to investigate whether further improvement in peak-to-peak resolution was possible. Temperature effects on separation efficiency in ion chromatography are thermodynamically complex (Hatsis and Lucy, 2001; Kulis, K., 2004; Rey and Pohl, 1996), but they typically result in increased peak resolution because of improvements in mobile-phase diffusivity, which increases the efficiency term from E3-2. Higher temperatures can replicate the separation effects observed when adding an organic mobile phase modifier (Hatsis and Lucy, 2001; Rey and Pohl, 1996). Figure 3-1a and 3-1b show gradient separations at 30 and 55 °C respectively. At 30 °C, K^+ and $DMAH^+$ overlap considerably ($R_S = 0.45$) and $DEAH^+$ and $TMAH^+$ coelute. By increasing the column temperature to 55 °C, the extent of peak overlap between K^+ and neighboring alkylamine cations is noticeably reduced ($R_S > 1$) and $DEAH^+$ and $TMAH^+$ are increasingly well resolved ($R_S = 1.48$). The effect of temperature on the separation of the alkylamines is demonstrated in Fig. 3-2, where the separation of $DEAH^+$ with $TMAH^+$ is achieved above 50 °C. The temperature increase also results in lower resolution between $DMAH^+$ and $MEAH^+$ from $R_S = 1.57$ to $R_S = 1.08$. In our method, a column temperature of 55 °C produced peak-to-peak resolutions greater than a value of 1 between all six alkylamine cations and inorganic cations in the final gradient method, giving a 95% separation between our target analytes and expected atmospheric interferences in the condensed phase. The peak-to-peak resolutions are summarized in Table 3-1. These represent a lower-limit in peak resolution since they were calculated using peak parameters at the upper limit of the working range, which was determined

based on maximum mixing ratios or mass loadings expected for the analysis of atmospheric samples containing these analytes.

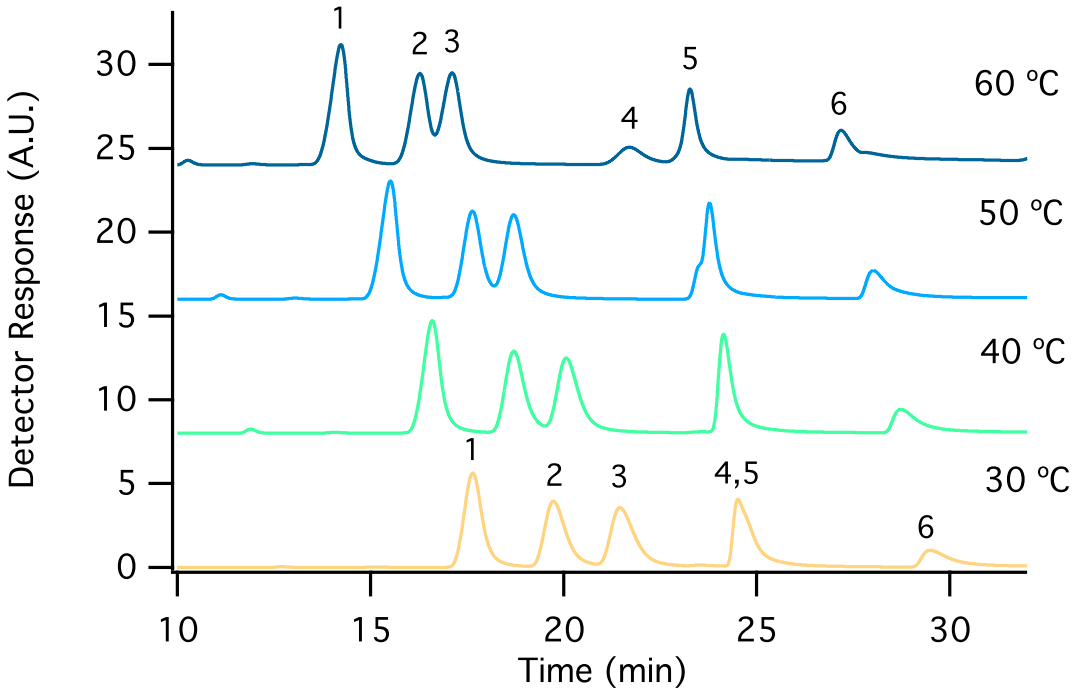

Figure 3-2. Separation of 1 µg ml^{-1} mixed amines standard with the final method gradient elution program at 30, 40, 50 and 60 °C. The peak elution order was MMAH$^+$ (1), MEAH$^+$ (2), DMAH$^+$ (3), TMAH$^+$ (4), DEAH$^+$ (5), and TEAH$^+$ (6). The separation of diethylamine (DEA) from trimethylamine (TEA) was achieved at column temperatures greater than 50 °C.

The separation method produced in this work is able to overcome previously reported IC coelution difficulties between DEAH$^+$ and TMAH$^+$ and between MEAH$^+$ and DMAH$^+$ (VandenBoer et al., 2012; Verriele et al., 2011). Both DMA and TMA have been identified as dominant amines in emission studies, so it is important to achieve accurate and specific quantitation of both species in gas and particulate atmospheric samples

(Facchini et al., 2008; Kuwata et al., 1983; Müller et al., 2009; Van Neste and Duce, 1987). Multiple field campaigns have detected large quantities of gas-phase and particle-phase MEA and DEA in ambient air as well (Facchini et al., 2008; Müller et al., 2009; Sorooshian et al., 2009; Yang et al., 2005; Yang et al., 2004). In some cases clean up steps have been used to alleviate IC interferences from common atmospheric cation species in the quantitation of amines despite the fact that an 85% evaporation loss of the amines, in addition to the extra sample handling, was reported when using a solid-phase extraction clean up (Huang et al., 2014). The CS19 IC method reported here is able to separate the most common atmospheric inorganic cations in addition to 11 common atmospheric amines (see separation of five additional alkylamines in Sect 3.4.1.3). It can be easily applied to water-soluble atmospheric gas and particulate samples since they can be directly analyzed - without coelution or a clean-up step - with separation times of similar duration to many previously reported methods, including those employing an online IC method (Huang et al., 2014; Murphy et al., 2007; VandenBoer et al., 2012; Verriele et al., 2011).

3.4.1.2 Instrumental Performance and Comparison for the Methylamines, Ethylamines and Inorganic Cations

The performance statistics of the CS19 gradient method for each cation are summarized in Table 3-1. The method shows high reproducibility, with method precisions better than 10% for most analytes. Although the instrumental response varied from month-to-month for each analyte, this variability was random and the calibration curve slopes for each analyte showed no systematic decrease over time. The larger

variability in the $TMAH^+$ and $TEAH^+$ calibration curves ($\pm$ 16% and $\pm$ 11%, respectively) is likely driven by their lower Henry's Law constants (K_H) in water (Christie and Crisp, 1967), resulting in volatilization losses from standards. Concurrently, this variability could be driven by partitioning losses along the flow path, particularly when the tri-subsituted amines reach the suppressor, which was not temperature controlled. In future investigations it may be worthwhile to acidify the standards to ensure the amines are maintained in their charged form in the aqueous phase. Alternatively, to combat losses to neutral forms, use of a Salt Converter suppressor accessory (ThermoScientific, SC-CSRS 300, P/N: 067530), which keeps weak electrolytes in a separated sample fully protonated prior to their conductance measurement, may also aid in increasing long-term $TMAH^+$ and $TEAH^+$ precision.

The LODs for each analyte are reported in Table 3-1 as both a range and as the average LOD ($\pm$ 1σ). The LODs are reported in this manner to reflect the high day-to-day variability in the calculated LODs. This variability may be driven by i) the purity of the deionized water used for eluent generation; ii) instrumental baseline noise and trace contamination on the day of analysis; and iii) quality of labware cleaning prior to preparation of calibration blanks. Outliers in the LOD dataset were found to result from trace contamination of analytical labware, sampling vials, or from systematic errors made in the preparation of standards or injection of samples on the IC (e.g. leaking autosampler caps, failing retention of concentrator column). The Grubb test was performed using a 95% confidence interval to statistically identify outliers from LOD data sets. Calculated detection limits were determined to lie in the picogram per injection range for all analytes.

Table 3-1. Separation characteristics and statistics for the CS19 gradient method. The retention time (t_r) ranges for the methyl amines, ethyl amines and inorganic cations were determined using retention time windows from a full calibration. The peak width and resolution were determined using the highest calibration standards amines (500 ng) and inorganic (160 – 520 ng) cations. The t_r range and peak width were back-calculated for $iMPAH^+$, $MPAH^+$, $MBAH^+$, $DABH^+$ and $DAPH^+$ based on the other alkyl amines responses to column degradation. Sensitivity, precision, average LOD, and LOD range were analyzed using multiple calibration standards and blanks (see Section 3.3.4). Upper and lower range accuracies were assessed using high and low check standards for the alkyl amines (n=6) and inorganic cations (n=4). The low check standards were 15 times more concentrated than the lowest calibration standard and the high check standards were 150 times more concentrated.

Cation	t_r (min)	Peak width (min)	Resolution	Sensitivity ($\mu S*min*mol^{-1}$)	Precision % ($\pm$ 1σ)	Upper range accuracy (%)	Lower range accuracy (%)	Average LOD (pg) ($\pm$ 1σ)	LOD range (pg)
Li^+	8.2 – 8.4	0.72	2.68	11.5E08	2	96 $\pm$ 5	82 $\pm$ 4	0.6 $\pm$ 0.2	0.3 - 0.8
Na^+	10.1 -10.3	0.73	1.87	5.04E08	2	95 $\pm$ 4	90 $\pm$ 6	8 $\pm$ 4	4 - 14
NH_4^+	11.8 – 12.1	1.18	0.65/1.85*	2.45E08	4	103 $\pm$ 4	50 $\pm$ 50	22 $\pm$ 17	7 - 47
$MEtAH^+$	12.7 – 13.0	0.99	0.56	2.2E08	---	---	---	3600 (n = 1)	---
$MMAH^+$	13.5 – 13. 8	0.86	1.09	1.42E08	5	98 $\pm$ 6	40 $\pm$ 30	300 $\pm$ 300	30 - 650
K^+	14.7 – 14.8	0.87	1.22	4.14E08	5	99 $\pm$ 2	94 $\pm$ 7	14 $\pm$ 11	4 - 28
$MEAH^+$	15.5 – 15.8	0.79	1.08	0.90E08	7	97 $\pm$ 5	40 $\pm$ 10	500 $\pm$ 200	200 - 700
$DMAH^+$	16.4 – 16.7	0.85	1.64	1.48E08	5	100 $\pm$ 10	30 $\pm$ 30	200 $\pm$ 300	40 - 650
$iMPAH^+$	18.2 – 18.5	0.79	2.24	0.84E08	4	90 $\pm$ 10	80 $\pm$ 80	70 $\pm$ 40	40 - 90
$MPAH^+$	20.1 – 20.4	0.88	1.55	0.62E08	12	88 $\pm$ 4	90 $\pm$ 90	50 $\pm$ 40	20 - 80
$TMAH^+$	21.2 -21.6	1.11	1.48	0.34E08	16	90 $\pm$ 10	30 $\pm$ 20	600 $\pm$ 300	300 - 1200
$DEAH^+$	22.6 – 22.7	1.18	2.51	0.76E08	8	97 $\pm$ 8	50 $\pm$ 30	400 $\pm$ 300	100 - 800
$MBAH^+$	25.3 – 25.6	0.43	3.12	0.62E08	1	80 $\pm$ 20	100 $\pm$ 80	910 $\pm$ 30	890 - 930
$TEAH^+$	27.3 – 27.7	0.95	3.40	0.85E08	12	96 $\pm$ 4	49 $\pm$ 6	800 $\pm$ 400	500 - 1400
Mg^{2+}	30.4 – 30.8	0.79	1.22	12.2E08	1	80 $\pm$ 20	100 $\pm$ 30	2000 $\pm$ 3000	200 - 4000
Ca^{2+}	31.6 – 32.9	1.05	3.16	14.3E08	2	90 $\pm$ 20	120 $\pm$ 20	3700 $\pm$ 200	3500 – 3800
$DABH^+$	36.6 – 36.9	1.48	0.98	4.5E08	---	---	---	1000 (n = 1)	---
$DAPH^+$	38.0 – 38.4	1.60	N/A	4.9E08	---	---	---	180 (n = 1)	---

The LODs for the inorganic cations were 10 to 100 times lower than those of the alkyl amines, with the exception of Mg^{2+} and Ca^{2+}. Trace contamination of Ca^{2+} in our ultrapure deionized water led to higher LODs for the divalent cations.

Our method shows high accuracy in the upper range of the calibrations for the methyl- and ethylamines, with accuracies ranging from 90 to 100%. The accuracy was much lower for each methyl- and ethylamine cation at the low end of the calibration range where amine concentrations were approximately 1.5 times the limit of quantitation (LOQ). Quantitation near the method LOQ was more sensitive to small integration changes, which affected the calculated peak area, even when performing integrations manually, and this resulted in greater accuracy error. This is a drawback inherent to IC since wide analyte peaks are a result of persistently large stationary-phase particle sizes, causing band broadening via longer flow paths and increased diffusion during separation (i.e. the A and B terms in Eq. 3-3). The low alkylamine accuracies may also be driven by their air-water partitioning properties, which could result in losses during sample handling and during sample injection. The low and high range accuracies for all inorganic cations, with the exception of ammonium, were high (80 – 120%) because concentrations were not near the LOQ for these analytes. The low check standard accuracy for ammonium likely arises due to similar issues as those discussed above for the tri-substituted amines.

It is important to note that the standard concentrations used to generate the method statistics for the alkylamines contained inherent uncertainty because they were derived from density calculations of non-standardized alkylamine stock solutions. Since the

alkylamine stock solution concentrations were not verified via inter-lab or inter-method comparison, there is no way to know for certain whether the reported %w/w values are the true stock solution values. Therefore, some or all of the calculated alkylamine method statistics may have an inherent systematic offset if the calculated concentrations differed from the true values.

To further test the efficacy of the separation method, a standard addition calibration was performed in the presence of the complex BB matrix. The calibration slopes and retention times for each analyte from the standard addition and external calibration performed on the same day are listed in Table B-1. The slopes for the two calibrations varied between 0 and 8%, which is within the method calibration precisions presented in Table 3-1. Thus, the BB sample extracts did not exhibit matrix effects. However, increasing retention times of approximately 0.3 – 0.5 min were observed for all cation analytes when performing the standard addition. This is an effect inherent in IC when samples with higher total quantities of cations are preconcentrated, resulting in a sample plug filling a greater quantity of the stationary-phase capacity. The initial weak mobile-phase of the gradient method will therefore take a greater amount of time to elute all of the analyte cations from the preconcentration and analytical columns. This same increase in retention times is present in the external calibration with increasingly concentrated standards (Table 3-1).

Previous IC instrumental precisions reported for use in quantifying the six atmospheric methyl- and ethylamines range from 0.4 to 17.2%, which is comparable to our method (Table B-2; Chang et al., 2003; Dawson et al., 2014; Erupe et al., 2010; Huang et al., 2014; Li et al., 2009; VandenBoer et al., 2012; Verriele et al., 2012;). Our

separation method shows greater average variability than others due to our numerous assessments (n = 9) over multiple months, a more comprehensive analysis compared to previous reports. The sensitivity of this instrument is also similar to that of all other reported IC methods as the instrumental detection limits are in the picogram range. Only VandenBoer et al. (2012) and Chang et al. (2003) report lower detection limits and these are likely a result of a lower background signal from running the IC instruments online. Our method does not achieve instrumental limits of detection as low as those achieved using derivatization methods coupled with GC-MS or HPLC analysis (Akyüz, 2007; Fournier et al., 2008; Possanzini and Di Palo, 1990). However, multistep derivatization methods are prone to losses that must be quantified with internal standards. These losses can lead to higher overall method detection limits, which is not the case for direct analysis of water-soluble samples. Derivatization methods are also difficult to employ for near-real-time analyses of the atmosphere, making the approach less analytically attractive. Further, the IC separation method presented here is able to address additional matrix effects that may result from other atmospheric species through the use of a sample pre-concentration column. Only positively charged species are retained in this pre-concentration step and injected through the IC system for analysis, negating matrix effects from non-charged and anion species, as demonstrated by the standard addition to the BB sample extract.

Employing a method that is capable of quantifying amines at very low mixing ratios is valuable since recent work has shown that parts per quadrillion by volume (ppqv) concentrations of gaseous amines can lead to particle formation and growth (Almeida et al., 2013). If our method were applied to online atmospheric ambient

sampling of gases or particles the method could be used to detect amines at ppqv mixing ratios. For example, a detectable signal for 100 ppqv mixing ratios could be attained by sampling through a bubbler, filter, or denuder at a low flow rate of 3 L min^{-1} for 1 – 10 hours, depending on the amine. It may be possible to shorten the sample collection duration to an hourly timescale to detect ppqv mixing ratios of atmospheric amines if the method is interfaced with a high sensitivity MS detector. Verriele et al. (2014) observed a 5 – 30 fold improvement in method detection limits when interfacing their IC method with a MS detector.

3.4.1.3 Expanded Amine Catalogue for other Common Atmospheric Species

The separation method developed was further investigated to elucidate its utility in quantifying MPA, iMPA, and MBA, three amines that have been frequently detected in ambient air (Ge et al., 2011). In particular, this test was performed to assess their potential coelution with the fully separated methyl- and ethylamines. Without modification of the gradient method, we observed separation of these three amines from the original 12 cations with $R_s > 0.85$ (Fig. 3-3a). $MPAH^+$ and $iMPAH^+$ eluted between $DMAH^+$ and $TMAH^+$ and $MBAH^+$ eluted later, but before $TEAH^+$. The resolution is sufficient between all analyte peaks to allow quantitative analysis of the nine alkylamine cations and six inorganic cations. The separation statistics for these additional amines are also presented in Table 3-1. Since the additional amines were injected after column degradation had occurred and retention times had noticeably shifted (see Fig. 3-3a vs. Fig. 3-1b and Sect 3.4.1.5 for further discussion), retention time and peak width were estimated using changes in separation parameters from the original method development for the methyl- and ethylamines.

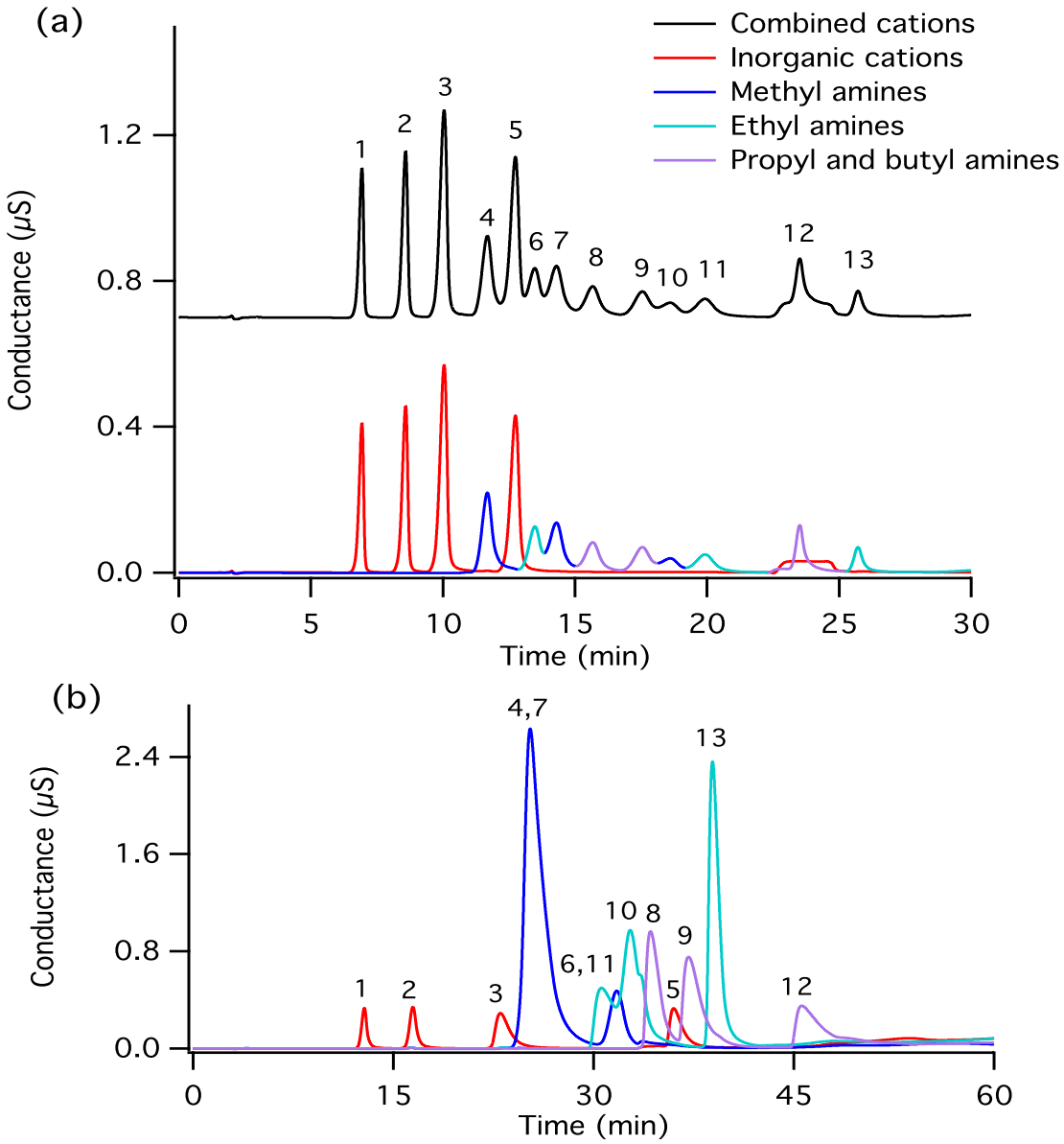

Figure 3-3. (a) Separation of amine and inorganic cation standards with the addition of $MPAH^+$, $iMPAH^+$ and $MBAH^+$ using the final gradient program. The order of elution and mass of cation injected in (a) is as follows: Li^+ (1, 1.6 ng), Na^+ (2, 16 ng), NH_4^+ (3, 17 ng), $MMAH^+$ (4, 50 ng), K^+ (5, 52 ng), $MEAH^+$ (6, 50 ng), $DMAH^+$ (7, 50 ng), $iMPAH^+$ (8, 50 ng), $MPAH^+$ (9, 50 ng), $TMAH^+$ (10, 50 ng), $DEAH^+$ (11, 50 ng), $MBAH^+$ (12, 50 ng), and $TEAH^+$ (13, 50 ng). (b) Separation of amine and inorganic cation standards with the addition of $MPAH^+$, $iMPAH^+$ and $MBAH^+$ and the addition of the CG15 column using a modified gradient program. Cation peaks are labeled accordingly to the same identities in (b) and the mass of analyte injected is as follows: Li^+ (1.6 ng), Na^+ (16 ng), NH_4^+ (17 ng), $MMAH^+$ (500 ng), K^+ (52 ng), $MEAH^+$ (500 ng), $DMAH^+$ (500 ng), $iMPAH^+$ (500 ng), $MPAH^+$ (500 ng), $TMAH^+$ (500 ng), $DEAH^+$ (500 ng), $MBAH^+$ (500 ng), and $TEAH^+$ (500 ng).

Peak widths for the propyl- and butylamines were assumed to have increased by approximately 50%, consistent for the same increases observed for the methyl- and ethylamines as a result of the column degradation. Retention times for $MPAH^+$, $iMPAH^+$, and $MBAH^+$ were back-calculated to reflect the initial column conditions using these corrected peak widths and the resolution values determined from the chromatogram presented in Fig. 3-3. The method precisions for $iMPAH^+$, $MPAH^+$ and $MBAH^+$ determined from two standard calibration injections ranged from 1 to 12%.

The reported average LODs for both propylamines are the lowest of the alkyl amines, while $MBAH^+$ has the highest method LOD because it elutes in a region with a high background due to the step change in eluent composition not being completely suppressed. The method accuracies for the three additional amines assessed by both the high and low check standards were within 80% for all analytes. However, the large standard deviations in the accuracies for all low check standards highlights the challenge of method reproducibility for these analytes near the LOQ. This CS19 IC method can resolve three sets of alkylamine structural isomers, thus not only allowing full speciation of the suite of common atmospheric amines but also overcoming a limitation of direct MS analysis of the atmospheric matrix.

Since diamines have recently been shown to be potent sources of new particle formation and have been detected in field campaigns across the U.S.A. (Jen et al., 2016b), as well as near livestock, food processing factories and sewage facilities (Ge et al., 2011), quantitation of $DABH^+$ and $DAPH^+$ was tested using the CS19 gradient method. The two diamines eluted after all 15 analytes, with $DABH^+$ and Ca^{2+} having a resolution of 3.16 and $DAPH^+$ and $DABH^+$ having a resolution of 0.98. A single

calibration curve was run to provide an estimate of the sensitivity and LOD for $DABH^+$ and $DAPH^+$ and the retention times for these two additional diamines were also back-calculated to reflect initial column conditions (Table 3-1). If the 10 mM MSA hold of the optimized method is extended by 5 min to give a total run time of 40 min, then $DABH^+$ and $DAPH^+$ can also be quantified. Ethanolamine (EAH^+), a compound employed in industry and CO_2 capture (Ge et al., 2011), was also analyzed by this IC method and found to have poor resolution with NH_4^+ and $MMAH^+$ ($R_S < 0.65$, Table 3-1). However, the peak is still identifiable in samples containing these analytes.

3.4.1.4 Method Development with the Addition of an Inline CG15 Guard Column

As mentioned previously, IC methods in the literature have been unable to separate potassium from the methyl- and ethylamines (Huang et al., 2014; VandenBoer et al., 2012), and in our current method K^+ has slight overlap with $MMAH^+$ ($R_S = 1.09$). We attempted to reduce peak overlap between K^+ and the alkylamines by adding a crown ether-functionalized CG15 guard column in-line after the CG19/CS19 columns. The addition of the CG15 column, which has increased selectivity for K^+, resulted in an increased retention time for K^+ of 13 min. The best separation achieved using the additional guard column is shown in Fig. 3-3b, where K^+ still elutes within the alkylamine retention region. The gradient method used to achieve the separation used a flow rate of 1 ml min^{-1}, a column temperature of 55 °C, and held a 1 mM MSA concentration for the first 30 min. The eluent concentration was step increased to 4 mM followed immediately by an exponential ramp to 10 mM over 20 min (Chromeleon curve factor of 7). The final concentration of 10 mM is held for an additional 15 min, yielding a total run time of 65 min. Even when holding the initial MSA concentration at 1 mM for

50 min, the separation was unable to fully resolve the alkylamine peaks. An increase in retentivity for K^+ and NH_4^+, as well as many of the alkylamines, indicated that the crown ether functionality was not selective for K^+ in this suite of analytes. With the addition of an organic modifier to the mobile phase or the ability to decrease column temperature, this increase in selectivity from the CG15 column might be harnessed to produce better separation. However, due to the limitations of the ICS-2100 system using RFIC we were unable to investigate these parameters. Furthermore, although a passable separation may be achieved when using a run time greater than 60 min, this would not be as applicable to online analyses as the CG/CS19 method developed without the addition of the CG15 column. A stationary phase similar to that of the CG/CS19 columns, but with some of this crown ether selectivity, could potentially yield better results than those presented here, particularly for the analysis of atmospheric samples containing large quantities of K^+ and amines.

3.4.1.5 Analytical Column Stability

Over the course of 5 months, peak retention times noticeably decreased and peak broadening of approximately 50% occurred for all analytes. After more than 1000 sample and standard injections retention times had decreased by 1.9 ± 0.1 min depending on the cation. Peak-to-peak resolution, however, remained largely unchanged throughout the column degradation during standard and sample analysis, even with observed peak broadening. This is consistent with what has been previously reported in the literature when hundreds to thousands of injections have been run through an IC column (VandenBoer et al., 2011). This may also be a result of column degradation from

operating the CS19 column at a temperature higher than that recommended by the manufacturers.

During the course of method development severe peak broadening and subsequent peak-to-peak resolution loss of Mg^{2+} and Ca^{2+} was also observed. After the analysis of hundreds of samples the unresolved coeluting divalent cations had a peak width greater than 10 min wide. The Mg^{2+} and Ca^{2+} peak areas eventually became unresolved, with their combined peak area precision in the highest standard within 6% ($\pm$ 1σ) after 12 months of analysis. It was determined that this broadening effect observed for the Mg^{2+} and Ca^{2+} peaks was due to a malfunctioning suppressor. After replacing the suppressor, a peak-to-peak resolution greater than 1 was restored for these analytes. Furthermore, the cumulative analyte peak broadening that had occurred throughout method development and sample analysis for all the monovalent cations was also mitigated by installing the new suppressor. Retention times however were still shifted by 1.9 $\pm$ 0.1 min, indicating that analytical column degradation had still occurred.

3.4.2 Biomass-Burning Particle Analysis and Discussion

3.4.2.1 Size-Resolved Alkylamines in Particles from an Aged Biomass-Burning Plume

BB particles often contain a complex mixture of water-soluble ions, organics, elemental carbon, and other insoluble components, making them nonpareil for testing the robustness of an atmospheric measurement technique. Ions such as NH_4^+ and K^+ are consistently detected in BB plumes, regardless of sampling location as they are well characterized as being co-emitted species (Capes et al., 2008; Hudson et al., 2004; Pósfai

et al., 2003). Particles released during forest fires have also been shown to contain highly oxidized large molecular weight organics (Di Lorenzo and Young, 2016; Saleh et al., 2014). We tested the robustness of our method on water-extracted aged BB particle samples collected by a cascade impactor in St. John's, Canada. Gas-sorption and reaction artifacts are minimized due to the gaseous flow path being directed around the nanoMOUDI impaction plates; therefore samples analyzed are representative of the particles in the atmosphere.

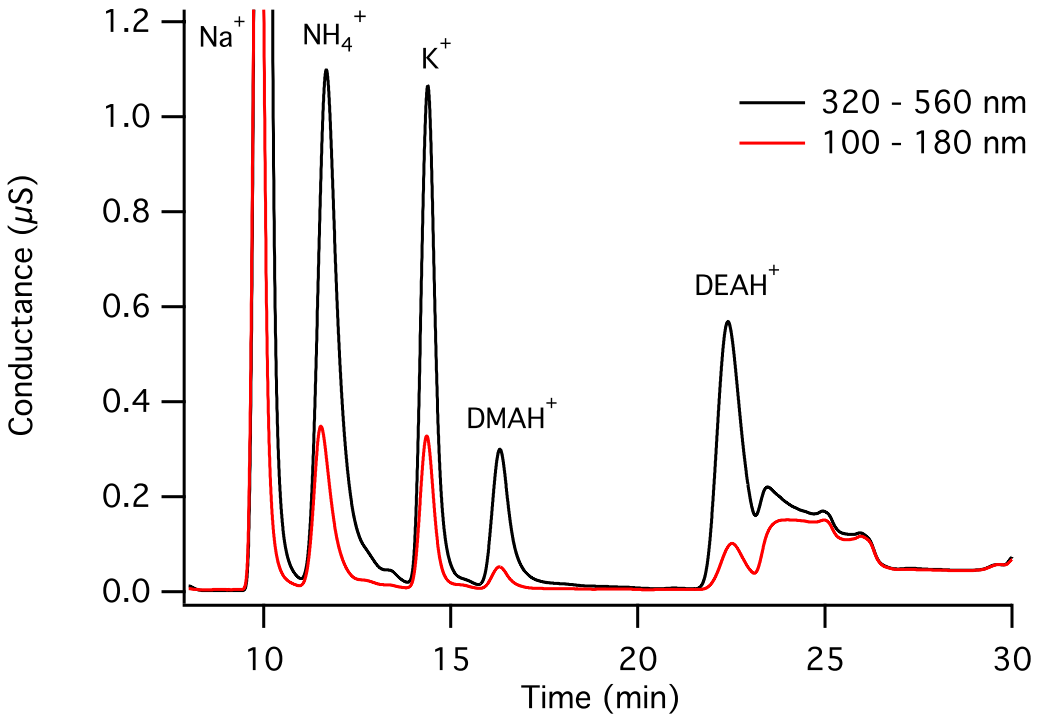

Figure 3-4. Overlaid chromatograms of MOUDI size-fractionated particle samples collected in St John's on July 6, 2013 during the intrusion of a biomass-burning plume that originated from Northern Labrador and Quebec. The robustness of the separation method for $MMAH^+$, $DMAH^+$ and $DEAH^+$ from the common inorganic cations is demonstrated for the 320-560 nm (Black) and 100-180 nm (Red) size bins.

An overlaid chromatogram of two different size-resolved particle samples (100 - 180 nm and 320 – 560 nm) shows the presence of $MMAH^+$, $DMAH^+$ and $DEAH^+$ in the aged BB samples with complete separation from K^+, NH_4^+ and Na^+ once the sample had been diluted to the working calibration range (Fig. 3-4). The maximum mass loadings for $MMAH^+$, $DMAH^+$ and $DEAH^+$ were found in particles with diameters of 320 – 560 nm and were 11 $\pm$ 3, 208 $\pm$ 4, and 1300 $\pm$ 200 ng m^{-3}, respectively (Table B-3). $TMAH^+$, $MEAH^+$, and $TEAH^+$ peaks were also detected in the BB size-resolved particle extracts. $TMAH^+$ and $TEAH^+$ reached mass loadings of 5 $\pm$ 3 ng m^{-3} and 4 $\pm$ 2 ng m^{-3}, respectively, while $MEAH^+$ never exceeded a concentration of 1 ng m^{-3} in any size-resolved particle fraction (Table B-3). Lobert et al (1990) reported detecting $C_1 - C_5$ aliphatic amines from controlled BB experiments, which is consistent with our findings. BB-derived amines were also identified during the 2007 San Diego forest fires (Zauscher et al., 2013) with primary amines observed at approximately 6% by mass of organic content from an aged BB particle sample in British Columbia (Takahama et al., 2011). However, few studies have addressed the speciation and quantitation of alkylamines emitted from BB events. Schade and Crutzen (1995) estimated the emission rates for MMA, DMA, TMA and MEA from BB sources based on controlled burn experiments, but do not include a BB emission rate for DEA or TEA. These emission estimates are yet to include emission rates from atmospheric BB measurements (Lobert et al., 1990; Schade and Crutzen, 1995).

In Fig. 3-5a we show the molar ratio of the sum of the methyl- and ethylamines to ammonium which is considered to be the main atmospheric base, as a function of the size-resolved particles collected. The summed amine moles exceeded ammonium in the

particle diameter range from 100 to 560 nm, and the ratio ranged from 0.5 to 1.9 in the fine mode ($PM_{1.0}$), with an average ratio of 0.92 in $PM_{1.0}$ calculated using nanoMOUDI bins up to this nominal cutoff. Quantities of NH_4^+ were below the detection limit above 1 μm, yielding no values for the ratio. The large error bars in the ratios are driven by the low molar quantities of ammonium in the samples as well as a higher variability in three extraction blanks (ultrapure deionized water sonicated in polypropylene tubes) injected on the day of analysis. For these reasons this method blank error was assigned to the size-resolved samples in place of the NH_4^+ error driven by the method precision and accuracy detailed in Table 3-1. To our knowledge, this is the first time that an amines to ammonium ratio greater than 1 has been reported in the $PM_{1.0}$ resolved fraction of atmospheric particles. An amine-to-ammonium ratio of 0.37 in fine-mode aerosol ($PM_{1.8}$) was reported by VandenBoer et al. (2011), but most reported ratios have been below 0.1 (Ge et al., 2011). These high ratios we observed can be attributed to large quantities of $DEAH^+$ and $DMAH^+$. $MMAH^+$ was found to be in molar quantities 100 times less than that of ammonium while $TMAH^+$, $MEAH^+$ and $TEAH^+$ were found to be in molar quantities 1000 to 10 000 times less than ammonium. Detecting such large molar ratio quantities of $DEAH^+$ and $DMAH^+$ to NH_4^+ in any particle sample is also unprecedented. Mono-substituted amines are the most frequently detected alkylamines in atmospheric particles and at molar ratios to ammonium of 1:100 or lower (Ge et al., 2011; Gorzelska et al., 1990; Mader, 2004, Müller et al., 2009; Yang et al., 2005; Yang et al., 2004; Zhang et al., 2003). In most instances where di-substituted or tri-substituted amines have been identified in the particle phase, they are present at molar quantities equal to or less than the mono-substituted amines (Healy et al., 2015; Suzuki et al., 2001).

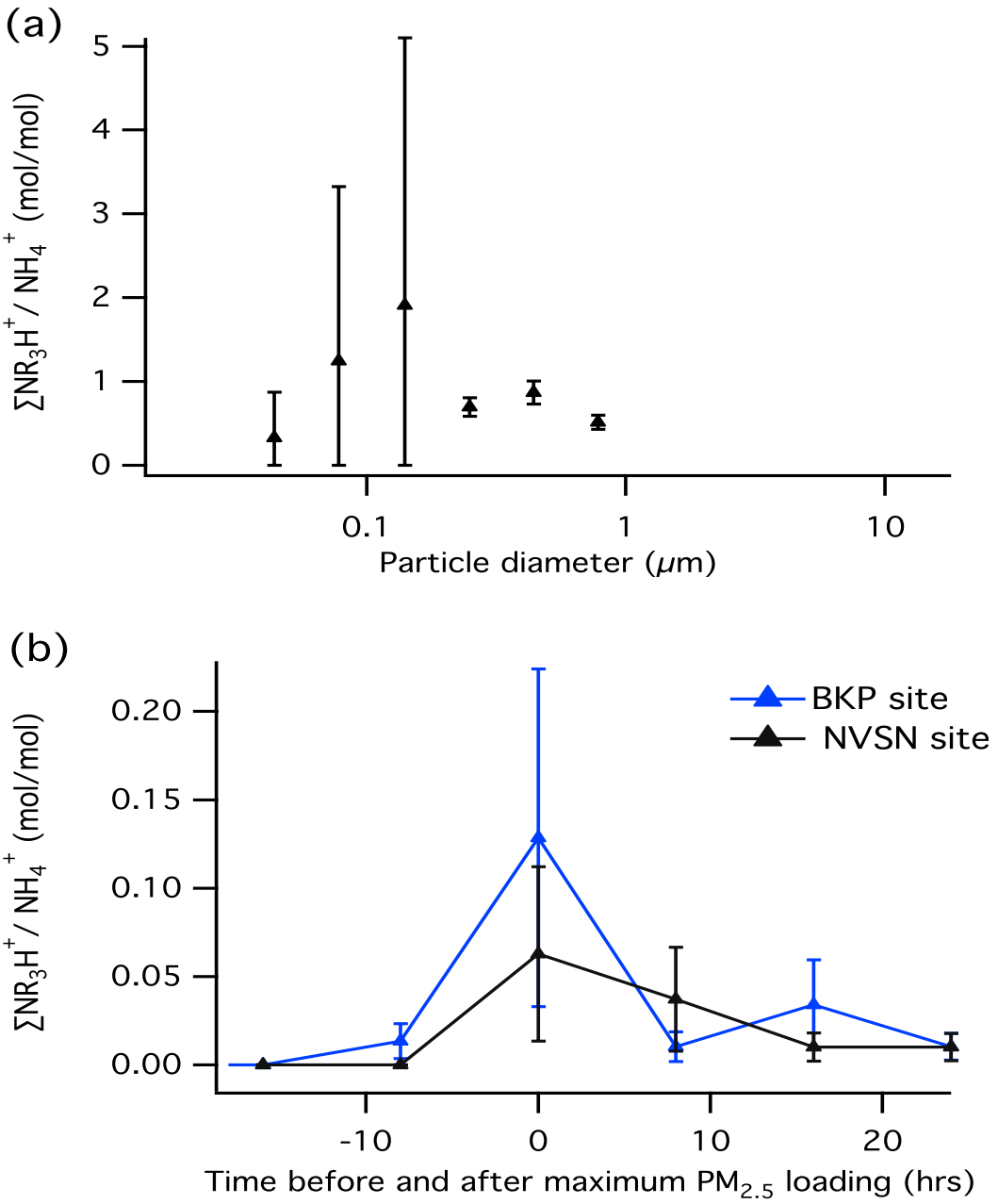

Figure 3-5. (a) Amines to ammonium ratio in the size-resolved aged biomass-burning sample originating from Quebec and Labrador in the summer of 2013. (b) Amines to ammonium ratio for the Burnaby/Kensington Park (BKP) site and North Vancouver/Second Narrows (NVSN) site in British Columbia during the summer 2015 wildfires. The error bars in the graph represent propagated error in the amine and ammonium quantities resulting from variability in the field blanks and check standards during the analysis of the samples.

Thus, such high quantities of $DMAH^+$ and $DEAH^+$ in these samples were unexpected and highly unusual compared to prior reports. In this case, the observation may be due to the fuel source of the fire or the interaction of the plume with a potent source of atmospheric amines. Previous work has identified di-substituted amines in large quantities from feedlot plumes (Sorooshian et al., 2008) and in marine particles (Facchini et al., 2008; Gibb et al., 1999a; Müller et al., 2009; Sorooshian et al., 2009; Van Pinxteren et al., 2015; Youn et al, 2015). In fact, DMA and DEA have been reported as the second and third most abundant organic species in marine fine aerosol behind MSA during periods of high biological activity in the North Atlantic (Facchini et al., 2008). Other researchers have also suggested a moderate to high correlation between high biological activity and di-substituted amine particle mass loadings (Müller et al., 2009; Sorooshian et al., 2009). Laboratory investigations have shown that methylamines can be produced by marine phytoplankton degradation of quarternary amines to maintain an osmotic gradient as well as during periods of known zooplankton grazing (Gibb et al., 1999b). Based on the HYSPLIT back trajectories calculated for these samples (Di Lorenzo, 2016), it is possible that the BB plume particles interacted with gaseous DMA and DEA emitted from inland agricultural sources along the St. Lawrence River, coastal phytoplankton blooms, or with enhanced amine emissions in the coastal zone, which has been observed in the marine boundary layer of California (Youn et al., 2015). The high concentrations of DMA and DEA produced by marine biological activity could then partition into the biomass burning particles and react to neutralize acids (e.g. sulfuric acid), form salts or amides with organic acids, or react with carbonyl moieties in the highly oxidized organic material produced via BB to form imines (Qiu and Zhang, 2013). If this explanation

holds true then there may be preferential uptake of these amines over ammonia into the plume, as there is no evidence yet that suggests a larger agricultural or marine source of amines relative to ammonia to the atmosphere. A marine amines hypothesis, while consistent with observations in the literature, is beyond the scope of this work in terms of assigning a definitive DMA and DEA source.

3.4.2.2 Time Series of Amines in Fresh Biomass Burning Plume Particles from British Columbia

Our method was also applied to a time series of $PM_{2.5}$ samples collected at two different locations (BKP and NVSN) during a forest fire in the Lower Fraser Valley in British Columbia in the summer of 2015. These $PM_{2.5}$ samples were collected every 8 h while the plume was traversing each site and during collection the $PM_{2.5}$ concentration was in excess of 200 μg m^{-3}. The relative ages for the smoke plumes sampled at both sites were calculated to be 20 h old, or less, and back trajectories indicated that the plume did not travel over the open ocean before being sampled (Di Lorenzo et al., 2016). In these test samples, the method was again able to detect the presence of four different amines ($iMPAH^+$, $TMAH^+$, $DEAH^+$, and $TEAH^+$) with loadings of Na^+, NH_4^+ and K^+ at ratios in excess of 100:1 (Figure B-6). Furthermore, the method was not only able to determine the presence of $iMPAH^+$ but also differentiate it from $MPAH^+$ and $TMAH^+$, its two structural isomers. $iMPAH^+$, $TMAH^+$, $DEAH^+$, and $TEAH^+$ had maximum mass loadings in these fresher BB samples of 60 ± 40, 9 ± 7, 1.6 ± 0.8, and 0.2 ± 0.1 ng m^{-3} respectively (Table B-4). $iMPAH^+$ was the amine detected in the largest molar quantities at both sampling sites in British Columbia. The detection of $iMPAH^+$ has not previously been reported in BB particles, and based on our measurements may be important to quantify in future

controlled burn experiments. Our results differ from the study conducted by Takahama et al (2011) on the 2009 forest fires in British Columbia that reports the detection of primary amine groups, which further suggest that amine emissions from BB and/or their incorporation into BB particles are not well understood. Although our observed suite of amines includes $iMPAH^+$, there was no indication of other primary amines from the analyses of the BB particles. The calculated quantities of amines for these samples may be biased high or low because the beta attenuation monitor used to sample the BB particles can be prone to gas-phase blow-on or blow-off artifacts via sorption or reactive mechanisms. Although the extracted field blank was corrected for any positive sorption biases on the filter tape (e.g. Müller et al., 2009), it was unable to account for any reactive uptake of gas-phase amines during the sampling period. Therefore, the filter tape BB samples presented here represent a time-integrated particulate composition assuming thermodynamic equilibrium between the gas and particulate phases for the duration of collection for each sample.

A time-series of the amine-to-ammonium molar ratio as the smoke plume intrudes into both the BKP and NVSN sites is presented in Fig. 3-5b. There were either no amines present or they were present in concentrations below our detection limits in the ambient particles collected on the front edge of the plume intrusions. When the maximum $PM_{2.5}$ mass loading of the plume reached the sampling site at $t = 0$, we saw an absolute maxima in total amine concentration as well as a relative maxima in the particulate amine-to-ammonium molar ratio (Fig. 3-5b). The particulate amine concentrations and the amine-to-ammonium ratio then tapered off as the plume diluted and passed through the site. The measured amine-to-ammonium ratio in these samples is consistent with previously

reported literature values (Ge et al., 2011). The measured amine species and quantities, as in the aged plume, could be indicative of the BB source fuel, fire type, or amine levels in air masses intercepted that were subsequently incorporated by partitioning and reacting into the condensed phase. Since the smoke plumes were less than a day old and the plume did not travel over the open ocean, it is less likely that offshore marine amine emissions interacted with the plume. However, the BKP and NVSN sampling sites are positioned in a coastal urban center and anthropogenic amine emissions from industry or animal husbandry operations nearby, as well as coastal amine emissions, may still have been incorporated into the plume before it was sampled.

3.5 Conclusions

We developed an ion chromatographic method that can separate and quantify the nine most abundant atmospheric alkylamines and two alkyl diamines from common inorganic atmospheric cations. Ion chromatography methods reported in the literature cannot fully resolve alkylamine peaks, nor separate interferences from K^+, Mg^{2+} and Ca^{2+}. In this work, we report the ability to overcome these prevalent issues for atmospheric sampling with a rapidity that can also be applied to near real-time analyses of aqueous atmospheric extracts by IC. Additionally, the method is able to separate and quantify three sets of structural isomers, a limitation for direct particle and gas sampling mass spectrometry instrumentation in quantifying atmospheric alkylamines. The method detection limits are comparable to other published IC methods in the literature, but the described method is not as sensitive as instrumentation used in conjunction with derivatization methods coupled with GC-MS or LC-MS, which can suffer from sample processing losses.

The IC method is robust. Two sets of BB particle samples collected at two different locations in Canada were injected onto the IC column and the method detected and quantified amines with the presence of a complex matrix where inorganic analytes, such as K^+, reached ratios of 1000:1 relative to the alkylamines. A standard addition demonstrated that the BB matrix does not have any influence on the ability of the IC method to quantify these analytes. This is a major improvement over all prior reports of the application of IC to the detection of amines in aqueous extracts of atmospheric particulate matter. Our results suggest that increasing focus on speciation and quantitation of various alkylamines from direct BB emissions and their propensity to undergo reactive uptake with BB particles is needed to constrain global budgets of atmospheric sources and fate of alkylamines.

Overall, the developed IC method shows promise for i) adoption into standard analysis of water soluble atmospheric extracts; ii) incorporation into online instrumentation already using ion chromatography for near real-time analysis of water-soluble atmospheric samples; and iii) interfacing with high-resolution mass spectrometry for even higher analytical sensitivity, particularly where supporting measurements for ppqv levels of amines may be stimulating new particle formation in the atmosphere.

3.6 References

Aiken, A. C., Salcedo, D., Cubison, M. J., Huffman, J. A., DeCarlo, P. F., Ulbrich, I. M., Docherty, K. S., Sueper, D., Kimmel, J. R., Worsnop, D. R., Trimborn, a., Northway, M., Stone, E. a., Schauer, J. J., Volkamer, R., Fortner, E., de Foy, B., Wang, J., Laskin, a., Shutthanandan, V., Zheng, J., Zhang, R., Gaffney, J., Marley, N. a., Paredes-Miranda, G., Arnott, W. P., Molina, L. T., Sosa, G. and Jimenez, J. L.: Mexico City aerosol analysis during MILAGRO using high resolution aerosol mass spectrometry at the urban supersite (T0) – Part 1: Fine particle composition and organic source apportionment, Atmos. Chem. Phys., 9, 6633–6653, doi:10.5194/acpd-9-8377-2009, 2009.

Akyüz, M.: Simultaneous determination of aliphatic and aromatic amines in indoor and outdoor air samples by gas chromatography-mass spectrometry, Talanta, 71(1), 486–492, doi:10.1016/j.talanta.2006.10.028, 2007.

Almeida, J., Schobesberger, S., Kürten, A., Ortega, I. K., Kupiainen-Määttä, O., Praplan, A. P., Adamov, A., Amorim, A., Bianchi, F., Breitenlechner, M., David, A., Dommen, J., Donahue, N. M., Downard, A., Dunne, E., Duplissy, J., Ehrhart, S., Flagan, R. C., Franchin, A., Guida, R., Hakala, J., Hansel, A., Heinritzi, M., Henschel, H., Jokinen, T., Junninen, H., Kajos, M., Kangasluoma, J., Keskinen, H., Kupc, A., Kurtén, T., Kvashin, A. N., Laaksonen, A., Lehtipalo, K., Leiminger, M., Leppä, J., Loukonen, V., Makhmutov, V., Mathot, S., McGrath, M. J., Nieminen, T., Olenius, T., Onnela, A., Petäjä, T., Riccobono, F., Riipinen, I., Rissanen, M., Rondo, L., Ruuskanen, T., Santos, F. D., Sarnela, N., Schallhart, S., Schnitzhofer, R., Seinfeld, J. H., Simon, M., Sipilä, M., Stozhkov, Y., Stratmann, F., Tomé, A., Tröstl, J., Tsagkogeorgas, G., Vaattovaara, P., Viisanen, Y., Virtanen, A., Vrtala, A., Wagner, P. E., Weingartner, E., Wex, H., Williamson, C., Wimmer, D., Ye, P., Yli-Juuti, T., Carslaw, K. S., Kulmala, M., Curtius, J., Baltensperger, U., Worsnop, D. R., Vehkamäki, H. and Kirkby, J.: Molecular understanding of sulphuric acid-amine particle nucleation in the atmosphere., Nature, 502(7471), 359–363, doi:10.1038/nature12663, 2013.

Angelino, S., Suess, D. T. and Prather, K. A.: Formation of aerosol particles from reactions of secondary and tertiary alkylamines: Characterization by aerosol time-of-flight mass spectrometry, Environ. Sci. Technol., 35(15), 3130–3138, doi:10.1021/es0015444, 2001.

Ault, A. P., Moffet, R. C., Baltrusaitis, J., Collins, D. B., Ruppel, M. J., Cuadra-Rodriguez, L. A., Zhao, D., Guasco, T. L., Ebben, C. J., Geiger, F. M., Bertram, T. H., Prather, K. A. and Grassian, V. H.: Size-dependent changes in sea spray aerosol composition and properties with different seawater conditions, Environ. Sci. Technol., 47(11), 5603–5612, doi:10.1021/es400416g, 2013.

Barsanti, K. C., McMurry, P. H. and Smith, J. N.: The potential contribution of organic salts to new particle growth, Atmos. Chem. Phys., 9(9), 2949–2957, doi:10.5194/acp-9-2949-2009, 2009.

Berndt, T., Stratmann, F., Sipilä, M., Vanhanen, J., Petäjä, T., Mikkilä, J., Grüner, A., Spindler, G., Lee Mauldin III, R., Curtius, J., Kulmala, M. and Heintzenberg, J.: Laboratory study on new particle formation from the reaction OH + SO_2: influence of experimental conditions, H_2O vapour, NH_3 and the amine tert-butylamine on the overall process, Atmos. Chem. Phys., 10, 7101–7116, doi:10.5194/acp-10-7101-2010, 2010.

Berndt, T., Sipilä, M., Stratmann, F., Petäjä, T., Vanhanen, J., Mikkilä, J., Patokoski, J., Taipale, R., Mauldin, R. L. and Kulmala, M.: Enhancement of atmospheric H_2SO4/H_2O nucleation: Organic oxidation products versus amines, Atmos. Chem. Phys., 14(2), 751–764, doi:10.5194/acp-14-751-2014, 2014.

Boucher, O., Randall. D., Artaxo, P., Bretherton, C., Feingold, G., Forster, P., Kerminen, V.-M., Kondo, Y., Liao, H., Lohmann, U., Rasch, P., Satheesh, S. K., Sherwood, S., Stevens, B. and Zhang, X. Y.: Clouds and Aerosols. In: Climate Change 2013: The Physical Science Basis. Contribution of Working Group I to the Fifth Assessment Report of the Intergovernmental Panel on Climate Change, Cambridge, United Kingdom and New York, NY, USA, 87 pp., 2013.

Bzdek, B. R., Ridge, D. P. and Johnston, M. V.: Amine exchange into ammonium bisulfate and ammonium nitrate nuclei, Atmos. Chem. Phys., 10, 3495–3503, doi:10.5194/acp-3495-2010, 2010.

Bzdek, B. R., Ridge, D. P. and Johnston, M. V.: Amine reactivity with charged sulfuric acid clusters, Atmos. Chem. Phys., 11(16), 8735–8743, doi:10.5194/acp-11-8735-2011, 2011.

Cadle, S. H. and Mulawa, P. A.: Low-molecular-weight aliphatic amines in exhaust from catalyst-equipped cars., Environ. Sci. Technol., 14(6), 718–723, doi:10.1021/es60166a011, 1980.

Capes, G., Johnson, B., McFiggans, G., Williams, P. I., Haywood, J. and Coe, H.: Aging of biomass burning aerosols over West Africa: Aircraft measurements of chemical composition, microphysical properties, and emission ratios, J. Geophys. Res. Atmos., 113(23), 1–13, doi:10.1029/2008JD009845, 2008.

Christie, A. O. and Crisp, D. J.: Activity coefficients of the n-primary, secondary and tertiary aliphatic amines in aqueous solution, J. Appl. Chem., 17, 1967.

Chang, I.-H., Lee, C.-G. and Lee, D. S.: Development of an automated method for simultaneous determination of low molecular weight aliphatic amines and ammonia in ambient air by diffusion scrubber coupled to ion chromatography, Anal. Chem., 75(22), 6141–6146, doi:10.1021/ac0347314, 2003.

Creamean, J. M., Ault, A. P., Ten Hoeve, J. E., Jacobson, M. Z., Roberts, G. C., Prather, K. A., Hoeve, J. E. Ten, Jacobson, Z., Roberts, G. C. and Prather, K. A.: Measurements of aerosol chemistry during new particle formation events at a remote rural mountain site,

Environ. Sci. Technol., 45(19), 8208–8216, doi:10.1021/es103692f, 2011.

Dabek-Zlotorzynska, E. and Maruszak, W.: Determination of dimethylamine and other low-molecular-mass amines using capillary electrophoresis with laser-induced fluorescence detection., J. Chromatogr. B. Biomed. Sci. Appl., 714(1), 77–85, 1998.

Dall'Osto, M., Ceburnis, D., Monahan, C., Worsnop, D. R., Bialek, J., Kulmala, M., Kurtén, T., Ehn, M., Wenger, J., Sodeau, J., Healy, R. and O'Dowd, C.: Nitrogenated and aliphatic organic vapors as possible drivers for marine secondary organic aerosol growth, J. Geophys. Res. Atmos., 117(12), 1-10, doi:10.1029/2012JD017522, 2012.

Dawson, M. L., Perraud, V., Gomez, a., Arquero, K. D., Ezell, M. J. and Finlayson-Pitts, B. J.: Measurement of gas-phase ammonia and amines in air by collection onto an ion exchange resin and analysis by ion chromatography, Atmos. Meas. Tech., 7(2), 1573–1602, doi:10.5194/amt-7-2733-2014, 2014.

Denkenberger, K. A., Moffet, R. C., Holecek, J. C., Rebotier, T. P. and Prather, K. A.: Real-time, single-particle measurements of oligomers in aged ambient aerosol particles, Environ. Sci. Technol., 41(15), 5439–5446, doi:10.1021/es070329l, 2007.

Di Lorenzo, R. A. and Young, C. J.: Size separation method for absorption characterization in brown carbon: Application to an aged biomass burning sample, Geophys. Res. Lett., 43(1), 458–465, doi:10.1002/2015GL066954, 2016.

Di Lorenzo, R. A., Washenfelder, R. A., Attwood, A. R., Guo, H., Xu, L., Ng, N. L., Weber, R. J., Baumann, K., Edgerton, E. and Young, C. J.: Molecular size separated brown carbon absorption for fresh and aged biomass burning plumes at multiple field sites, Environ. Sci. Technol. (under review), 2016.

Ehn, M., Thornton, J. A., Kleist, E., Sipilä, M., Junninen, H., Pullinen, I., Springer, M., Rubach, F., Tillmann, R., Lee, B., Lopez-Hilfiker, F., Andres, S., Acir, I.-H., Rissanen, M., Jokinen, T., Schobesberger, S., Kangasluoma, J., Kontkanen, J., Nieminen, T., Kurtén, T., Nielsen, L. B., Jørgensen, S., Kjaergaard, H. G., Canagaratna, M., Maso, M. D., Berndt, T., Petäjä, T., Wahner, A., Kerminen, V.-M., Kulmala, M., Worsnop, D. R., Wildt, J. and Mentel, T. F.: A large source of low-volatility secondary organic aerosol, Nature, 506(7489), 476–479, doi:10.1038/nature13032, 2014.

Erupe, M. E., Liberman-Martin, A., Silva, P. J., Malloy, Q. G. J., Yonis, N., Cocker, D. R. and Purvis-Roberts, K. L.: Determination of methylamines and trimethylamine-N-oxide in particulate matter by non-suppressed ion chromatography, J. Chromatogr. A, 1217(13), 2070–2073, doi:10.1016/j.chroma.2010.01.066, 2010.

Erupe, M. E., Viggiano, A. A. and Lee, S. H.: The effect of trimethylamine on atmospheric nucleation involving H_2SO_4, Atmos. Chem. Phys., 11(10), 4767–4775, doi:10.5194/acp-11-4767-2011, 2011.

Facchini, M. C., Decesari, S., Rinaldi, M., Carbone, C., Finessi, E., Mircea, M., Fuzzi, S., Moretti, F., Tagliavini, E., Ceburnis, D. and O'Dowd, C. D.: Important source of marine secondary organic aerosol from biogenic amines., Environ. Sci. Technol., 42(24), 9116–9121, doi:10.1021/es8018385, 2008.

Fekete, A., Frommberger, M., Ping, G., Lahaniatis, M. R., Lintelman, J., Fekete, J., Gebefugi, I., Malik, A. K., Kettrup, A. and Schmitt-Kopplin, P.: Development of a capillary electrophoretic method for the analysis of low-molecular-weight amines from metal working fluid aerosols and ambient air, Electrophoresis, 27(5–6), 1237–1247, doi:10.1002/elps.200500724, 2006.

Fournier, M., Lesage, J., Ostiguy, C. and Tra, H. V: Sampling and analytical methodology development for the determination of primary and secondary low molecular weight amines in ambient air, J Env. Monit, 10(3), 379–386, doi:10.1039/b719091n, 2008.

Ge, X., Wexler, A. S. and Clegg, S. L.: Atmospheric amines - Part I. A review, Atmos. Environ., 45(3), 524–546, doi:10.1016/j.atmosenv.2010.10.012, 2011.

Gibb, S. W., Mantoura, R. F. C., Liss, P. S. and Barlow, R. G.: Distributions and biogeochemistries of methylamines and ammonium in the Arabian Sea, Deep. Res. Part II Top. Stud. Oceanogr., 46(3–4), 593–615, doi:10.1016/S0967-0645(98)00119-2, 1999a.

Gibb, S. W., Mantoura, R. F. C. and Liss, P. S.: Ocean-atmosphere exchange and atmospheric speciation of ammonia and methylamines in the region of the NW Arabian Sea, Global Biogeochem. Cycles, 13(1), 161–178, doi:10.1029/98GB00743, 1999b.

Gorzelska, K. and Galloway, J. N.: Amine nitrogen in the atmospheric environment over the North Atlantic Ocean, Global Biogeochem. Cycles, 4(3), 309–333, doi:10.1029/GB004i003p00309, 1990.

Hatsis, P. and Lucy, C. A.: Evaluation of column temperature as a means to alter selectivity in the cation exchange separation of alkali metals, alkaline earth metals and amines., Analyst, 126(12), 2113–2118, doi:10.1039/b106639k, 2001.

Healy, R. M., Evans, G. J., Murphy, M., Sierau, B., Arndt, J., McGillicuddy, E., O'Connor, I. P., Sodeau, J. R. and Wenger, J. C.: Single-particle speciation of alkylamines in ambient aerosol at five European sites, Anal. Bioanal. Chem., 407(20), 5899–5909, doi:10.1007/s00216-014-8092-1, 2015.

Hodshire, A. L., Lawler, M. J., Zhao, J., Ortega, J., Jen, C., Yli-Juuti, T., Brewer, J. F., Kodros, J. K., Barsanti, K. C., Hanson, D. R., McMurry, P. H., Smith, J. N. and Pierce, J. R.: Multiple new-particle growth pathways observed at the US DOE Southern Great Plains field site, Atmos. Chem. Phys., 16, 9321–9348, doi:10.5194/acp-16-9321-2016, 2016.

Huang, G., Hou, J. and Zhou, X.: A measurement method for atmospheric ammonia and primary amines based on aqueous sampling, OPA derivatization and HPLC analysis, Environ. Sci. Technol., 43(15), 5851–5856, doi:10.1021/es900988q, 2009.

Huang, R. J., Li, W. B., Wang, Y. R., Wang, Q. Y., Jia, W. T., Ho, K. F., Cao, J. J., Wang, G. H., Chen, X., Ei Haddad, I., Zhuang, Z. X., Wang, X. R., Prèvôt, A. S. H., O'Dowd, C. D. and Hoffmann, T.: Determination of alkylamines in atmospheric aerosol particles: A comparison of gas chromatography-mass spectrometry and ion chromatography approaches, Atmos. Meas. Tech., 7(7), 2027–2035, doi:10.5194/amt-7-2027-2014, 2014.

Hudson, P. K., Murphy, D. M., Cziczo, D. J., Thomson, D. S., de Gouw, J. A., Warneke, C., Holloway, J., Jost, H. J. and Hübler, G.: Biomass-burning particle measurements: Characteristics composition and chemical processing, J. Geophys. Res. D Atmos., 109(23), 1–11, doi:10.1029/2003JD004398, 2004.

IARC Monographs on the Evaluation of Carcinogenic Risks to Humans: Outdoor Air Pollution (World Health Organization), http://monographs.iarc.fr/ENG/Classification (accessed Aug 9, 2016), 2016.

Jen, C. N., Zhao, J., McMurry, P. H. and Hanson, D. R.: Chemical ionization of clusters formed from sulfuric acid and dimethylamine or diamines, Atmos. Chem. Phys., 16, 12513–12529, doi:10.5194/acp-2016-492, 2016a.

Jen, C. N., Bachman, R., Zhao, J., Mcmurry, P. H. and Hanson, D. R.: Diamine-sulfuric acid reactions are a potent source of new particle formation, Geophys. Res. Lett., 43(2), 867–873, doi:10.1002/2015GL066958, 2016b.

Key, D., Stihle, J., Petit, J.-E., Bonnet, C., Depernon, L., Liu, O., Kennedy, S., Latimer, R., Burgoyne, M., Wanger, D., Webster, A., Casunuran, S., Hidalgo, S., Thomas, M., Moss, J. A. and Baum, M. M.: Integrated method for the measurement of trace nitrogenous atmospheric bases, Atmos. Meas. Tech., 4(12), 2795–2807, doi:10.5194/amt-4-2795-2011, 2011.

Kovač, N., Glavaš, N., Dolenec, M., Šmuc, N. R. and Šlejkovec, Z.: Chemical Composition of Natural Sea Salt from the Sečovlje Salina (Gulf of Trieste, northern Adriatic), Acta Chim. Slov., 60(3), 706–714, 2013.

Kuhn, U., Sintermann, J., Spirig, C., Jocher, M., Ammann, C. and Neftel, a.: Basic biogenic aerosol precursors: Agricultural source attribution of volatile amines revised, Geophys. Res. Lett., 38(16), 1–8, doi:10.1029/2011GL047958, 2011.

Kulisa, K.: The effect of temperature on the cation-exchange separations in ion chromatography and the mechanism of zone spreading, Chem. Anal., 49, 665.

Kulmala, M., Kontkanen, J., Junninen, H., Lehtipalo, K., Manninen, H. E., Nieminen, T.,

Petäjä, T., Sipilä, M., Schobesberger, S., Rantala, P., Franchin, A., Jokinen, T., Järvinen, E., Äijälä, M., Kangasluoma, J., Hakala, J., Aalto, P. P., Paasonen, P., Mikkilä, J., Vanhanen, J., Aalto, J., Hakola, H., Makkonen, U., Ruuskanen, T., Mauldin, R. L., Duplissy, J., Vehkamäki, H., Bäck, J., Kortelainen, A., Riipinen, I., Kurtén, T., Johnston, M. V, Smith, J. N., Ehn, M., Mentel, T. F., Lehtinen, K. E. J., Laaksonen, A., Kerminen, V.-M. and Worsnop, D. R.: Direct observations of atmospheric aerosol nucleation., Science, 339(6122), 943–946, doi:10.1126/science.1227385, 2013.

Kurtén, T., Loukonen, V., Vehkamäki, H. and Kulmala, M.: Amines are likely to enhance neutral and ion-induced sulfuric acid-water nucleation in the atmosphere more effectively than ammonia, Atmos. Chem. Phys., 8, 4095–4103, doi:10.5194/acp-8-4095-2008, 2008.

Kürten, A., Bergen, A., Heinritzi, M., Leiminger, M., Lorenz, V., Piel, F., Simon, M., Sitals, R., Wagner, A. and Curtius, J.: Observation of new particle formation and measurement of sulfuric acid, ammonia, amines and highly oxidized molecules using nitrate CI-APi-TOF at a rural site in central Germany, Atmos. Chem. Phys. Discuss., 0(June), 1–47, doi:10.5194/acp-2016-294, 2016.

Kuwata, K., Akiyama, E., Yamasaki, H., Kuge, Y. and Kisa, Y.: Trace determination of low molecular weight aliphatic amines in air by gas chromatography, Anal. Chem., 55, 2199–2201, 1983.

Leach, J., Blanch, A. and Bianchi, A. C.: Volatile organic compounds in an urban airborne environment adjacent to a municipal incinerator, waste collection centre and sewage treatment plant, Atmos. Environ., 33(26), 4309–4325, doi:10.1016/S1352-2310(99)00115-6, 1999.

Li, F., Liu, H., Xue, C., Xin, X., Xu, J., Chang, Y., Xue, Y. and Yin, L.: Simultaneous determination of dimethylamine, trimethylamine and trimethylamine-n-oxide in aquatic products extracts by ion chromatography with non-suppressed conductivity detection, J. Chromatogr. A, 1216(31), 5924–5926, doi:10.1016/j.chroma.2009.06.038, 2009.

Lloyd, J. A., Heaton, K. J. and Johnston, M. V.: Reactive uptake of trimethylamine into ammonium nitrate particles, J. Phys. Chem. A, 113(17), 4840–4843, doi:10.1021/jp900634d, 2009.

Lobert, J. M., Scharffe, D. H., Hao, W. M. and Crutzen, P. J.: Importance of biomass burning in the atmospheric budgets of nitrogen-containing gases, Nature, 346(6284), 552–554, doi:10.1038/346552a0, 1990.

Lohmann, U. and Feichter, J.: Global indirect aerosol effects: a review, Atmos. Chem. Phys., 5, 715–737, doi:10.5194/acp-5-715-2005, 2005.

Loukonen, V., Kurtén, T., Ortega, I. K., Vehkamäki, H., Pádua, A. A. H., Sellegri, K. and Kulmala, M.: Enhancing effect of dimethylamine in sulfuric acid nucleation in the presence of water – a computational study, Atmos. Chem. Phys., 10, 4961–4974,

doi:10.5194/acp-10-4961-2010, 2010.

Loukonen, V., Kuo, I. F. W., McGrath, M. J. and Vehkamäki, H.: On the stability and dynamics of (sulfuric acid)(ammonia) and (sulfuric acid)(dimethylamine) clusters: A first-principles molecular dynamics investigation, Chem. Phys., 428, 164–174, doi:10.1016/j.chemphys.2013.11.014, 2014.

Lunn, F. and Van de Vyver, J.: Sampling and analysis of air in pig houses, Agric. Environ., 3, 159–169, doi:10.1016/0304-1131(77)90007-8, 1977.

Mader, B. T., Yu, J. Z., Xu, J. H., Li, Q. F., Wu, W. S., Flagan, R. C., and Seinfeld, J. H.: Molecular composition of the water-soluble fraction of atmospheric carbonaceous aerosols collected during ACE-Asia, J. Geophys. Res., 109(D6), 1–13, doi:10.1029/2003JD004105, 2004.

Müller, C., Iinuma, Y., Karstensen, J., van Pinxteren, D., Lehmann, S., Gnauk, T. and Herrmann, H.: Seasonal variation of aliphatic amines in marine sub-micrometer particles at the Cape Verde islands, Atmos. Chem. Phys., 9, 14825–14855, doi:10.5194/acp-9-9587-2009, 2009.

Murphy, S. M., Sorooshian, A., Kroll, J. H., Ng, N. L., Chhabra, P., Tong, C., Surratt, J. D., Knipping, E., Flagan, R. C. and Seinfeld, J. H.: Secondary aerosol formation from atmospheric reactions of aliphatic amines, Atmos. Chem. Phys., 7, 2313–2337, doi:10.5194/acp-7-2313-2007, 2007.

Myhre, G., Shindell, D., Bréon, F.-M., Collins, W., Fuglestvedt, J., Huang, J., Koch, D., Lamarque, J.-F., Lee, D., Mendoza, B., Nakajima, T., Robock, A., Stephens, G., Takemura, T. and Zhang, H.: Anthropogenic and Natural Radiative Forcing. In: Climate Change 2013: The Physical Science Basis. Contribution of Working Group I to the Fifth Assessment Report of the Intergovernmental Panel on Climate Change, Cambridge, United Kingdom and New York, NY, USA, 81 pp., 2013.

Nadykto, A., Herb, J., Yu, F., Xu, Y. and Nazarenko, E. S.: Estimating the lower limit of the impact of amines on nucleation in the Earth's atmosphere, Entropy, 17(5), 2764–2780, doi:10.3390/e17052764, 2015.

Ortega, I. K., Kupiainen, O., Kurtén, T., Olenius, T., Wilkman, O., McGrath, M. J., Loukonen, V. and Vehkamäki, H.: From quantum chemical formation free energies to evaporation rates, Atmos. Chem. Phys., 12(1), 225–235, doi:10.5194/acp-12-225-2012, 2012.

Ortega, I. K., Donahue, N. M., Kurtén, T., Kulmala, M., Focsa, C. and Vehkamäki, H.: Can highly oxidized organics contribute to atmospheric new particle formation?, J. Phys. Chem. A, 120(9), 1452–1458, doi:10.1021/acs.jpca.5b07427, 2016.

Pósfai, M., Simonics, R., Li, J., Hobbs, P. V and Buseck, P. R.: Individual aerosol

particles from biomass burning in southern Africa: 1. Compositions and size distributions of carbonaceous particles, J. Geophys. Res. Atmos., 108(D13), n/a-n/a, doi:10.1029/2002JD002291, 2003.

Possanzini, M. and Di Palo, V.: Improved HPLC determination of aliphatic amines in air by diffusion and derivatization techniques, Chromatographia, 29(3–4), 151–154, doi:10.1007/BF02268702, 1990.

Qiu, C., Wang, L., Lal, V., Khalizov, A. F. and Zhang, R.: Heterogeneous reactions of alkylamines with ammonium sulfate and ammonium bisulfate, Environ. Sci. Technol., 45(11), 4748–4755, doi:10.1021/es1043112, 2011.

Qiu, C. and Zhang, R.: Multiphase chemistry of atmospheric amines., Phys. Chem. Chem. Phys., 15(16), 5738–5752, doi:10.1039/c3cp43446j, 2013.

Rabaud, N. E., Ebeler, S. E., Ashbaugh, L. L. and Flocchini, R. G.: Characterization and quantification of odorous and non-odorous volatile organic compounds near a commercial dairy in California, Atmos. Environ., 37(7), 933–940, doi:10.1016/S1352-2310(02)00970-6, 2003.

Rey, M. A. and Pohl, C. A.: Novel cation column for separation of amines and six common inorganic cations. J. Chrom. A., 739, 87-97, 1996.

Rey, M. and Pohl, C.: Novel cation-exchange column for the separation of hydrophobic and/or polyvalent amines, J. Chromatogr. A, 997(1–2), 199–206, doi:10.1016/S0021-9673(03)00113-4, 2003.

Rogge, W. F., Hildemann, L. M., Mazurek, M. A., Cass, G. R. and Simonelt, B. R. T.: Sources of fine organic aerosol. 1. charbroilers and meat cooking operations, Environ. Sci. Technol., 25(6), 1112–1125, doi:10.1021/es00018a015, 1991.

Ruiz-Jimenez, J., Parshintsev, J., Laitinen, T., Hartonen, K., Petäjä, T., Kulmala, M. and Riekkola, M. L.: Influence of the sampling site, the season of the year, the particle size and the number of nucleation events on the chemical composition of atmospheric ultrafine and total suspended particles, Atmos. Environ., 49, 60–68, doi:10.1016/j.atmosenv.2011.12.032, 2012.

Saleh, R., Robinson, E. S., Tkacik, D. S., Ahern, A. T., Liu, S., Aiken, A. C., Sullivan, R. C., Presto, A. A., Dubey, M. K., Yokelson, R. J., Donahue, N. M. and Robinson, A. L.: Brownness of organics in aerosols from biomass burning linked to their black carbon content, Nat. Geosci., 7, 647-650, doi:10.1038/ngeo2220, 2014.

Schade, G. W. and Crutzen, P. J.: Emission of aliphatic amines from animal husbandry and their reactions: Potential source of N_2O and HCN, J. Atmos. Chem., 22(3), 319–346, doi:10.1007/BF00696641, 1995.

Schauer, J. J., Kleeman, M. J., Cass, G. R. and Simoneit, B. R. T.: Measurement of emissions from air pollution sources. 1. C_1 through C_{29} organic compounds from meat charbroiling, Environ. Sci. Technol., 33(10), 1566–1577, doi:10.1021/es980076j, 1999.

Schmeltz, I., and Hoffmann, D.: Nitrogen-containing compounds in tobacco and tobacco smoke, Chemical Review, 77(3), 295-311, doi: 10.1021/cr60307a001, 1977.

Seo, S. -G., Ma, Z. -K., Jeon, J. -M., Jung, S. -C., and Lee, W. -B..: Measurements of key offensive odorants in a fishery industrial complex in Korea, Atmos. Environ., 45(17), 2929–2936, doi:10.1016/j.atmosenv.2011.01.032, 2011.

Silva, P. J., Erupe, M. E., Price, D., Elias, J., Malloy, Q. G. J., Li, Q., Warren, B. and Cocker, D. R.: Trimethylamine as precursor to secondary organic aerosol formation via nitrate radical reaction in the atmosphere, Environ. Sci. Technol., 42(13), 4689–4696, doi:10.1021/es703016v, 2008.

Smith, J. N., Dunn, M. J., VanReken, T. M., Iida, K., Stolzenburg, M. R., McMurry, P. H. and Huey, L. G.: Chemical composition of atmospheric nanoparticles formed from nucleation in Tecamac, Mexico: Evidence for an important role for organic species in nanoparticle growth, Geophys. Res. Lett., 35(4), 2–6, doi:10.1029/2007GL032523, 2008.

Smith, J. N., Barsanti, K. C., Friedli, H. R., Ehn, M., Kulmala, M., Collins, D. R., Scheckman, J. H., Williams, B. J. and McMurry, P. H.: Observations of aminium salts in atmospheric nanoparticles and possible climatic implications., Proc. Natl. Acad. Sci. U. S. A., 107(15), 6634–6639, doi:10.1073/pnas.0912127107, 2010.

Sobanska, S., Hwang, H., Choël, M., Jung, H. -J., Eom, H. -J., Kim, H., Barbillat, J. and Ro, C. U.: Investigation of the chemical mixing state of individual asian dust particles by the combined use of electron probe X-ray microanalysis and raman microspectrometry, Anal. Chem., 84(7), 3145–3154, doi:10.1021/ac2029584, 2012.

Sorooshian, A., Murphy, S. M., Hersey, S., Gates, H., Padro, L. T., Nenes, a., Brechtel, F. J., Jonsson, H., Flagan, R. C. and Seinfeld, J. H.: Comprehensive airborne characterization of aerosol from a major bovine source, Atmos. Chem. Phys., 8, 5489–5520, doi:10.5194/acp-8-5489-2008, 2008.

Sorooshian, A., Padró, L. T., Nenes, A., Feingold, G., McComiskey, A., Hersey, S. P., Gates, H., Jonsson, H. H., Miller, S. D., Stephens, G. L., Flagan, R. C. and Seinfeld, J. H.: On the link between ocean biota emissions, aerosol, and maritime clouds: Airborne, ground, and satellite measurements off the coast of California, Global Biogeochem. Cycles, 23(4), 1–15, doi:10.1029/2009GB003464, 2009.

Stephen and et al.: A comparative risk assessment of burden of disease and injury attributable to 67 risk factors and risk factor clusters in 21 regions, 1990–2010: a systematic analysis for the Global Burden of Disease Study 2010, Lancet, 380(9859), 2224–2260, doi:10.1016/S0140-6736(12)61766-8.A, 2012.

Sun, Y., Zhuang, G., Tang, A., Wang, Y. and An, Z.: Chemical characteristics of $PM_{2.5}$ and PM_{10} in haze−fog episodes in Beijing, Environ. Sci. Technol., 40(10), 3148–3155, doi:10.1021/es051533g, 2006.

Suzuki, Y., Kawakami, M. and Akasaka, K.: ^{1}H NMR application for characterizing water-soluble organic compounds in urban atmospheric particles, Environ. Sci. Technol., 35(13), 2656–2664, doi:10.1021/es001861a, 2001.

Takahama, S., Schwartz, R. E., Russell, L. M., MacDonald, A. M., Sharma, S. and Leaitch, W. R.: Organic functional groups in aerosol particles from burning and non-burning forest emissions at a high-elevation mountain site, Atmos. Chem. Phys., 11(13), 6367–6386, doi:10.5194/acp-11-6367-2011, 2011.
Tao, Y., Ye, X., Jiang, S., Yang, X., Chen, J., Xie, Y. and Wang, R.: Effects of amines on particle growth observed in new particle formation events, J. Geos. Res. Atmos., 121, 1-12, doi: 10.1002/2015JD024245, 2015

Tröstl, J., Chuang, W. K., Gordon, H., Heinritzi, M., Yan, C., Molteni, U., Ahlm, L., Frege, C., Bianchi, F., Wagner, R., Simon, M., Lehtipalo, K., Williamson, C., Craven, J. S., Duplissy, J., Adamov, A., Almeida, J., Flagan, R. C., Franchin, A., Fuchs, C., Guida, R., Gysel, M., Pet, T. and Steiner, G.: The role of low-volatility organic compounds in initial particle growth in the atmosphere, Nature, 527-531, doi:10.1038/nature18271, 2016.

Vandenboer, T. C., Petroff, A., Markovic, M. Z. and Murphy, J. G.: Size distribution of alkyl amines in continental particulate matter and their online detection in the gas and particle phase, Atmos. Chem. Phys., 11(9), 4319–4332, doi:10.5194/acp-11-4319-2011, 2011.

VandenBoer, T. C., Markovic, M. Z., Petroff, A., Czar, M. F., Borduas, N. and Murphy, J. G.: Ion chromatographic separation and quantitation of alkyl methylamines and ethylamines in atmospheric gas and particulate matter using preconcentration and suppressed conductivity detection, J. Chromatogr. A, 1252(3), 74–83, doi:10.1016/j.chroma.2012.06.062, 2012.

Van Neste, A., Duce, R. A., Lee, C.: Methylamines in the marine atmosphere, Geophys. Res. Lett., 14(7), 711-714, 1987.

van Pinxteren, M., Fiedler, B., van Pinxteren, D., Iinuma, Y., Körtzinger, A. and Herrmann, H.: Chemical characterization of sub-micrometer aerosol particles in the tropical Atlantic Ocean: marine and biomass burning influences, J. Atmos. Chem., 105–125, doi:10.1007/s10874-015-9307-3, 2015.

Verriele, M., Plaisance, H., Depelchin, L., Benchabane, S., Locoge, N. and Meunier, G.: Determination of 14 amines in air samples using midget impingers sampling followed by analysis with ion chromatography in tandem with mass spectrometry., J. Environ. Monit.,

14(2), 402–408, doi:10.1039/c2em10636a, 2012.

Wang, L., Khalizov, A. F., Zheng, J., Xu, W., Ma, Y., Lal, V. and Zhang, R.: Atmospheric nanoparticles formed from heterogeneous reactions of organics, Nat. Geosci., 3(4), 238–242, doi:10.1038/ngeo778, 2010a.

Wang, L., Vinita, L., Khalizov, A. F. and Zhang, R.: Heterogeneous chemistry of alkylamines with sulfuric acid: Implications for atmospheric formation of alkylaminium sulfates, Environ. Sci. Technol., 44(7), 2461–2465, doi:10.1021/es9036868, 2010b.

Willis, M. D., Burkart, J., Thomas, J. L., Köllner, F., Schneider, J., Bozem, H., Hoor, P. M., Aliabadi, A. A., Schulz, H., Herber, A. B., Leaitch, W. R. and Abbatt, J. P. D.: Growth of nucleation mode particles in the summertime Arctic: a case study, Atmos. Chem. Phys., 16, 7663–7679, doi:10.5194/acp-16-7663-2016, 2016.

Yang, H., Xu, J., Wu, W. S., Wan, C. H. and Yu, J. Z.: Chemical characterization of water-soluble organic aerosols at Jeju Island collected during ACE-Asia, Environ. Chem., 1(1), 13–17, doi:10.1071/EN04006, 2004.

Yang, H., Jian, Z. Y., Hang Ho, S. S., Xu, J., Wu, W. S., Chun, H. W., Wang, X., Wang, X. and Wang, L.: The chemical composition of inorganic and carbonaceous materials in $PM_{2.5}$ in Nanjing, China, Atmos. Environ., 39(20), 3735–3749, doi:10.1016/j.atmosenv.2005.03.010, 2005.

Yao, L., Wang, M.-Y., Wang, X.-K., Liu, Y.-J., Chen, H.-F., Zheng, J., Nie, W., Ding, A.-J., Geng, F.-H., Wang, D.-F., Chen, J.-M., Worsnop, D. R. and Wang, L.: Detection of atmospheric gaseous amines and amides by a high resolution time-of-flight chemical ionization mass spectrometer with protonated ethanol reagent ions, Atmos. Chem. Phys. Discuss., 1–32, doi:10.5194/acp-2016-484, 2016.

Youn, J. -S., Crosbie, E., Maudlin, L. C., Wang, Z. and Sorooshian, A.: Dimethylamine as a major alkyl amine species in particles and cloud water: Observations in semi-arid and coastal regions, Atmos. Environ., 122, 250–258, doi:10.1016/j.atmosenv.2015.09.061, 2015.

Yu, H., McGraw, R. and Lee, S. H.: Effects of amines on formation of sub-3 nm particles and their subsequent growth, Geophys. Res. Lett., 39(2), 2–7, doi:10.1029/2011GL050099, 2012.

Zauscher, M. D., Wang, Y., Moore, M. J. K., Gaston, C. J. and Prather, K. A.: Air quality impact and physicochemical aging of biomass burning aerosols during the 2007 San Diego wildfires, Environ. Sci. Technol., 47(14), 7633–7643, doi:10.1021/es4004137, 2013.

Zhang, Q. and Anastasio, C.: Free and combined amino compounds in atmospheric fine particles ($PM_{2.5}$) and fog waters from Northern California, Atmos. Environ., 37(16),

2247–2258, doi:10.1016/S1352-2310(03)00127-4, 2003.

Zhao, J., Smith, J. N., Eisele, F. L., Chen, M., Kuang, C. and McMurry, P. H.: Observation of neutral sulfuric acid-amine containing clusters in laboratory and ambient measurements, Atmos. Chem. Phys., 11(21), 10823–10836, doi:10.5194/acp-11-10823-2011, 2011.

Zollner, J. H., Glasoe, W. A., Panta, B., Carlson, K. K., McMurry, P. H. and Hanson, D. R.: Sulfuric acid nucleation: Power dependencies, variation with relative humidity, and effect of bases, Atmos. Chem. Phys., 12(10), 4399–4411, doi:10.5194/acp-12-4399-2012, 2012.

Chapter 4. Conclusions

4.1 Summary and General Findings

The development of analytical methods for quantifying reduced and oxidized atmospheric nitrogen species within remote regions is essential to understanding the role of increased anthropogenic atmospheric nitrogen emissions into the atmosphere. In this thesis, analytical methods have been developed for quantifying trace quantities of gaseous nitric acid and alkyl amines. $HNO_{3(g)}$ has been shown to be the dominant source of new nitrogen to rural and remote environments (Flechard et al., 2011; Zhang et al., 2009), and therefore is an important input to N cycles within these regions. Alkylamines on the other hand, may represent a source of organic nitrogen entering and/or cycling in remote ecosystems, but more importantly influence Earth's climate at ultra-trace atmospheric concentrations through particle formation (Qiu and Zhang, 2013). The developed methods for measuring these species have been demonstrated to be sensitive and robust when applied to remote atmospheric environments. Further, the data collected using these methods was shown to be reliable through the implementation of multiple quality assurance and quality control procedures, comparison to other related field measurements, and comparison to atmospheric chemical transport model estimates. The development of these analytical techniques now allows for the accurate quantitation of $HNO_{3(g)}$ and $NR_{3(g)}$ in all ecosystems, no matter how remote. Ideally these techniques will be used to fully characterize these two species in the atmosphere and provide a better global understanding of their roles and impact on the nitrogen cycle in more remote ecosystems.

4.2 Summary of the Passive Sampling of $HNO_{3(g)}$ Across the NL-BELT

The developed analytical method for measuring $HNO_{3(g)}$ was comprised of a passive sampling technique employing custom-built physisorption-based samplers coupled with an ion chromatography separation technique. The design and implementation of $HNO_{3(g)}$ passive samplers employing nylon membrane filters has been carried out previously (Bytnerowicz et al., 2001; Bytnerowicz et al., 2005), but the effectiveness of the passive samplers in remote ecosystems had yet to be demonstrated. In this work we have shown that the custom-built $HNO_{3(g)}$ samplers were able to quantify $HNO_{3(g)}$ mixing ratios ranging from 4 – 200 pptv across the Newfoundland and Labrador - Boreal Ecosystem Latitudinal Transect. Further, through the use of a pre-concentration step during IC analysis, the method detection limit approached 2 pptv for a monthly sampling period.

The measured $HNO_{3(g)}$ mixing ratios across the NL-BELT during the summers of 2015 and 2016 showed a seasonal trend, with higher $HNO_{3(g)}$ quantities observed in May, June, and July. However, no latitudinal trends were observed. An air mass back trajectory analysis showed that $HNO_{3(g)}$ formation across the NL-BELT had some correlation to the short-range transport of precursor NO_x emissions from the eastern side of Newfoundland, where a majority of the province's population resides. However, by using an atmospheric chemistry steady-state approximation coupled with supporting NL-BELT measurements, it was determined that local biogenic and anthropogenic production of NO_x dominated overall $HNO_{3(g)}$ formation at the NL-BELT sites. The down welling of PANs from the upper troposphere in the springtime likely attributed to $HNO_{3(g)}$ formation in the months of May and June at the sites as well.

4.3 Summary of the IC Method for Quantifying Atmospheric Alkylamines

The developed analytical method for quantifying atmospheric alkyl amines consisted of an ion chromatography method capable of separating 11 abundant atmospheric alkyl amines from 5 common cation interferences. The developed IC method is capable of separating $MMAH^+$, $DMAH^+$, $TMAH^+$, $MEAH^+$, $DEAH^+$, $TEAH^+$, $MPAH^+$, $iMPAH^+$, $MBAH^+$, $DABH^+$, $DAPH^+$, Na^+, K^+, NH_4^+, Ca^{2+}, and Mg^{2+} with a peak-to-peak resolution greater than one for all cation analytes. Not only does the IC method overcome previous issues with co-eluting peaks (Chang et al., 2003; Dawson et al., 2014; Erupe et al., 2010; Huang et al., 2014; Li et al., 2009; Murphy et al., 2007; VandenBoer et al., 2012), but it is also able to separate and quantify three sets of amine structural isomers, which is not possible by direct MS analysis. The method is able to achieve ppqv mixing ratio detection limits when coupled to an active air scrubber technique operating at a low flow rate for an hour or less depending on the alkylamine sampled.

The IC method was applied to two sets of biomass-burning samples to test the robustness of the method in the presence of a complex organic and cation matrix. The use of a pre-concentration column eliminated all neutral and anionic species, and the method was able to detect and quantify alkylamines in the presence of inorganic cations that reached molar ratios of 1000:1 relative to the alkylamines. A standard addition was performed on the biomass-burning matrix, which further confirmed that the quantitation of alkylamines in the sample was unaffected by high concentrations of Na^+, NH_4^+ and K^+ in the sample. In the aged BB analyzed sample, the di-substituted alkylamines were detected in molar quantities greater than ammonium. These alkylamines may have been

initially present in the plume as BB degradation products or preferentially partitioned into the plume as the plume transported over agricultural and marine regions, known alkylamine sources, as it traveled from Quebec to Newfoundland. Further, monoisopropylamine was detected in the fresh BB sample, and has not previously been reported in BB emission inventories. These findings suggest that the reactive uptake of BB plumes as well as the speciation of direct BB emissions, with respect to alkylamines, needs future focus and characterization. Further, monitoring alkylamine emissions along with other N_r species may become increasingly important as the frequency of wildfires continue to increase each year across Canada (e.g. Vancouver Sun, 2017).

4.4 References

Bytnerowicz, A., Padgett, P. E., Arbaugh, M. J., David, R. and Jones, D. P.: Passive sampler for measurements of atmospheric nitric acid vapor (HNO_3) concentrations, The Scientific World, 1, 815–822, doi:10.1100/tsw.2001.323, 2001.

Bytnerowicz, A., Sanz, M. J., Arbaugh, M. J., Padgett, P. E., Jones, D. P. and Davila, A.: Passive sampler for monitoring ambient nitric acid (HNO_3) and nitrous acid (HNO_2) concentrations, Atmos. Environ., 39(14), 2655–2660, doi:10.1016/j.atmosenv.2005.01.018, 2005.

Chang, I.-H., Lee, C.-G. and Lee, D. S.: Development of an automated method for simultaneous determination of low molecular weight aliphatic amines and ammonia in ambient air by diffusion scrubber coupled to ion chromatography, Anal. Chem., 75(22), 6141–6146, doi:10.1021/ac0347314, 2003.

Dawson, M. L., Perraud, V., Gomez, A., Arquero, K. D., Ezell, M. J. and Finlayson-Pitts, B. J.: Measurement of gas-phase ammonia and amines in air by collection onto an ion exchange resin and analysis by ion chromatography, Atmos. Meas. Tech., 7(2), 1573–1602, doi:10.5194/amt-7-2733-2014, 2014.

Erupe, M. E., Liberman-Martin, A., Silva, P. J., Malloy, Q. G. J., Yonis, N., Cocker, D. R. and Purvis-Roberts, K. L.: Determination of methylamines and trimethylamine-N-oxide in particulate matter by non-suppressed ion chromatography, J. Chromatogr. A, 1217(13), 2070–2073, doi:10.1016/j.chroma.2010.01.066, 2010.

Flechard, C. R., Nemitz, E., Smith, R. I., Fowler, D., Vermeulen, A. T., Bleeker, A., Erisman, J. W., Simpson, D., Zhang, L., Tang, Y. S. and Sutton, M. A.: Dry deposition of reactive nitrogen to European ecosystems: A comparison of inferential models across the NitroEurope network, Atmos. Chem. Phys., 11(6), 2703–2728, doi:10.5194/acp-11-2703-2011, 2011.

Hot, dry conditions see 28 new B.C. wildfires in less than two days, Vancouver Sun, August 8, 2017. Accessed on: September 12, 2017.

Huang, R. J., Li, W. B., Wang, Y. R., Wang, Q. Y., Jia, W. T., Ho, K. F., Cao, J. J., Wang, G. H., Chen, X., Ei Haddad, I., Zhuang, Z. X., Wang, X. R., Prèvôt, A. S. H., O'Dowd, C. D. and Hoffmann, T.: Determination of alkylamines in atmospheric aerosol particles: A comparison of gas chromatography-mass spectrometry and ion chromatography approaches, Atmos. Meas. Tech., 7(7), 2027–2035, doi:10.5194/amt-7-2027-2014, 2014.

Li, F., Liu, H., Xue, C., Xin, X., Xu, J., Chang, Y., Xue, Y. and Yin, L.: Simultaneous determination of dimethylamine, trimethylamine and trimethylamine-n-oxide in aquatic products extracts by ion chromatography with non-suppressed conductivity detection, J. Chromatogr. A, 1216(31), 5924–5926, doi:10.1016/j.chroma.2009.06.038, 2009.

Murphy, S. M., Sorooshian, A., Kroll, J. H., Ng, N. L., Chhabra, P., Tong, C., Surratt, J. D., Knipping, E., Flagan, R. C. and Seinfeld, J. H.: Secondary aerosol formation from atmospheric reactions of aliphatic amines, Atmos. Chem. Phys., 7, 2313–2337, doi:10.5194/acp-7-2313-2007, 2007.

Qiu, C. and Zhang, R.: Multiphase chemistry of atmospheric amines., Phys. Chem. Chem. Phys., 15(16), 5738–5752, doi:10.1039/c3cp43446j, 2013.

VandenBoer, T. C., Markovic, M. Z., Petroff, A., Czar, M. F., Borduas, N. and Murphy, J. G.: Ion chromatographic separation and quantitation of alkyl methylamines and ethylamines in atmospheric gas and particulate matter using preconcentration and suppressed conductivity detection, J. Chromatogr. A, 1252(3), 74–83, doi:10.1016/j.chroma.2012.06.062, 2012.

Zhang, L., Vet, R., O'Brien, J. M., Mihele, C., Liang, Z. and Wiebe, A.: Dry deposition of individual nitrogen species at eight Canadian rural sites, J. Geophys. Res. Atmos., 114(2), 1–13, doi:10.1029/2008JD010640, 2009.

Appendix A: Supporting Information for Chapter 2

```
#pragma rtGlobals=3// Use modern global access method and strict wave access.

function assign_sector(latitude_points, longitude_points, site_coordinates)
	wave latitude_points, longitude_points, site_coordinates


	make/N=5/D sector_points
	variable i=0

	for(i=0;i<(numpnts(latitude_points));i+=1)
		if(latitude_points[i] > site_coordinates[0] && longitude_points[i] >
		site_coordinates[1])
			sector_points[0]= sector_points[0]+1
			sector_points[4]=sector_points[4]+1
		elseif(latitude_points[i] > site_coordinates[0] && longitude_points[i] <
		site_coordinates[1])
			sector_points[1]= sector_points[1]+1
			sector_points[4]=sector_points[4]+1
		elseif(latitude_points[i] < site_coordinates[0] && longitude_points[i] >
		site_coordinates[1])
			sector_points[2]= sector_points[2]+1
			sector_points[4]=sector_points[4]+1
		elseif(latitude_points[i] < site_coordinates[0] && longitude_points[i] <
		site_coordinates[1])
			sector_points[3]= sector_points[3]+1
			sector_points[4]=sector_points[4]+1
		endif
	endfor

	AppendToTable sector_points

end
```

Figure A-1. Procedure developed for geographical sector assignment of air mass back trajectory endpoints for use with Igor Pro. Trajectory endpoints are assigned to one of four quadrants (NE, NW, SW, SE) surrounding the coordinates centered on the desired NL-BELT field site. Any trajectory endpoints directly on top of the field site were not counted in the analysis. The procedure takes in 3 waves (columns) named latitude_points, longitude_points, and site_coordinates and creates the wave sector_points. The wave latitude_points contains all the latitude coordinates of the air mass trajectory endpoints for a given sampling period, while longitude_points contains all of the matching longitude coordinates. The wave site_coordinates contains the latitude and longitude points in that order within the wave for the field site of interest (ie. GC, HR, SR or ER). The procedure then takes each longitude and latitude trajectory endpoint and decides whether it is greater than or less than the corresponding site coordinate. It outputs the final result in the wave sector_points, which is a counting-based wave that contains the following rows: northwest points, northeast points, southwest points, southeast points, and total points. The procedure adds a value of one to the quadrant in which the trajectory endpoint lies and then adds a value of one to the total points. The probability density for air transit duration in each sector is calculated later by dividing the quadrant points by the total points counted.

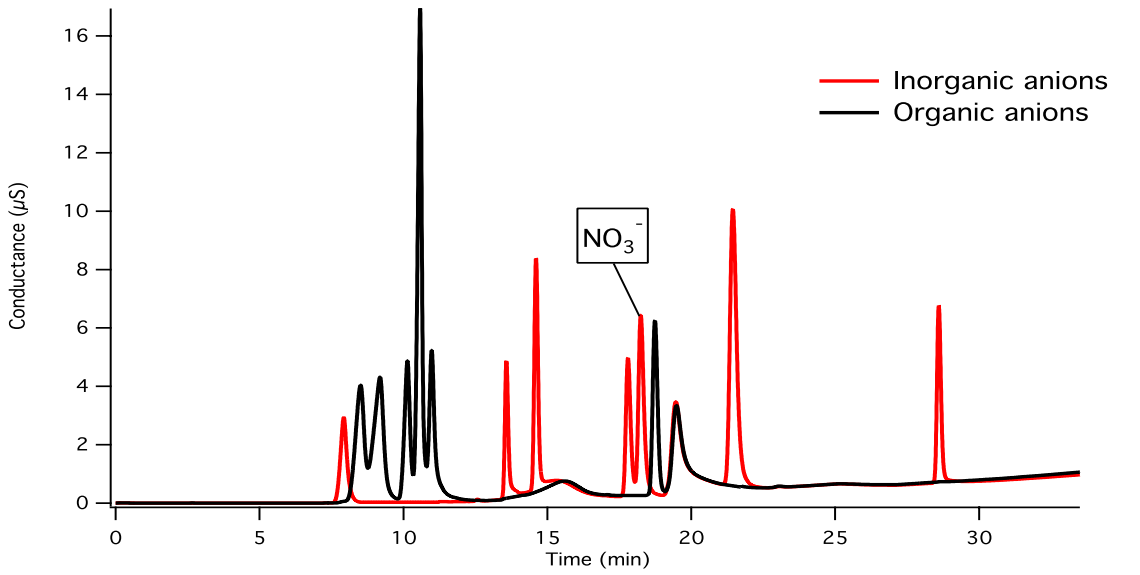

Figure A-2. Ion chromatograph of separations achieved between the inorganic anions (red line: fluoride, nitrite, chloride, nitrate, bromide, sulfate, and phosphate) and organic anions (black line: succinate, formate, acetate, lactate, propionate, and butyrate) running the gradient program described in Sect 2.3.4.2. Ions are listed in order of appearance from left to right. The two system peaks present in the chromatogram where both traces overlap result from carbonate and bicarbonate present in the ultrapure water eluent source.

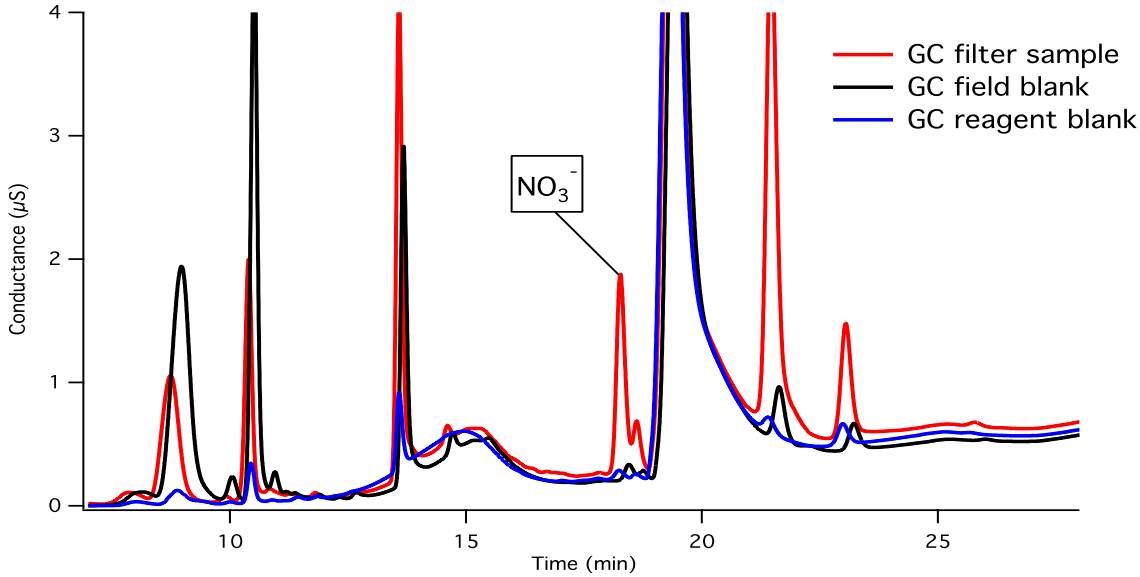

Figure A-3. Overlaid chromatograms of a nylon filter sample extract, a nylon filter field blank extract, and a 1 mM KOH reagent blank collected from GC in November 2015.

Table A-1. Geographical grid sector assignment of air-mass source regions for each month of the study period across all four study sites.

	Grand Codroy				Humber River				Salmon River				Eagle River			
	NE	**NW**	**SW**	**SE**	**NE**	**NW**	**SW**	**SE**	**NE**	**NW**	**SW**	**SE**	**NE**	**NW**	**SW**	**SE**
Oct 2016	16%	62%	18%	4%	14%	62%	21%	3%	15%	60%	23%	2%	12%	69%	16%	3%
Sept 2016	15%	53%	26%	6%	16%	53%	24%	7%	12%	67%	17%	4%				
Aug 2016	17%	37%	30%	16%	17%	37%	36%	10%	23%	30%	35%	12%	30%	34%	23%	13%
July 2016	24%	27%	33%	16%	24%	27%	38%	11%	33%	19%	39%	9%				
June 2016	30%	27%	24%	18%	32%	33%	13%	22%	33%	43%	16%	8%				
Nov 2015	26%	58%	9%	7%	14%	63%	16%	7%	14%	72%	10%	4%				
Oct 2015	10%	59%	23%	8%					7%	62%	29%	2%	10%	59%	23%	8%
Sept 2015	15%	54%	25%	6%	13%	51%	27%	9%	15%	53%	22%	10%				

Appendix B: Supporting Information for Chapter 3

```
{Initial Time}     Instrument Setup
        Pump_ECD.Pressure.UpperLimit                    3000 [psi]
        Sampler.DelayVolume                             125 [µl]
        Pump_ECD.%A.Equate                              "MSA"
        Pump_ECD.Pressure.LowerLimit                    200 [psi]
        Pump_ECD.ColumnTemperature.Nominal              55.0 [°C]
        Pump_ECD.CellTemperature.Nominal                30.0 [°C]
        Pump_ECD.Data_Collection_Rate                   5.0 [Hz]
        Pump_ECD.Suppressor_Type                        CERS_4mm
        Pump_ECD.Suppressor_MSA                         10.0 [mM]
        Pump_ECD.Suppressor_RecommendedCurrent          37 [mA]
        Pump_ECD.Suppressor_Current                     37 [mA]
        Pump_ECD.CR_TC                                  On
        Sampler.FlushFactor                             1
        Sampler.DeliverSpeed                            1.0 [ml/min]
        Sampler.InjectPosition
        Sampler.DeliverRinse                            500,Position=Rinse
        Sampler.DeliverSample                           Volume=Bleed
        Sampler.LoadPosition
        Sampler.DeliverSample
        Sampler.EndSamplePrep
        Pump_ECD.Flow                                   1.25
        Pump_ECD.EluentGenerator_2.Concentration        1.00 [mM]
-5.000  Equilibration                                   Duration = 5.000 [min]
        Pump_ECD.EluentGenerator_2.Concentration        1.00 [mM]
0.000   Inject
        Wait    Sampler.CycleTimeState,
                Run=Hold,
                Timeout=Infinite
        Sampler.Inject
        Start Run
        Pump_ECD.Channel_Pressure.AcqOn
        Pump_ECD.Autozero
        Pump_ECD.ECD_1.AcqOn
        Pump_ECD.ECD_Total.AcqOn
        Run                                             Duration = 45.000 [min]
        Pump_ECD.EluentGenerator_2.Concentration        1.00 [mM]
        Pump_ECD.EluentGenerator_2.Curve                5
20.000
        Pump_ECD.EluentGenerator_2.Concentration        1.00 [mM]
        Pump_ECD.EluentGenerator_2.Curve                7
        Pump_ECD.EluentGenerator_2.Concentration        4.00 [mM]
        Pump_ECD.EluentGenerator_2.Curve                7
30.000
        Pump_ECD.EluentGenerator_2.Concentration        10.00 [mM]
        Pump_ECD.EluentGenerator_2.Curve                7
40.000
        Pump_ECD.EluentGenerator_2.Concentration        10.00 [mM]
        Pump_ECD.EluentGenerator_2.Curve                5
        Pump_ECD.EluentGenerator_2.Concentration        1.00 [mM]
        Pump_ECD.EluentGenerator_2.Curve                5
45.000  Stop Run
        Pump_ECD.Channel_Pressure.AcqOff
        Pump_ECD.ECD_1.AcqOff
        Pump_ECD.ECD_Total.AcqOff
End
```

Figure B-1. Chromeleon method data file for final gradient method at 55 °C.

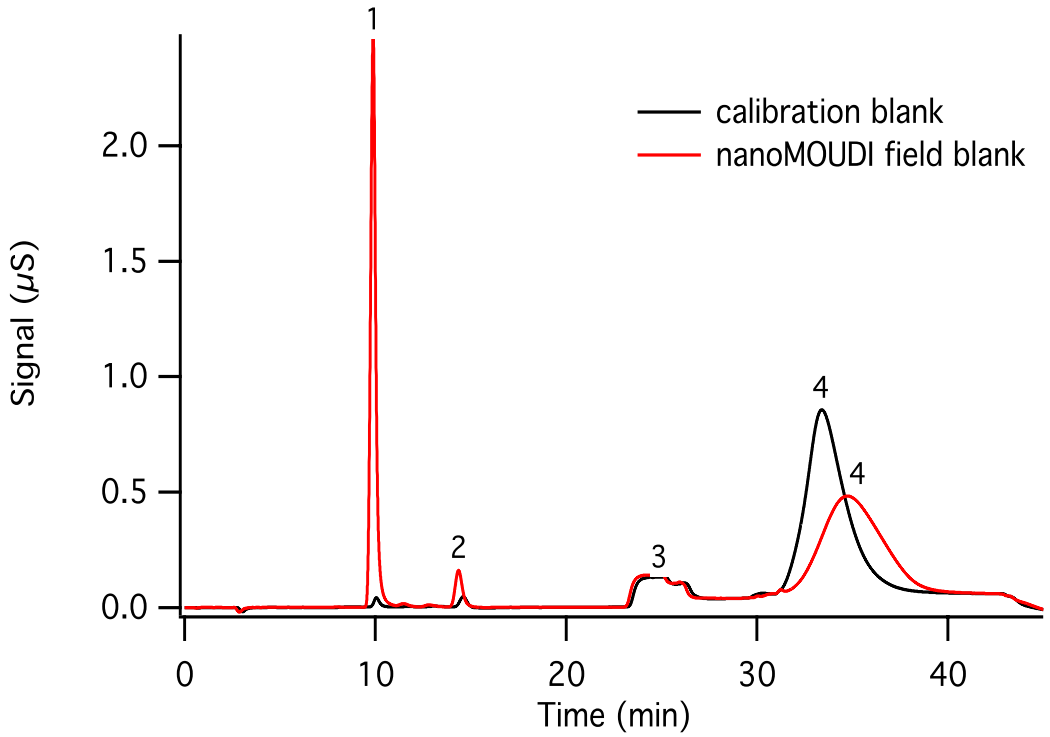

Figure B-2. Sample chromatograms of a calibration blank and a size-resolved BB MOUDI foil substrate field blank. The peaks labelled above are as follows: Na^+ (1), K^+ (2), System peak (3), and Ca^{2+} (4).

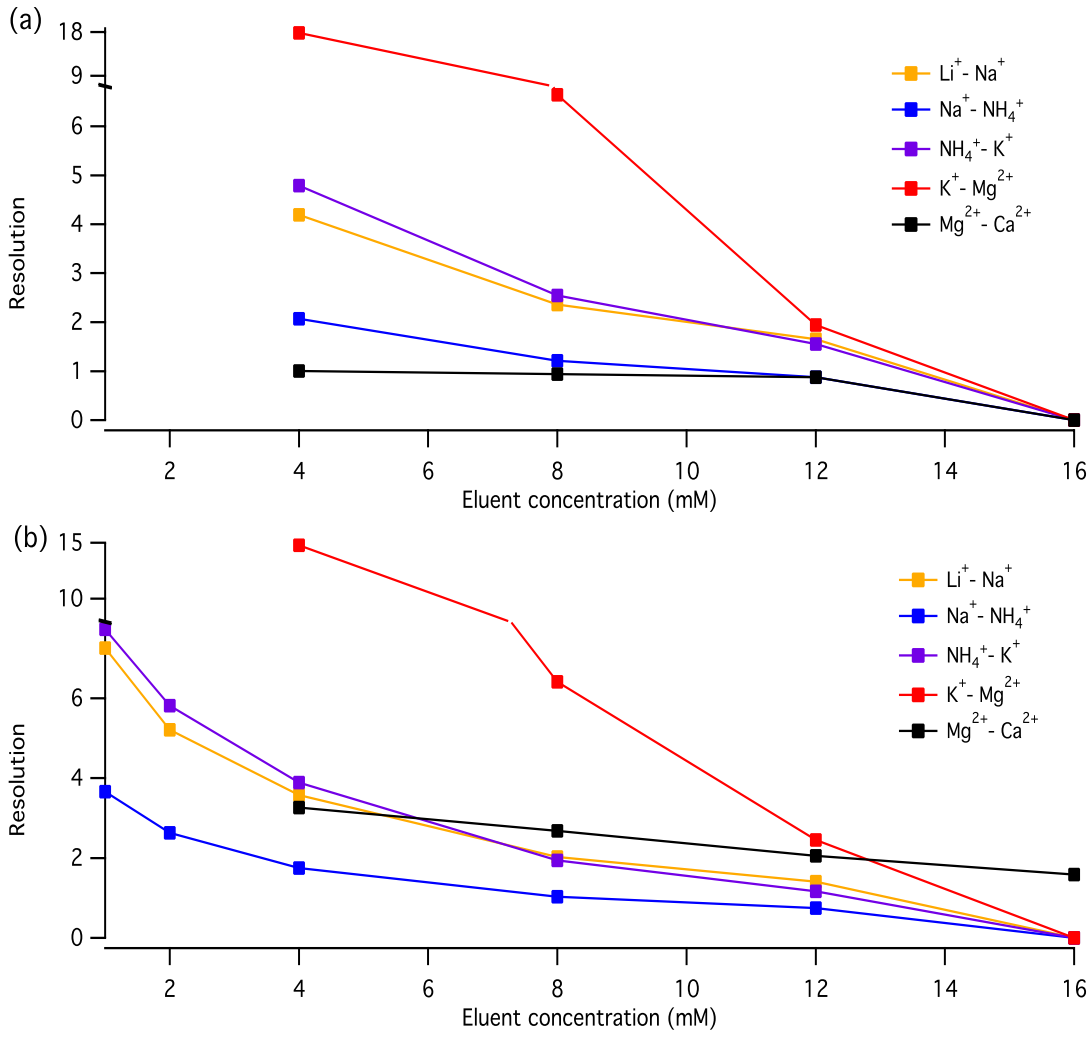

Figure B-3. (a) Resolution of the six inorganic cation peak pairs using isocratic eluent methods at a flow rate of 0.75 ml min^{-1}. (b) Resolution of the six inorganic cation peak pairs using isocratic eluent methods at a flow rate of 1.25 ml min^{-1}. The resolution axis is split to indicate eluent concentrations where dramatic increases in separation occurred.

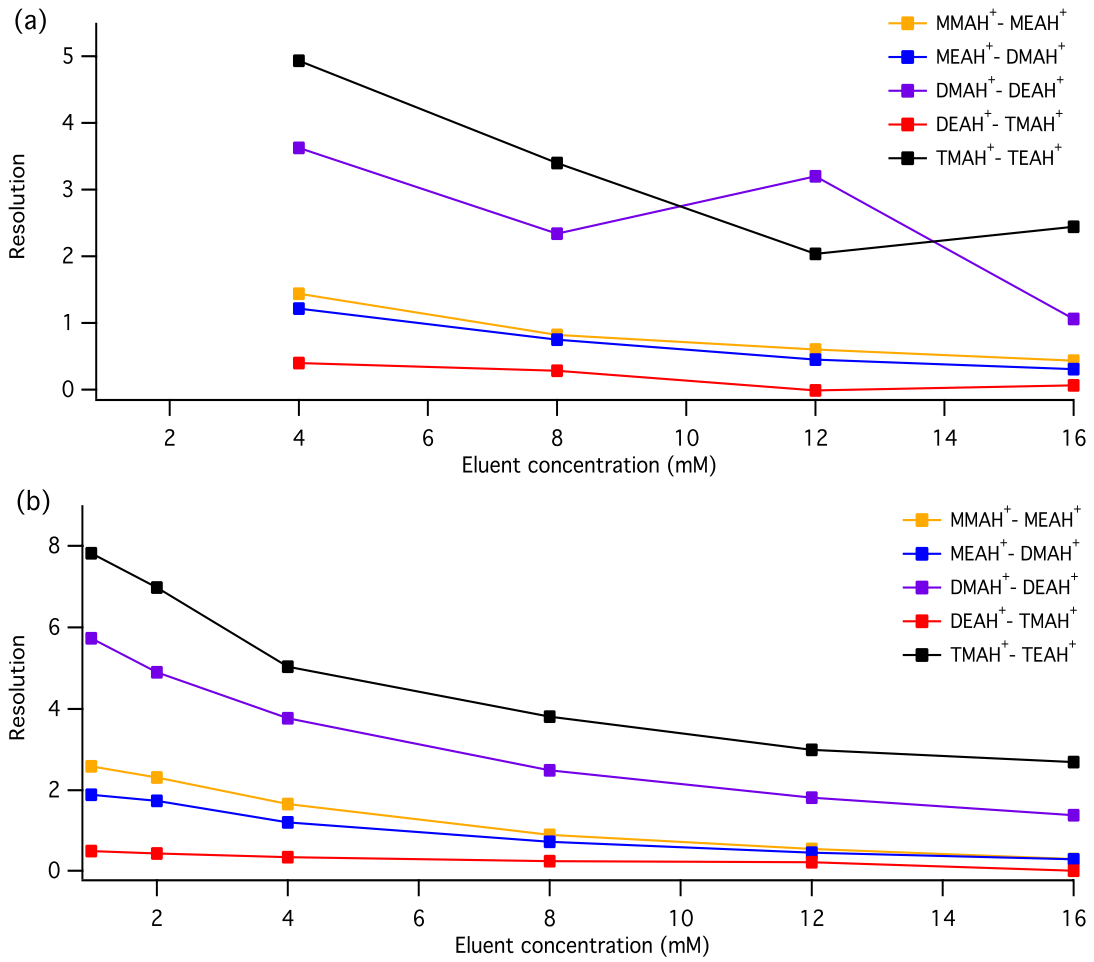

Figure B-4. (a) Resolution of the six alkyl amine cation peak pairs using isocratic eluent methods at a flow rate of 0.75 ml min^{-1}. (b) Resolution of the six alkyl amine cation peak pairs using isocratic eluent methods at a flow rate of 1.25 ml min^{-1}.

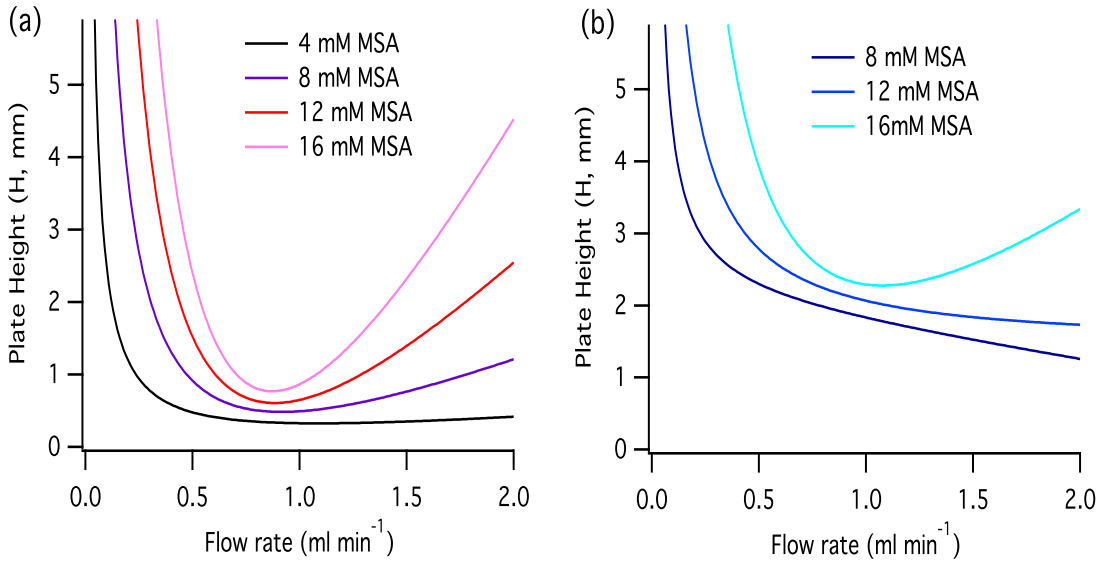

Figure B-5. Calculated Van Deemter plots for the isocratic elutions of (a) $MMAH^+$ and (b) $TEAH^+$ at various MSA eluent concentrations and flow rates.

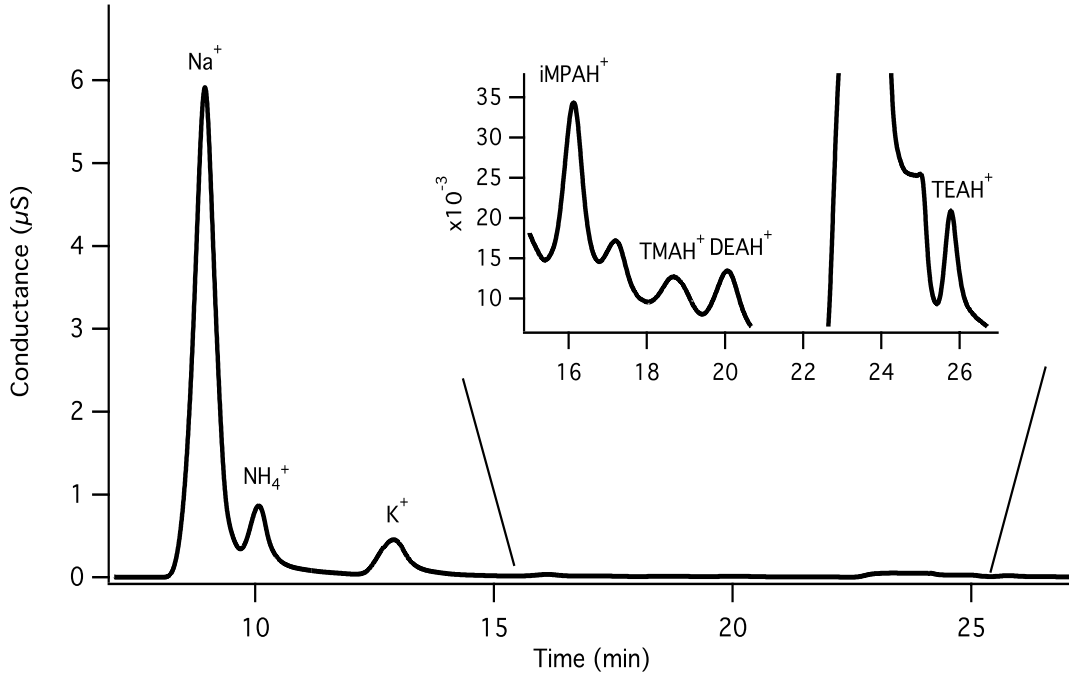

Figure B-6. A chromatogram from an extracted $PM_{2.5}$ sample collected during a biomass-burning event in British Columbia at the Burnaby Kensington Park site.

Table B-1. Comparison of methyl and ethylamine external and standard addition calibration slopes and retention times (t_r).

Analyte	External (μS*min mol^{-1})	Standard addition (μS*min mol^{-1})	Difference (%)	External t_r range (mins)	Standard Addition t_r range (mins)
$MMAH^+$	0.41E08	0.42E08	2	9.0 – 9.4	9.3 – 9.6
$DMAH^+$	0.98E08	1.01E08	3	10.4 – 10.8	10.6 – 11.0
$TMAH^+$	0.13E08	0.13E08	0	13.2 – 13.5	13.4 – 13.8
$MEAH^+$	0.47E08	0.51E08	8	10.1 – 10.5	10.3 – 10.8
$DEAH^+$	1.06E08	1.08E08	2	13.9 – 14.2	14.1 – 14.5
$TEAH^+$	0.57E08	0.57E08	0	23.6 – 24.0	23.9 -24.2

Table B-2. Analytical performance of other IC methods used for the determination of atmospheric methyl and ethylamines.

Analyte	Detection method	Pre-conc	Column	LOD (pg)	Precision (%)	Reference
$MMAH^+$	CD	Yes	CS10	31	2 – 2.7	Chang et al., 2003
	CD	Yes	CS12A	18	4.5	VandenBoer et al.,
	CD	No	CS14	2500	3.8	2012
	MS	No	CS14	500	5.8	Verriele et al., 2012
	CD	Yes	CS17	540	4.8	Verriele et al., 2012
	CD	Yes	CS19	30 - 650	5	VandenBoer et al.,
	CD	No	Metrosep	21500	0.4	2012
	CD	Yes	C2	2100	12.2	This work
	CD	No	Metrosep	160	7.3	Erupe et al., 2010
			C4			Huang et al., 2014
			Metrosep			Dawson et al., 2014
			C4			
$DMAH^+$	CD	Yes	CS10	40	2 – 2.7	Chang et al., 2003
	CD	Yes	CS12A	25	1	VandenBoer et al.,
	CD	No	CS14	4000	10.5	2012
	MS	No	CS14	150	11.4	Verriele et al., 2012
	CD	Yes	CS17	870	14	Verriele et al., 2012
	CD	No	CS17	1500	1.2	VandenBoer et al.,
	CD	Yes	CS19	40 - 650	5	2012
	CD	No	Metrosep	23000	1.4	Li et al., 2009
	CD	Yes	C2	3800	15.7	This work
	CD	No	Metrosep	320	1.1	Erupe et al., 2010
			C4			Huang et al., 2014
			Metrosep			Dawson et al., 2014
			C4			

$TMAH^+$	CD	Yes	CS10	26	2 – 2.7	Chang et al., 2003
	CD	Yes	CS12A	220	1	VandenBoer et al.,
	CD	No	CS14	2500	N/A	2012
	MS	No	CS14	500	12.2	Verriele et al., 2012
	CD	Yes	CS17	1580	3.3	Verriele et al., 2012
	CD	No	CS17	2000	3.5	VandenBoer et al.,
	CD	Yes	CS19	300 -	16	2012
	CD	No	Metrosep	1200	1.1	Li et al., 2009
	CD	No	C2	38000	6.1	This work
			Metrosep	970		Erupe et al., 2010
			C4			Dawson et al., 2014
$MEAH^+$	CD	Yes	CS10	37	2 – 2.7	Chang et al., 2003
	CD	Yes	CS12A	33	12	VandenBoer et al.,
	CD	No	CS14	1000	5.1	2012
	MS	No	CS14	500	7.9	Verriele et al., 2012
	CD	Yes	CS17	790	10	Verriele et al., 2012
	CD	Yes	CS19	200 -	7	VandenBoer et al.,
	CD	Yes	Metrosep	700	4.3	2012
			C4	2200		This work
						Huang et al., 2014
$DEAH^+$	CD	Yes	CS12A	195	14	VandenBoer et al.,
	CD	No	CS14	N/A	N/A	2012
	MS	No	CS14	35	9	Verriele et al., 2012
	CD	Yes	CS17	1140	3.5	Verriele et al., 2012
	CD	Yes	CS19	100 -	8	VandenBoer et al.,
	CD	Yes	Metrosep	800	4.6	2012
			C4	4100		This work
						Huang et al., 2014
$TEAH^+$	CD	Yes	CS12A	32000	2	VandenBoer et al.,
	CD	Yes	CS17	1870	5.9	2012
	CD	Yes	CS19	500 -	12	VandenBoer et al.,
	CD	Yes	Metrosep	1400	5.1	2012
			C4	15900		This work
						Huang et al., 2014

Table B-3. Mass loadings of amines and ammonium in size-resolved particle samples from an aged biomass burning plume sampled in St. John's, Newfoundland on July 6, 2013.

D_p (μm)	Mass loading (ng m^{-3})						
	NH_4^+	MMA	DMA	TMA	MEA	DEA	TEA
10 - 18	BDL	2.0 ± 0.2	0.6 ± 0.2	BDL	BDL	3 ± 1	2 ± 1
5.6 - 10	BDL	BDL	0.7 ± 0.3	2 ± 2	BDL	2.2 ± 0.9	2 ± 1
3.2 – 5.6	BDL	0.11 ± 0.03	0.4 ± 0.1	BDL	BDL	BDL	BDL
1.8 – 3.2	BDL	0.10 ± 0.03	0.25 ± 0.09	2 ± 1	BDL	1.4 ± 0.6	1.3 ± 0.7
1 – 1.8	BDL	2.9 ± 0.8	3 ± 1	3 ± 2	BDL	27 ± 4	4 ± 2
0.56 – 1	719 ± 7	1.4 ± 0.4	190 ± 4	5 ± 3	0.4 ± 0.2	1300 ± 200	2 ± 1
0.32 – 0.56	443 ± 4	11 ± 3	208 ± 4	4 ± 3	0.21 ± 0.08	1300 ± 200	4 ± 2
0.18 – 0.32	236 ± 2	6 ± 2	80 ± 2	BDL	BDL	560 ± 90	2 ± 1
0.10 – 0.18	30 ± 50	0.4 ± 0.1	30 ± 10	BDL	0.6 ± 0.2	200 ± 30	BDL
0.056 – 0.10	20 ± 30	3 ± 1	6 ± 2	4 ± 3	BDL	58 ± 9	3 ± 2
0.032 – 0.056	40 ± 70	0.11 ± 0.03	7 ± 3	BDL	BDL	49 ± 8	BDL
0.018 – 0.032	BDL	0.10 ± 0.03	BDL	BDL	BDL	4 ± 2	BDL
0.010 – 0.018	BDL	0.30 ± 0.08	BDL	BDL	BDL	BDL	BDL

BDL = below detection limits

Table B-4. Mass loadings of amines and ammonium in a fresh biomass burning plume at Burnaby Kensington Park and North Vancouver/Second Narrows sites in British Columbia in July 2015.

Sampling site	Relative time	Mass loading (ng m^{-3})				
		NH_4^+	iMPA	TMA	DEA	TEA
BKP	- 24	70 ± 20	1.4 ± 0.9	0.6 ± 0.5	0.9 ± 0.5	0.2 ± 0.1
BKP	- 16	90 ± 30	6 ± 4	3 ± 2	1.6 ± 0.8	0.08 ± 0.06
BKP	- 8	130 ± 40	BDL	5 ± 4	BDL	BDL
BKP	0	90 ± 30	20 ± 10	9 ± 7	8 ± 4	BDL
BKP	8	90 ± 30	2 ± 1	2 ± 1	1.2 ± 0.7	BDL
BKP	16	80 ± 20	BDL	BDL	BDL	BDL
BKP	24	31 ± 9	BDL	BDL	BDL	BDL
NVSN	- 24	130 ± 40	5 ± 3	BDL	BDL	BDL
NVSN	- 16	400 ± 100	14 ± 9	BDL	BDL	BDL
NVSN	0	300 ± 100	40 ± 30	BDL	BDL	BDL
NVSN	8	300 ± 100	60 ± 40	BDL	BDL	BDL
NVSN	16	70 ± 20	BDL	BDL	BDL	BDL
NVSN	24	100 ± 30	BDL	BDL	BDL	BDL

BDL = below detection limits